# Università degli Studi di Napoli Federico II

# Xenobiotics in the environment: an investigation on the transformation kinetics, the environmental metabolites and their formation mechanisms

*Monica Passananti*

Tutor
Prof. Maria Rosaria Iesce
Co-tutor
Dr. Fabio Temussi

# ABSTRACT

Xenobiotics are continually introduced into the environment and it is very important to draw up an "*environmental risk assessment*" for these pollutants. Xenobiotics can be persistent and accumulate in the environment or undergo biotic and/or abiotic transformations leading to transformation products. The latter are known as environmental metabolites and may be more toxic and/or persistent than the parent compounds. Therefore, it is important to have information on the xenobiotic behavior in the different compartments (water, atmosphere, soil) as well as on the nature of their transformation products.

The photochemical processes play an essential role in the environmental degradation of pollutants. Phototransformation studies may be used in combination with physical chemical properties and data from other studies (abiotic hydrolysis; biotransformation; adsorption/desorption) to help the assessment of the overall environmental transformations and transport of chemical pollutants. The photochemical behavior of a molecule depends on the presence of peculiar functional groups. However, given the heterogeneity and complexity of xenobiotics, it is often difficult to predict or rationalize the photochemical behavior of these molecules.

In this PhD thesis the photochemical behavior of some chemical pollutants (mainly drugs and pesticides) under environmental-like conditions has been investigated. The selected xenobiotics are characterized by the presence in the molecular structure of a carbamate function or an indole moiety, two functions present in widely used bioactive compounds. In particular, direct photolysis studies have been carried out on drugs indomethacin, etodolac, loratidine and rivastigmine, on pesticides chlorpropham and phenisopham and on carbamic model compounds. Indirect photolysis of rivastigmine and nicotine have also been investigated. Moreover, for some xenobiotics photochemical experiments in soil have been performed.

Direct photolysis studies have led to the determination of phototransformation kinetics, isolation and characterization of photoproducts and interpretation of the involved mechanisms.

Investigation on indomethacin, a non-steroidal anti-inflammatory drug (NSAID), has evidenced the role of the aryl portion in the formation of ionic species prior to the decarboxylation, and the results give a further support to the general photodecarboxylation mechanism of arylalkanoic acids. The photochemical oxidative

cleavage of C2-C3 bond through the intermediacy of peroxidic species has also been observed, and this supports the tendency of indoles to give self-sensitized photooxygenation. This type of reaction has also been observed for the other indolic drug examined, etodolac.

Investigation on rivastigmine and its main human metabolite has evidenced a peculiar photochemical behavior. Both compounds undergo a β-cleavage of the benzylamine moiety resulting in photosolvolysis reaction, previously reported for benzyl ethers or esters. In particular, the photodegradation involves the tertiary amino site and leads mainly to ion-derived products characterized by departure of the $Me_2N$-group. It is reported that amines bearing *N*-substituents that are capable of stabilizing the formed aminium radicals have lower oxidation potentials as compared to those with *N*-electron withdrawing substituents as amides and carbamates. This could account for the unreactivity of the carbamic-N function of rivastigmine as compared with the reactivity of the benzylaminic function.

Loratidine is rapidly transformed either under UV-B or by sunlight exposure. In this case the reactive site is the double bond, while the carbamate moiety is unreactive.

Pesticides chlorpropham and phenisopham contain a carbamate and a bis-carbamate function, respectively; in phenisopham one of the functions is similarly substituted as in chlorpropham. Neverthless, the two pesticides behave differently: the first one undergoes a nucleophilic photosubstitution of chlorine with water on the aromatic ring, while in phenisopham photo-Fries rearrangements occur involving the cleavage of the *N*-aryl *O*-aryl carbamate moiety. However investigation on model compounds evidences that *N*-aryl *O*-aryl substitution is not a sufficient condition to have a photo-induced breaking of the carbamate bond. This breaking is completely overcome in the presence of a chlorine on the aromatic ring. Moreover, substitution on the carbamic nitrogen as well as the presence of a *N*-substituent in the *O*-aryl moiety appears determinant to accelerate the photo-Fries reaction.

All photochemical experiments evidence the determinant role of water. This is probably due to the fact that water can favor photoionization reactions, stabilize ionic intermediates and trap electrophilic species.

Indirect photolysis investigations have been performed on rivastigmine and nicotine in Clermont-Ferrand (France) in collaboration with *Laboratoire de Photochimie Moléculaire et Macromoléculaire*-University Blaise Pascal. The results show that the degradation rate of both compounds depends on the HO˙ source ($H_2O_2$, nitrates,

nitrites). Faster degradation has been observed in the presence of nitrates and nitrites and is probably due to reactions between the xenobiotics and photogenerated reactive nitrogen species. For rivastigmine the formation of nitro derivatives has been confirmed by LC-MS. Nitro compounds are often more toxic than the parent compounds, and hence for a complete environmental risk assessment the reactivity toward hydroxyl radical and also toward nitro reactive species that are naturally present in surface waters should be considered.

Less satisfying has been the investigation on the photochemistry in soils. Despite the simple synthetic model soils used each compound examined behaves differently depending on the light absorption property and on the formation of saline bonds due to the presence of acidic or basic reactive sites. In addition to these factors in real soils other factors should be considered as the presence of microorganisms or xenobiotics, the type of texture, the pH, etc.

In conclusion, the whole of the results give information on the photochemical behavior of different xenobiotics under environmental-like conditions. From a chemical point of view they give a deeper insight into the substituent and solvent effects in the photochemistry of some important compound classes as indoles, benzyl derivatives and carbamates. Therefore, these studies could allow to develop theoretical models for the prediction of the environmental fate of xenobiotics.

# INDEX

# 1.0 INTRODUCTION

With population growth, urbanisation and economic development xenobiotics are continually introduced into the environment and it becomes very important to draw up an *"environmental risk assessment"* for these pollutants. In order to know the risks and the impact of xenobiotics on the environment it is necessary to investigate on their environmental fate. Indeed, xenobiotics can be persistent and accumulate in the environment or undergo biotic and/or abiotic transformations leading to transformation products. The latter are known as environmental metabolites and may be more toxic and/or persistent than parent compounds. Therefore, it is important to have information on the behavior of a xenobiotic in the different compartments (water, atmosphere, soil) as well as on the nature of their transformation products.

The photochemical processes play an essential role in the environmental degradation of pollutants. Studies about the phototransformation in combination with other studies (physico-chemical properties of the molecule, abiotic hydrolysis, biotransformation, adsorption/desorption, toxicity) can be used to assess the overall environmental risk of chemical pollutants. Furthermore, these studies could allow to develop theoretical models for the prediction of the environmental fate of xenobiotics. The photochemical behavior of a molecule depends on the presence of peculiar functional groups. However, given the heterogeneity and the complexity of xenobiotics, it is often difficult to predict or rationalize the photochemical behavior of these molecules.

In this PhD thesis the potential effects of solar and solar-simulated irradiation on some chemical pollutants (mainly drugs and pesticides) under environmental-like conditions have been investigated. It has been chosen to study the photochemical reactivity of xenobiotics characterized by the presence of common functional groups. In particular investigation has been focused on pollutants characterized by the presence of a carbamate moiety or of an indole ring, two functions present in widely used bioactive compounds.

In this chapter a brief summary is reported about the regulations on chemicals, the main pollution sources and the environmental fate of xenobiotics (transport and degradation processes). An introduction on photochemical processes is also described together with literature data on the photochemistry of indoles and carbamates.

In the second chapter the results about the direct irradiation (direct photolysis) of some xenobiotics in aqueous solutions are reported. The work concerns with the determination of phototransformation kinetics, isolation and characterization of

photoproducts and elucidation of the involved mechanisms. These data contribute to estimate the environmental impact of these pollutants, and give information about the photoreactivity of some functional groups. In some cases, in an attempt to rationalize the functional group photoreactivity in different molecular environments, photoreactivity studies of synthetic model compounds have also been performed.

In the third chapter a study on the phototransformation of some pollutants mediated by other species (indirect photolysis) present in natural waters is reported. In the environment there are many compounds that may absorb solar light and contribute to degradation of xenobiotics. The indirect photolysis of pollutants in the environment is the main photodegradation process when xenobiotics do not absorb sunlight or are slowly degraded by direct sunlight irradiation. The xenobiotics transformation has been investigated under irradiation of synthetic waters using different natural hydroxyl radical sources (*i.e.* $H_2O_2$, $NO_3^-$, $NO_2^-$). Some irradiations have been performed in natural waters (lake, river, rain).

In the end, phototransformation experiments have been carried out in synthetic soils (chapter four). This preliminary investigation has been performed with the aim of highlighting the analogies and the differences with xenobiotics phototransformations in aqueous solutions.

The results reported in this thesis on the phototransformation rate and on the transformation photoproducts of xenobiotics under environmental-like conditions give significant information on their environmental fate.


## 1.1 ENVIRONMENTAL POLLUTION

All products fabricated by humans, from electric material of computers to packages, from soaps to drugs, after use, are finally released into the environment and are introduced into all environmental compartments (air, soil and water) by intentional disposal or accidental spills.

The use and production of chemical substances are in continuous growth. Each year between 50 and 1˙000 new synthetic compounds are introduced to the market and over 70˙000 different chemicals are used daily worldwide. Seas and oceans have been used as dump and even now are used as disposal waste. Although large bodies of water have the capacity to dilute and disperse contaminants, the wastes and the pollution sources are continually growing. For example, during the 90s, more than 500 tons of sewage *per*

2

year have been dumped into the Mediterranean, and more than 60% of these haven't been treated at all (Kress et al. 2004). The impact of these substances on the ecosystem and on the human health is of considerable concern and in the last decades has involved also the governmental authorities. The latter have intervened by imposing limits on production, use and disposal of chemicals and promoting restrictive regulations. Since 1 June 2007, in Europe, REACH (**R**egistration, **E**valuation, **A**uthorisation and Restriction of **Ch**emical substances) has entered into force (The European Parliament and of the Council 2006). It is the European Community Regulation on chemicals and their safe use and environmental impact. The aim of REACH is to improve the protection of human health and the environment through the better and earlier identification of the intrinsic properties of chemical substances.
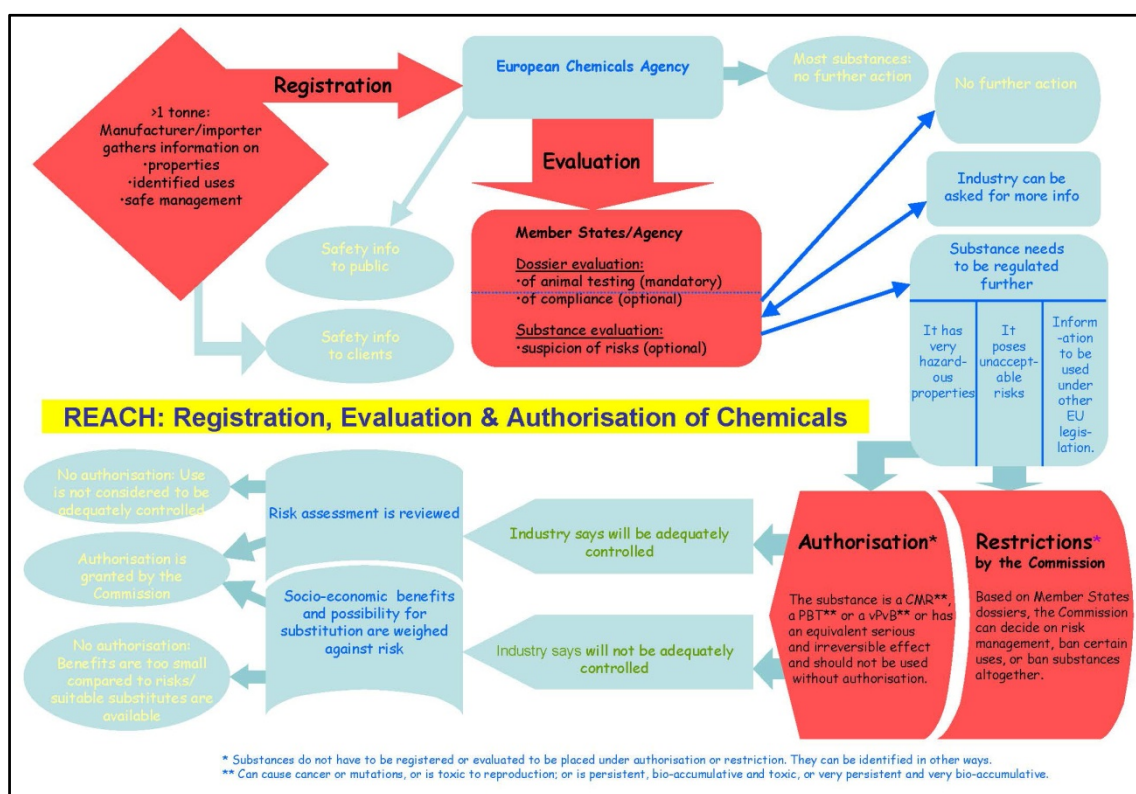


**Figure 1**. Flowchart on REACH regulation from http://ec.europa.eu/.

The REACH regulation places greater responsibility on industry to manage the risks from chemicals and to provide safety information on the substances. If substances are manufactured or imported in an annual quantity of 10 metric tons or more, REACH requires not only the submission of technical data but also a Chemical Safety Assessment (CSA) (Fig. 1). Within REACH, the chemical safety assessment plays a major role since it is the instrument to ensure that all risks are identified and under

control. The Chemical Safety Assessment (CSA) is the process that identifies and describes the conditions under which the manufacturing and use of a substance is considered to be safe. Based on this chemical safety assessment, the Chemical Safety Report (CSR) is prepared which also describes the necessary risk management measures to ensure safe use of the substance. Along with the information on the intrinsic properties of the substance, it is necessary to collect data on the potential environmental fate of the substance, exposure scenarios and risk characterization.

In addition to regulations on chemicals and their safety assessment, there are several governmental and non-governmental authorities that supply information on xenobiotics and more in generally on the environment issues, in order to implement and evaluate the economic development and environmental policy. These organizations promote the information acquisition on human health and environmental risks connected to chemicals. In particular, they develop guidelines to evaluate human and environmental risk of xenobiotics. All these data are used to draw up an "*environmental risk assessment*" (ERA) for chemicals (Fig. 2).
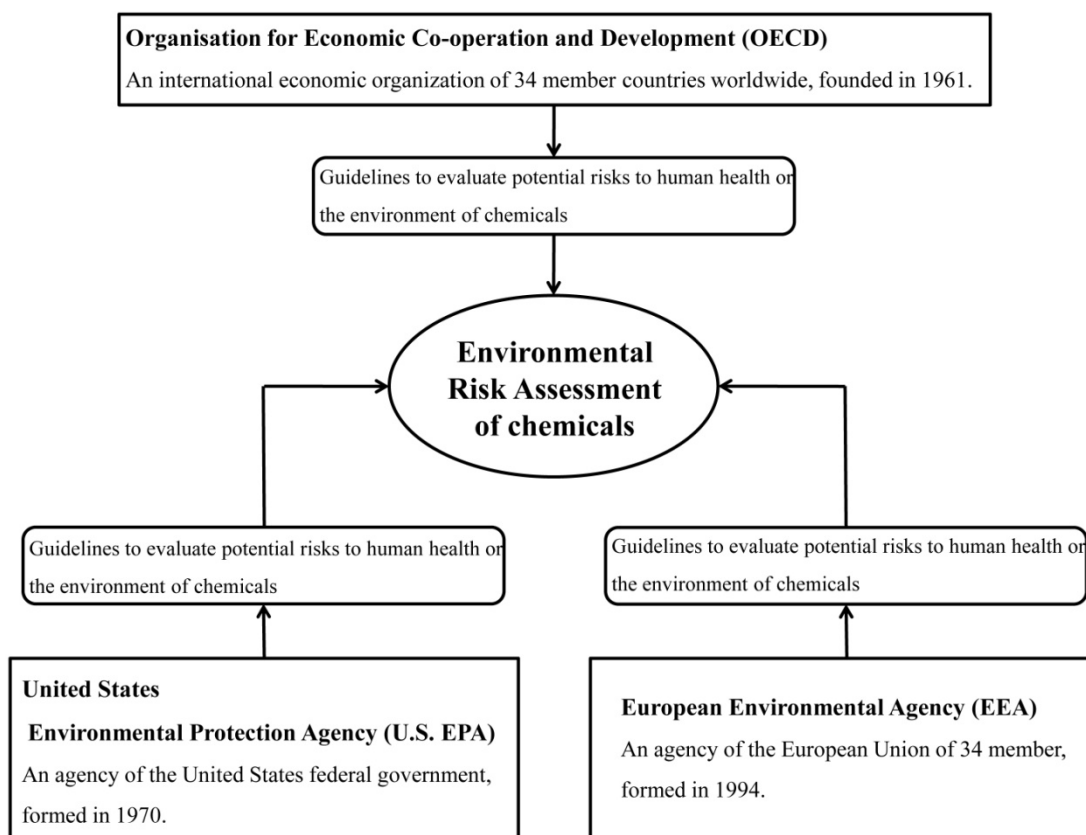


**Figure 2**. Main organizations developing guidelines on the environmental risk assessment of chemicals.

4

The main organizations are: the United States Environmental Protection Agency (U.S. EPA), the European Environmental Agency (EEA) and the Organization for Economic Co-operation and Development (OECD), this latter is formed by 34 countries from all around the world. In particular, the European Environmental Agency recommends to draw up an ERA for xenobiotics because it provides a systematic procedure for predicting potential risks to human health or the environment. An environmental risk assessment is a process of predicting whether there may be a risk of adverse effects on the environment caused by a chemical substance. Environmental exposure concentrations of a chemical are predicted and compared to predicted no-effect concentrations (PNECs) for different environmental compartments. ERA can also reveal if measures are needed to limit the potential environmental consequences of a substance and it can point out if further testing and knowledge about a substance is needed. Basic principles of environmental risk assessment have been developed by the European Commission and are available at http://www.eea.europa.eu/publications/GH-07-97-595-EN-C2/riskindex.html (EEA 2011).

The main pollution sources are exhaust gases of industries and of vehicles, industrial sewage, effluents of wastewater treatment plants and the use of hazardous substances such as household chemicals, fertilizers and pesticides (Fig. 3).
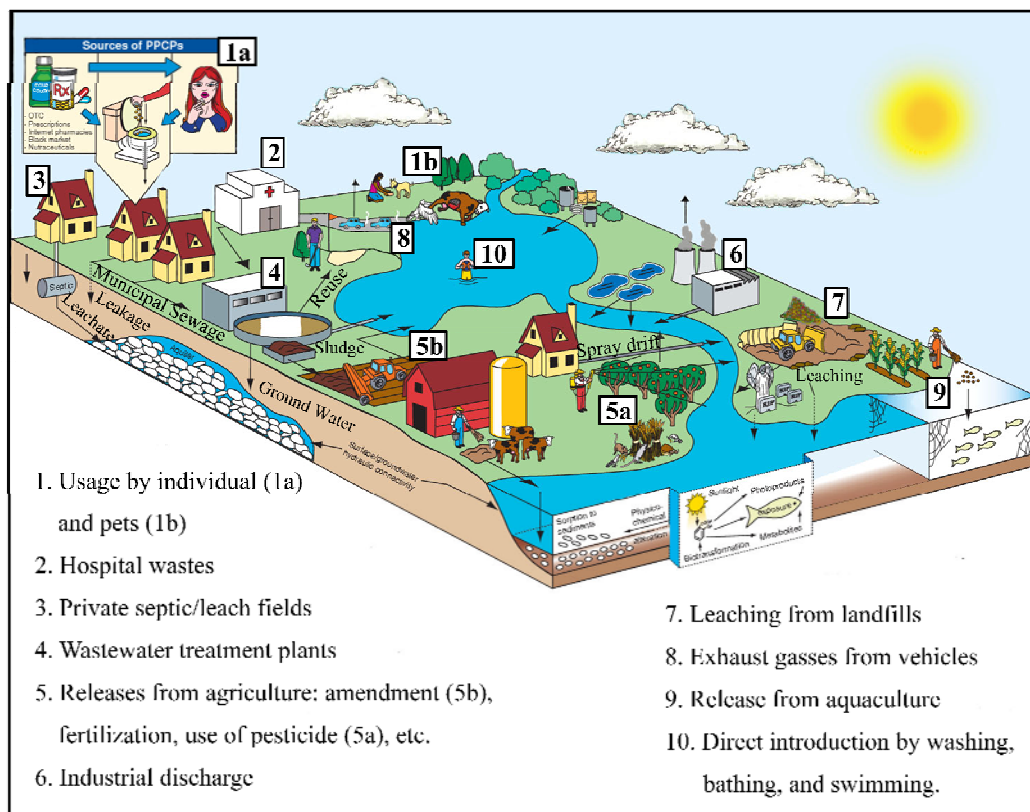


**Figure 3**. Main pollution sources (http://www.epa.gov/).

The pollutants released into the environment may bioaccumulate, undergo transformation and/or be transferred into the different compartments. If the pollutant is a persistent molecule, it may accumulate in the food chain presenting an important human and ecological risk. The movement of xenobiotics in the environment is very complex and the transfers occur continually among different compartments, depending on the physicochemical properties of the compounds. In some cases, these exchanges occur not only between areas that are close together, but may also involve transportation of pollutants over long distances (see Fig. 4).

The interest about environmental pollution has begun during mid-50s; in those years industrial wastes, industrial products and pesticides started to be studied from an environmental point of view. In particular, in 1962, the book *Silent Spring* written by scientist Rachel Carson was published. It was one of the signature events in the birth of the environmental movement. The book focused attention on the problem of pollution in the environment and condemned the use of long-lasting pesticides in general, and DDT in particular. Ten years later DDT was banned in the US. Actually the intensive agricultural methods and the large scale development of the agrochemical industry has led to a massive use of synthetic compounds in agriculture. Only in 1996, more than 2.5 million tons of pesticides were applied to soil and foliage (Brown et al. 1996). Due to their intensive use, pesticides are often found in soil and in water. For example, in Italy groundwaters, used for drinking, were analysed, and some pesticides were found at concentrations higher than 0.1 μg/L. This value represents the European Union limit of the single pesticide in drinking water. The maximum level was recorded for desethylatrazine that was found at a concentration of 0.62 μg/L (Fava et al. 2010). There are many other studies that attest the presence of pesticides in the environment. In a study published last year many organochlorine pesticides were found in sediments sampled in Keoladeo National Park in India (Bhadouria et al. 2012). In this case DDT was still found although banned many years ago. Most of the chlorinated pesticides are toxic and persistent and were replaced by carbamate pesticides that are less toxic. The massive use of carbamic pesticides in the last years has led to an increase of these compounds in the environment. In Bangladesh carbamic pesticide carbofuran was found in surface water samples at a concentration of nearly 200 μg/L (Chowdhury et al. 2012). Generally, pesticides are directly applied to soil or applied to irrigation waters; they may be adsorbed by soil or crops, but may also move in the environment. Pesticides may reach the atmosphere by volatilization or by spray drift. The runoff from the soil carries

these compounds in surface waters. Moreover pesticides may reach groundwater by percolation through the soil. Pesticides are projected and synthesized to kill or repel pests, hence they are biological active compounds and may interact with the ecosystem. Many pesticides exhibit acute and chronic toxicity to aquatic and terrestrial organisms (Iesce et al. 2006; Weyman et al. 2012). Pesticides can also pose risks to people. The health effects of pesticides depend on the type of the pesticide. Some of them, such as the organophosphates and carbamates, affect the nervous system; others may irritate the skin or the eyes, some others may be carcinogenic. The US Environmental Protection Agency (EPA) furnishes an human health risk assessments for many pesticides (US EPA 2012).

Pesticides and industry products are generally called classic pollutants. In the last decade new pollutants have been found in the environment. These compounds, that are not covered by existing water quality regulations, are generally called emerging pollutants. They include diverse groups of chemicals: surfactants, industrial additives and agents, perfluorinated compounds, flame retardants, pharmaceutical and personal care products (PPCPs) and many others (Farre et al. 2008). PPCPs are compounds used for personal health, cosmetic reasons or used to enhance growth or health of livestock. They include thousands of chemical substances as drugs, dietary supplements, veterinary drugs, fragrances, and cosmetics, laundry and cleaning products. The way that these xenobiotics enter into the environment depends on their use and application mode. One of the main point discharge sources of PPCPs into the environment are the sewage treatment plants (STPs) effluents. Many of these compounds, mainly drugs, after application are excreted by urine and feces and are transported into sewage. Sewage treatment plants (STPs) often are not able to completely remove these xenobiotics. Many studies reported the detection of PPCPs, specially drugs and their metabolites, in input and output STPs effluents in the range of ng $L^{-1}$ – µg $L^{-1}$ (Kim et al. 2009). In this way PPCPs enter into the environment, where they are frequently found (Andreozzi et al. 2003; Ellis 2006; Murray et al. 2010). Drugs are compounds made to have a biological activity and in the environment, even in very small concentration, can interact with aquatic or non aquatic organisms with effects often unknown on the ecosystem (Daughton and Ternes 1999; Halling-Sorensen et al. 1998; Jjemba 2006; Jorgensen and Halling-Sorensen 2000; Vaal et al. 1997).

The environmental fate of pollutants is very difficult to be predicted and depends on several factors among which the most important are the point discharge and the

physical-chemical properties of xenobiotics. The environment fate of pollutants involves many different processes, such as bioaccumulation, transfer and degradation (Fig. 4). The latter may be due to microorganisms (biotic process) or involves abiotic processes.
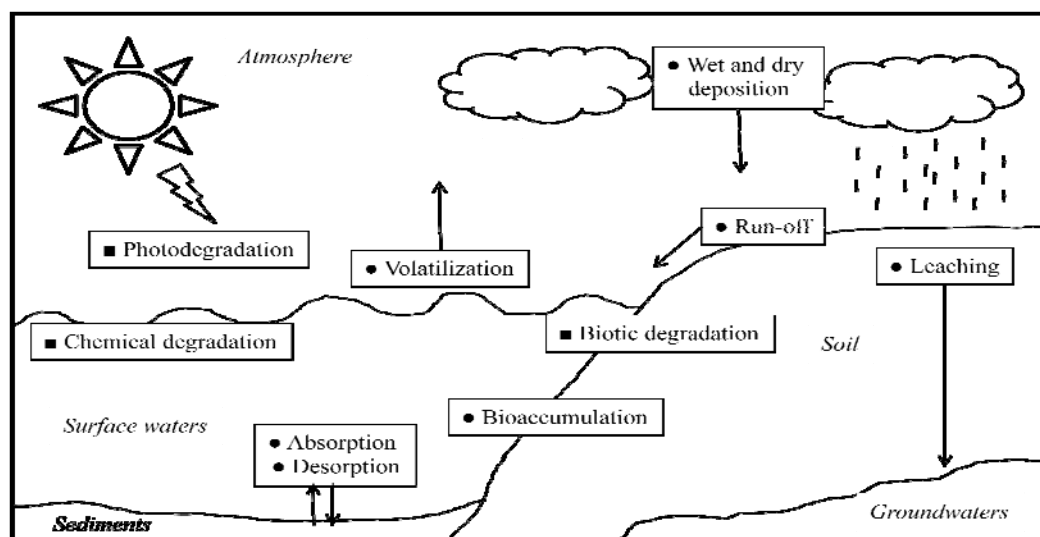


**Figure 4**. Environmental fate of pollutants (● transport, ■ transformation processes).

The environmental transformation processes may lead to complete degradation of xenobiotics, that are transformed in very small molecule as carbon dioxide; this process is generally known as mineralization (Mateen et al. 1994). In some cases the xenobiotics transformation is not complete and leads to the formation of novel compounds, called environmental metabolites. These compounds may differ in their environmental and ecotoxicological behavior from their corresponding parent compounds. For example, they may be more toxic and persistent than the parent compounds (DellaGreca et al. 2004a; Jahan et al. 2008). Indeed, they may have a different mode of action from parent compounds, in some cases due to the increase in hydrofobicity (Escher and Fenner 2011). One example is given by carbaryl and its environmental metabolite that has more potent mode of action and is more toxic than the parent compound (Boxall et al. 2004). Hence, data on pollutant degradates are crucial for understanding the environmental fate of xenobiotics and predicting their potential impact on the environment (Sinclair and Boxall 2003).

The degradation routes of pollutants depend on the environmental compartments in which the xenobiotic is located. For example, if a pesticide is directly applied to soil, the biotic degradation may be an important process.

The fate and behavior of organic pollutants in soil are governed by many different factors including soil characteristics, chemical properties and environmental factors such as temperature and precipitation (Semple et al. 2001). The persistence of several organic pollutants in soil was proposed to be related to their hydrophobicity (Cerniglia 1992). In this environmental compartment the degradation by microorganisms is one of the main transformation processes. The biodegradation rate depends very much on soil temperature, soil moisture content, concentration of the compound and on composition of the microbial community (Sinkkonen and Paasivirta 2000). The abiotic processes may also take place in soil. In particular, photochemical degradation is possible only near the air-soil interface, generally it is restricted to less than the top 1 mm of soil. Direct photolysis is restricted to the photic depth of soils ($0.2 \pm 0.4$ mm), while the indirect photolysis can take place a little deeper (Hebert and Miller 1990; Sinkkonen and Paasivirta 2000).

In soil, such as in atmosphere (mainly in hydrosphere) abiotic transformations of pollutants involve heterogeneous reactions. The latter differ substantially from analogous homogeneous reactions in respect to reaction rates, product distributions and stereochemistry. In heterogeneous environments sorption, ion-exchange, dissolution, precipitation and heterogeneous redox processes bear a decisive role on transformation processes (Wayne 2005). The complexity of the natural environment renders the understanding of photochemical environmental processes through basic laboratory experiments very difficult. For this reason the studies about the environmental fate of xenobiotics are generally carried out in aqueous solutions.

In water the most important degradation processes are abiotic, in particular hydrolysis, oxidation-reduction and photolysis. Hydrolysis, generally, produces molecules more polar than parent compounds, and depends strongly on pH. Redox reactions of organic pollutants may occur in the environment. Only a few functional groups are oxidized or reduced abiotically, such as acids, halides and nitrogenous compounds. This contrasts with biologically mediated redox processes by which organic pollutants may be completely mineralized to $CO_2$, $H_2O$ and so on.

An important role in the environmental fate of xenobiotics, in natural waters, is the sunlight mediated photodegradation, that may occur *via* direct or indirect reactions. Direct photolysis involves the transformation of a molecule resulting from the direct absorption of a solar light. Accordingly, direct photolysis can be a degradation pathway

only for chemical pollutants that exhibit light absorption above the 290 nm cutoff of solar irradiation at the earth's surface (OECD 2008).

When a molecule (R) absorbs light it is promoted to an excited state (R*). This is an unstable species with a surplus of energy that is fast dissipated by several processes(Fig. 5). There are various physical or chemical processes that the excited species may undergo.

The physical processes are generally represented by:

$$R + h\nu \rightarrow R^* \rightarrow R$$
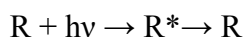
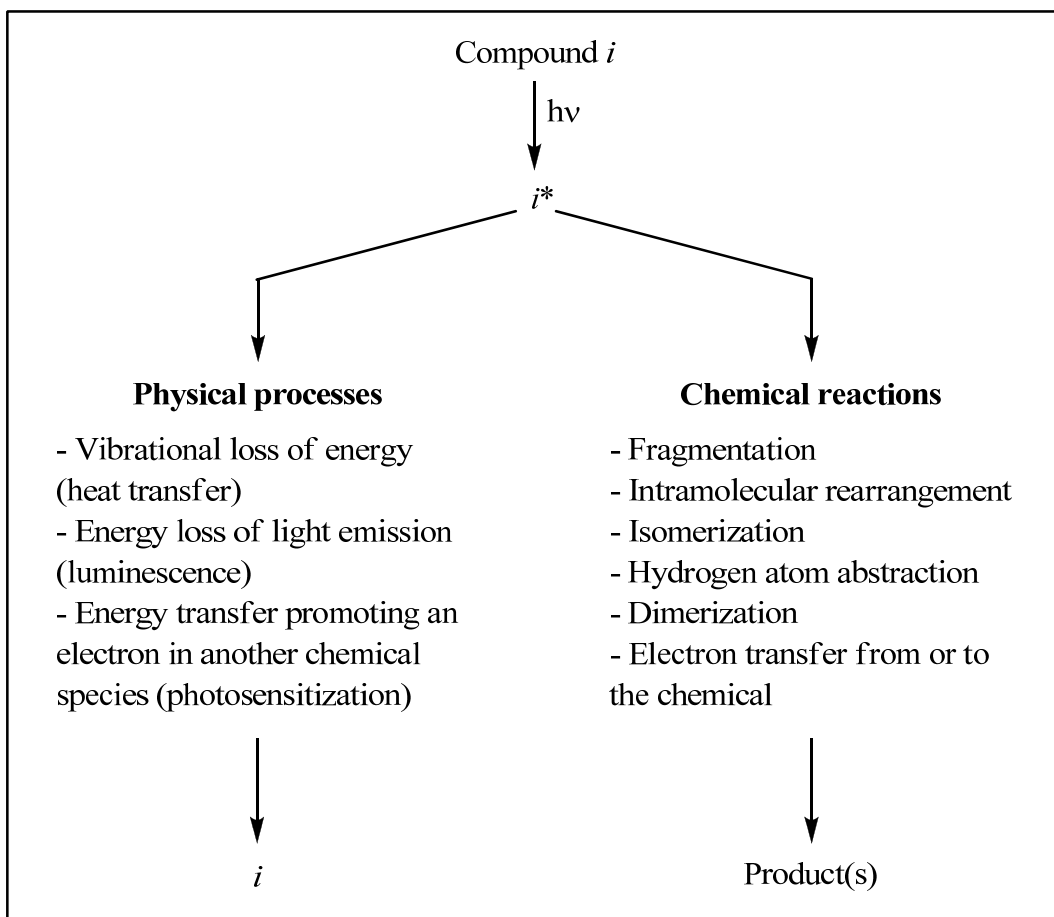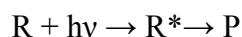In this case the excited species returns by deactivation processes to the ground state.



**Figure 5**. Possible photophysical and photochemical processes (Schwarzenbach et al. 2003).

On the other hand in a photochemical process the molecule in the excited state undergoes transformation to form a new compound (P):

$$R + h\nu \rightarrow R^* \rightarrow P$$

There are various physical deactivation processes that are illustrated by a Jablonski diagram (Fig. 6). Here non-radiative transitions are indicated by wavy arrows and radiative transitions by straight arrows. One of non-radiative transitions is the *internal conversion*, in which the excited species converts to a lower level of the same multiplicity by giving off its energy in small increments of heat to the environment.
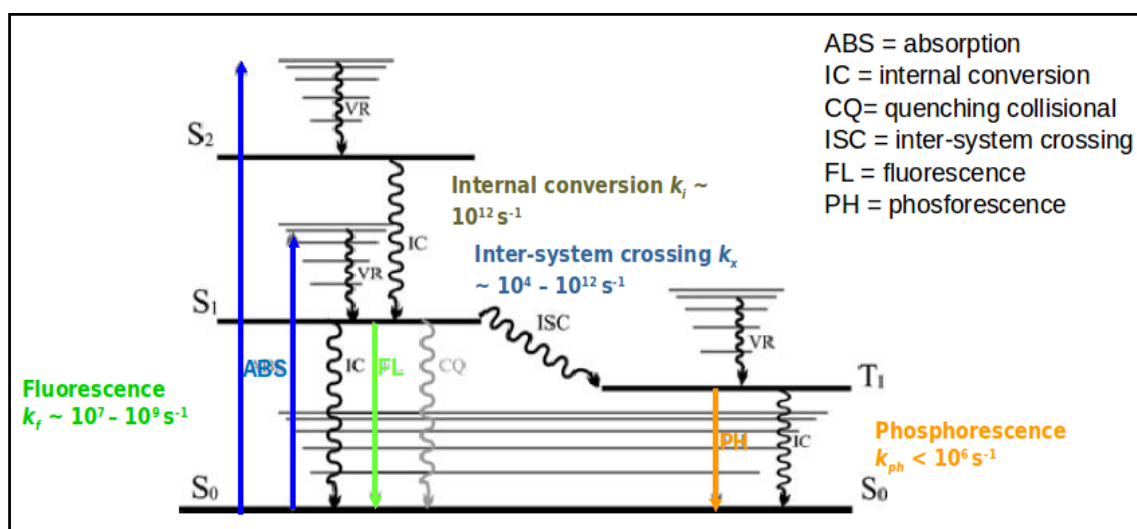


**Figure 6**. Jablonski diagram.

Alternatively, the *intersystem crossing* involves the transition between two electronic states with different spin multiplicity, generally $S_1 \rightarrow T_1$. The excited molecule may directly, or after *intersystem crossing*, drop to the ground state by giving off the energy in the form of light. These luminescent processes are called fluorescence and phosphorescence, respectively.

Finally, an excited species may undergo an intermolecular process transferring its energy to another molecule in the ground state (A):

$$R^* + A \rightarrow R + A^*$$
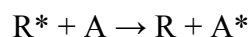
This process can be considered through two different points of view depending on the scope:

- if the scope is to generate the excited molecule A* by energy transfer, the species R is called *sensitizer* and the process *photosensitization;*

11

- if the scope is to deactivate R* to ground state (R), the process is called *quenching* and A *quencher*

(Schwarzenbach et al. 2003; Turro et al. 2010).

In the environment, intermolecular processes play an important role. Indeed, abiotic degradation pathways may involve indirect photolysis, that occurs through reactions with reactive intermediates (photosensitizers or reactive oxygen species) generated by light-absorbing molecules. These photosensitized processes may involve energy transfer, electron transfer and/or the formation of reactive oxygenated species (ROS). In the environment indirect photolysis can be induced by naturally occurring compounds such as inorganic ions (nitrate and nitrite), transition metals ($Fe^{III}$ salts) and chromophoric dissolved organic matter (CDOM), for example humic substances. These substances produce radical or oxidizing species by sunlight irradiation (Vione et al. 2005). Chromophoric dissolved organic matter (CDOM), after excitation, may lead to direct transformation of an organic pollutant (P), as well as to the formation of a variety of reactive species, such as alkyl peroxy radicals and hydroxyl radical (Lam et al. 2003). Hydroxyl radical $HO^{\bullet}$ is a strong and not selective photooxidant and reacts with many organic compounds at nearly diffusion-controlled rates. It is produced in the environment also through the photolysis of $Fe^{II}$ and $Fe^{III}$ species, nitrate and nitrite.

Nitrate ions are usually present in natural waters and their photolysis is a relevant source of hydroxyl radical in natural waters. Nitrogen dioxide is also produced by sunlight irradiation of nitrate ions and this species can interact with organic compounds inducing nitration and nitrosation processes.

Nitrite is usually present in the environment at a lower concentration than nitrate, but due to its higher molar absorptivity and photolysis quantum yield it represents an important $HO^{\bullet}$ environmental source (Fischer and Warneck 1996; Vione et al. 2005).

Another reactive species present in natural water is the carbonate radical ($CO_3^{\bullet-}$), that is generated from the reaction of $HO^{\bullet}$ with carbonate or bicarbonate ions. Carbonate radicals may react with electron-rich compounds such as anilines and phenols, but react mainly with sulfur compounds. It is reported that carbonate radicals are involved in the degradation of some sulfurated pesticides such as fenthion and thioanisole (Huang and Mabury 2000; Larson and Zepp 1988).

In the environment both direct and indirect photolysis may contribute to the degradation of xenobiotics.

## 1.2 PHOTOCHEMISTRY OF INDOLES

The indole moiety is a basic element for a large number of biologically active natural and synthetic products. Indole (Fig. 7) is present into amino acid tryptophan and in neurotransmitter serotonin. It is one of the most frequently encountered heterocycles in medicinal chemistry (Kalshetty et al. 2012; Kaneko et al. 2000; Leonard 1995). One of the largest classes of alkaloids (indole alkaloids) is constituted by compounds containing the structural moiety of indole. Many of these indole alkaloids possess significant biological activity and are used in medicine. In fact, the active ingredients of many drugs with different activities, such as Lescol (fluvastatin sodium), Cialis (tadalafil), Indoxen (indometachin) and many other, are indole derivatives. Some other derivatives show herbicidal activity, as indole-3-acetic acid (IAA) that is the most common plant hormone and has profound effects on plant growth and development (Zhao 2010). Many synthetic indolic molecules are used in agriculture, as indole-3-butirric acid extensively used in floriculture.
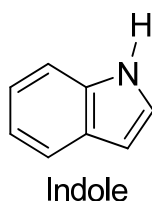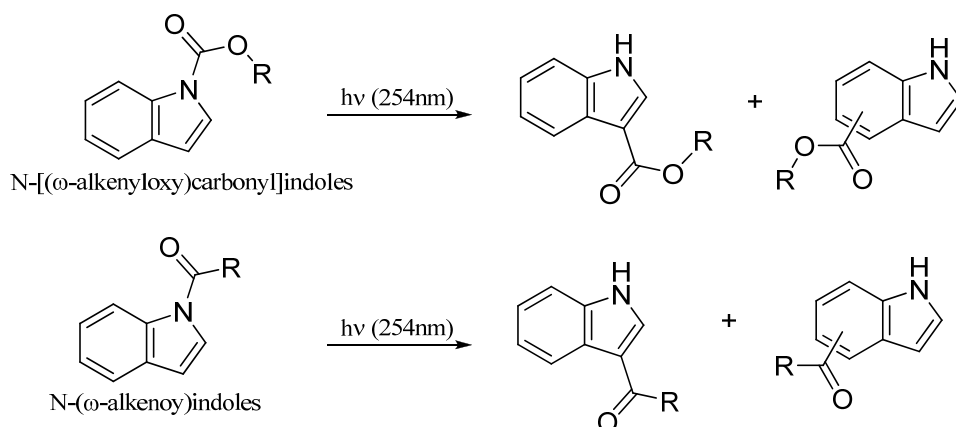


Indole

**Figure 7**. Indole structure.

In literature many studies about spectroscopic and photophysical properties of indoles, for biological applications, are reported, but studies about photoreactivity under environmental-like conditions are few. In some cases the photochemical behavior of indoles has been investigated in organic solvents and/or for synthetic purposes. Photo-Fries rearrangements have been reported for *N*-acylindoles and a dependence on irradiation wavelength has been observed. The total quantum yield for the photo-Fries products decreases as the irradiation wavelength increases (Oldroyd and Weedon 1991). In particular, ultraviolet light (254 nm) irradiation of *N*-[(ω-alkenyloxy)carbonyl]indoles and *N*-(ω-alkenoy)indoles in organic solvents (mainly benzene) gives the 3-, and in smaller amounts 4-, and 6-substituted isomers by Fries-type rearrangement (Scheme 1). With light of wavelength $\lambda$ < 300 nm the photo-Fries rearrangement doesn't take place (Oldroyd and Weedon 1994).

**Scheme 1.** Photoreactivity of *N*-[(ω-alkenyloxy)carbonyl]indoles and *N*-(ω-alkenoy) indoles.

Recently, the photoreactivity of an indole derivative, the drug fluvastatin, has been investigated in environmental-like conditions (Fig. 8) (Cermola et al. 2007).



Fluvastatin

Dihydrobenzocarbazole

Azonane-2,7-dione

Spiro[4.4]azononane
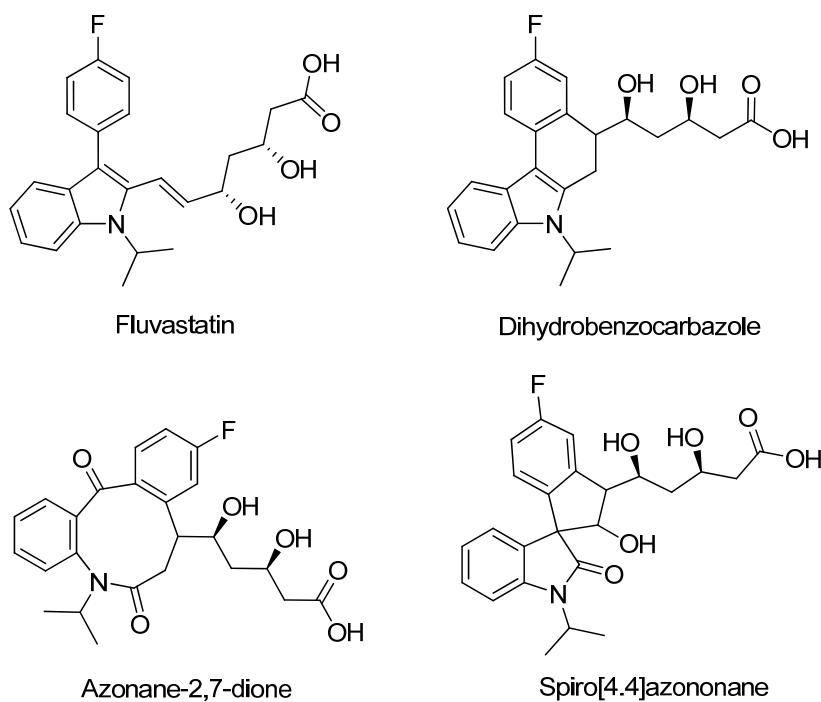
**Figure 8.** Fluvastatin and its main photoproducts.

Fluvastatin is easily transformed in water by solar irradiation. Photocyclization and photooxygenation are the main reactions involved in the formation of the products. As reported for *o*-vinylbiphenyl compounds (Mallory and Mallory 1988), the photochemical electrocyclization is the main reaction that leads to dihydrobenzocarbazoles. Photooxygenation of the indole moiety of this photoproduct gives an azonane-2,7-dione and a spiro[4.4]azononane. The experiments suggest that

singlet oxygen may be involved in the photooxygenation pathways, probably formed through a self-sensitized mechanism. The capacity of polycyclic nitrogen heterocycles to generate singlet oxygen has been observed in other cases (Pari et al. 2000). Photooxygenation of indoles has been extensively studied, often with the aim to synthetize alkaloids (Iesce et al. 2005; Nakagawa et al. 1982). On the other hand, it is possible that different oxygenated species (e.g. $O_2^{\bullet-}$) can be involved in the formation of spiro compounds. This hypothesis is supported by the reported superoxide scavenging properties of fluvastatin and its metabolites (Suzumura et al. 1999).

Another study about indoles photobehavior is on the photochemistry of the drug tadalafil (Fig. 9) in aqueous solutions (Temussi et al. 2010).
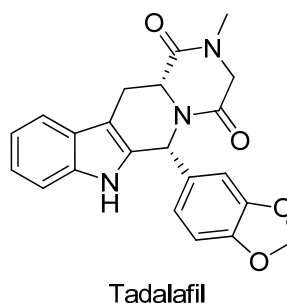


Tadalafil

**Figure 9.** Structure of drug tadalafil.

Under irradiation at $\lambda > 290$ nm the drug undergoes heterolytic β-cleavage of benzyl-like amide. The indole moiety isn't directly involved in the formation of photoproducts, but probably influences the β-cleavage, not observed in other benzyl amides.

## 1.3  PHOTOCHEMISTRY OF CARBAMATES

Due to their broad spectrum of biological activity, carbamates (Fig. 10) are used in medical field as active ingredients of many drugs, and in cosmetic field (Meyer et al. 2010; Vielhaber et al. 2010).



Carbamate

**Figure 10.** Carbamate structure.

Moreover carbamates represent one of the main categories of synthetic organic pesticides and are used as insecticides, nematocides, fungicides, acaracides, molluscicides, sprout inhibitors or herbicides (Morais et al. 2012). They were introduced to the agrochemical market in the 1950s (Tomlin 1997) and are used annually on a large scale worldwide (Paiga et al. 2009). The carbamates attack the insect nervous system, in particular they bind with the acetylchlorinesteras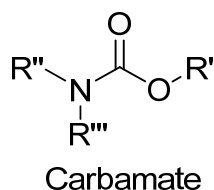e, an enzyme found in the synapses (Wright 2003). Although carbamates present low bioaccumulation potentials and short-term toxicity they are known to have potential harmful effects towards non-target organisms (Morais et al. 2012). In fact, they are considered hazardous to the environment and human health being included in the priority list released by the U.S. EPA (US EPA 1992). In general, oral and dermal exposures to carbamate pesticides produce nausea, stomach cramps, diarrhea and excess salivation. At higher dosage sweating, lack of co-ordination and convulsions may result (Wright 2003).

Carbamate pesticides and their transformation products are often found in the environment; for example benfuracarb and carbosulfan and their hydrolysis products, carbofuran and carbofuran-3-hydroxy, have been recently detected in the Sakura River (Iwafune et al. 2010). The literature survey reveals that photoreactivity of carbamate pesticides is sufficiently studied, but in many cases the experimental set-up is far from environmental conditions. Many studies report the photochemical behavior of carbamate pesticides in organic solvents (cyclohexane, isopropanol, etc.) under UV-C irradiation (Burrows et al. 2002) and in some cases the results are conflicting. For example, photodegradation kinetics of ethiofencarb has been studied (Sanz-Asensio et al. 1999) and it has been observed that the reaction rate increases with the polarity of the reaction medium. In another study the efficiency of the photodegradation of this pesticide has been found higher in less polar solvents, with variation of the half-lives from 75 min to more than 20 h (Kopf and Schwack 1995). Different products have been found in the irradiation of ethiofencarb depending on the solvent and light source. Ethiofencarb sulfoxide is the main product in cyclohexane, while photooxidation, hydrolysis and addition product formation are observed when the photodegradation takes place in isopropanol. In water, 2-(methyl)phenyl-*N*-methylcarbamate deriving from photocleavage of the C–S bond is the main photoproduct (Scheme 2) (Burrows et al. 2002).
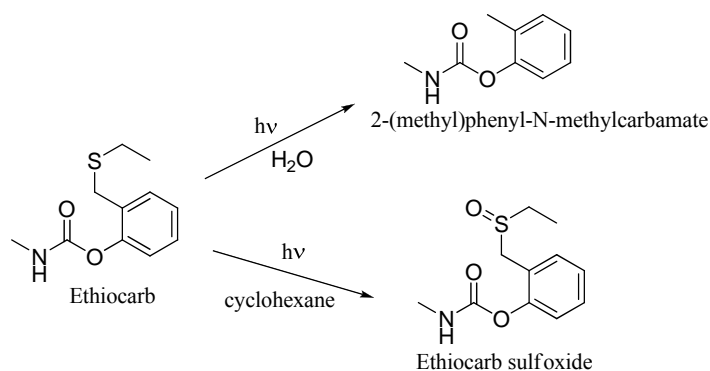
**Scheme 2.** Photoreactivity of ethiocarb in different solvents.

Carbamate pesticides that have been extensively studied, also under environmental-like conditions, are carbofuran and carbaryl. The latter was the first carbamate pesticide to be used worldwide. The photochemistry of these compounds has been examined in distilled water, in natural waters and artificial water (in presence of humic acid and/or nitrate) under sunlight, suntest apparatus and high pressure mercury lamp irradiation (De Bertrand and Barcelo 1991; Iesce et al. 2006; Samanidou et al. 1988). The main photochemical event observed is the cleavage of C-O bond and the resulting formation of α-naphtol from carbaryl and of phenol derivative from carbofuran (Scheme 3).
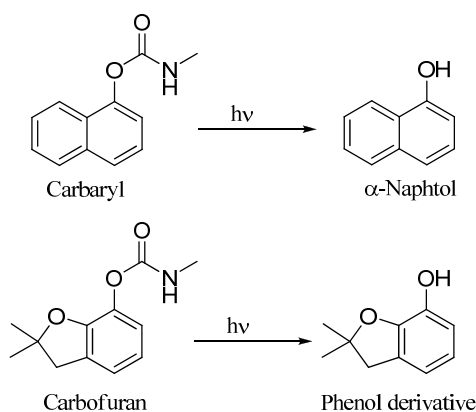


**Scheme 3.** Photoreactivity of carbaryl and carbofuran.

Carbofuran is quite photostable and a half-life time of 693 h has been calculated under high pressure mercury lamp irradiation in water. For carbaryl a half-life time of 5 h has been calculated under solar simulator irradiation in vary dilute seawater solution (5 x $10^{-7}$ M) (Armbrust and Crosby 1991). The literature survey reveals that carbamate pesticides under irradiation undergo mainly cleavage of carbamic moiety to form phenols and anilines from *O*-aryl carbamates and *N*-aryl carbamates, respectively.

17

In some cases photo-Fries rearrangement products were observed. However, in aqueous solutions, hydrolysis may efficiently compete with photodegradation, and in some cases may even be the dominant pathway (Burrows et al. 2002).

## 2.0 DIRECT PHOTOLYSIS

Direct photolysis involves the transformation of xenobiotics resulting from the direct absorption of solar radiation. This chapter reports the results about the direct photolysis experiments of xenobiotics containing an indole moiety (indomethacin (**1a**), etodolac (**1b**)) or a carbamic function (rivastigmine (**1c**), loratidine (**1d**), chlorpropham (**1e**), phenisopham (**1f**)), and studies about the direct photolysis of model carbamic compounds (**1g-1m**). For each xenobiotic the studies led to the determination of phototransformation kinetics and quantum yield, isolation and characterization of photoproducts, and to the mechanistic interpretation of phototransformation pathways.

Preliminarily, the UV-Vis absorption of the xenobiotic was measured in aqueous solutions at different concentrations. The radiation absorption of the molecule is a necessary condition, although not sufficient, to undergo transformation *via* direct photolysis. Moreover, the stability in solution and in the dark was always tested. Various compound solutions (different pH, concentration, solvent) were stored in the dark, and analysed time by time, generally by HPLC.

Two photoreactors equipped with UV-B lamps were used as radiation sources. In some experiments UV-C and UV-A lamps were also used. For environmental information sunlight exposure (Naples, latitude 40°51'46''80 N) was also used as a radiation source for environmental information. Irradiations were followed by HPLC and, when necessary, also by TLC and NMR. Products were irradiated in aqueous solution using, in some cases, an organic solvent (acetonitrile or methanol) as co-solvent to obtain clear solutions. Concentration values were within the range $1 \times 10^{-5}$ M – $1 \times 10^{-3}$ M. Concentrated solutions ($1 \times 10^{-3}$ M) were used to isolate the photoproducts. The latter were separated by chromatographic techniques (TLC, CC, HPLC) and were fully characterized by spectroscopic techniques, mainly mono- and bi-dimensional NMR and mass spectrometry.

## 2.1 KINETICS AND QUANTUM YIELDS

### 2.1.1 *Actinometry*

The incident photon flux of the lamps was measured by *p*-nitroanisole (PNA)/pyridine (Py) actinometer (Dulin and Mill 1982). The PNA transformation rate in presence of

pyridine depends, in some conditions, only on pyridine concentration. The quantum yield of actinometer PNA/Py is:

$$\Phi_{PNA/Py} = 0.44[Py] + 0.00023 \qquad (Eq.1)$$

where [Py] is the molar concentration of pyridine. The quantum yield depends on absorbed photon flux ($I_a$) according to the following relationship:

$$I_a = \frac{\Delta N_{PNA}}{\Phi_{PNA/Py}} \qquad (Eq.2)$$

where $\Delta N_{PNA}$ is the number of PNA molecules degraded *per* time unit and surface unit. It is possible to determine $\Delta N_{PNA}$ by irradiation experiments. The absorbed photon flux depends on incident photon flux ($I_0$) and on absorbance of PNA/Py solution (A) at different $\lambda$, according to the following relationship:

$$I_a = \sum_{\lambda=300}^{\lambda=350} I_0(\lambda)\left[1 - 10^{-A(\lambda)}\right] \qquad (Eq.3)$$

The sum range ($\lambda$ from 300 nm to 350 nm) is defined by overlapping of the UV absorbent spectrum of PNA/Py solution with lamp emission spectrum. The incident photon flux, for a system of specific geometry and in a well defined spectral domain, may be calculated by Eq.3.

The incident photon flux in solution for photoreactor System II is 4.98 x $10^{21}$ photons $m^{-2} s^{-1}$ (see experimental section, *6.1.2*).

The incident photon flux in solution for photoreactor System IV is 6.10 x $10^{19}$ photons $m^{-2} s^{-1}$ (see experimental section, *6.1.2*).

## 2.1.2 *Quantum yield*

The quantum yield is an important parameter in photochemistry, it is defined as follows:

$$\Phi = \frac{number\ of\ reacted\ molecules\ per\ time\ unit}{number\ of\ photons\ absorbed\ per\ time\ unit} = \frac{dn(X)/dt}{I_a} \qquad (Eq.4)$$

The quantum yield represents the fraction of photoexcited molecules that undergo phototransformation, usually it is a number less than 1, only for radical chain processes is $\Phi > 1$. The absorbed energy by molecules must be sufficient to cause the transformation, for example a bond cleavage, rearrangement, oxidation or reduction. Not all excited molecules react to form new molecules, because there are many other possible deactivation processes such as quenching, radiation-less processes and radiative processes. For this reason, the quantum yield generally assumes a value lower than 0.1 (Harris 1982; Mill 1999).

Assuming that the xenobiotic is the only absorbing specie present in solution, the polychromatic quantum yield degradation ($\Phi$) of the xenobiotic has been calculated in the overlap range of the UV-Vis spectrum of the molecule with the lamp emission spectrum, as follows:

$$\Phi = \frac{R_X^d}{I_a} \qquad \text{(Eq.5)}$$

where $R_X^d$ is the xenobiotic degradation rate (M s$^{-1}$) and $I_a$ is the absorbed photon flux *per* unit of surface and unit of time. The latter is calculated from:

$$I_a = \int_{\lambda_1}^{\lambda_2} I_0(\lambda)\left(1 - 10^{-\varepsilon(\lambda)d[X]}\right) d\lambda \qquad \text{(Eq.6)}$$

where $\varepsilon$ is the molar absorption coefficient of the xenobiotic, *d* the optical path length inside the cells and [X] the initial xenobiotic concentration.

### 2.1.3 *Kinetic constant*

If the photon irradiance remains constant over time, it is possible to assume that the direct photolysis kinetic is of first order and the rate of transformation of the xenobiotic follows the equation:

$$\frac{dc}{dt} = -k\,c \qquad \text{(Eq.7)}$$

where $c$ is the xenobiotic concentration in molarity (mol L$^{-1}$) and $k$ is the rate constant in s$^{-1}$. With opportune transformations Eq.7 can be written as follow:

$$ln\frac{c_0}{c_t} = k\,t \qquad\qquad (Eq.8)$$

where $t$ is the time (s) and $c_0$ and $c_t$ are respectively the xenobiotic concentration (M) at time $t = 0$ and at time $t$. The kinetic constants ($k$) were determined fitting data by linear regression with Eq.8. The half-life time ($t_{1/2}$) of the xenobiotic was calculated using the following equation:

$$t_{1/2} = \frac{ln2}{k} \qquad\qquad (Eq.9)$$

The variation of xenobiotics concentration during irradiation was monitored by HPLC. At fixed time intervals an aliquot of the irradiation mixture was withdrawn and analysed by HPLC. Preliminary, a calibration curve was obtained by analyzing stock solutions of xenobiotics by HPLC and plotting the peak areas versus the theoretical concentrations. The data were subjected to the least squares regression analysis.

## 2.2 LASER FLASH PHOTOLYSIS (LFP)

In a photochemical reaction a molecule (R) is promoted to an excited state (R*), this latter is an unstable species that decays rapidly. To understand the phototransformation mechanism it is important to monitor the formation of transient species. Laser time-resolved techniques are able to observe excited states and metastable intermediates (Cosa and Scaiano 2004; Demtroeder 2008). The laser flash photolysis is one of these techniques that detects the short lived intermediates *via* their absorption. The most common laser flash photolysis system are equipped by lasers with a pulse duration of nanosecond (2-20 ns). By these devices it is possible to study triplet states, diradicals, radicals, ions and other long life intermediates.

A typical nanosecond laser system is composed of a laser source for sample excitation, a continues lamp (generally a xenon lamp) for the monitoring beam, an optic system (filters, monochromator, etc…) for sample excited analysis and a detection system (photomultiplier) (Fig. 11).
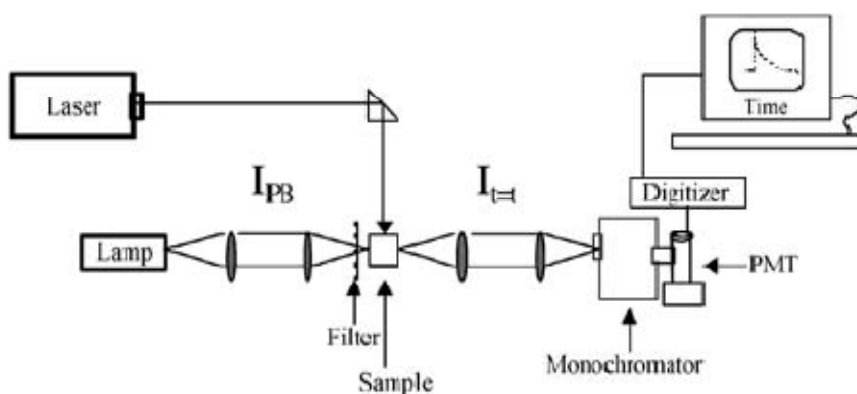
**Figure 11**. Schematic diagram of a nanosecond laser system (Cosa and Scaiano 2004).

The experimental magnitude measured is a change in absorbance (ΔOD) reflecting changes in transmitted light from the continuous lamp (probe beam) before ($I_{t=0}$) and after ($I_{t=t}$) laser excitation:

$$\Delta OD_{t=t} = -\log\left(\frac{I_{t=t}}{I_{t=0}}\right)$$

Eq. (10)

The output is a plot of ΔOD versus time at a given wavelength. It is possible to construct an absorption spectrum of species in solution by monitoring time-resolved traces at many wavelengths and extracting absorbance data at a given time from each trace. The transient species are characterized by their absorption spectrum and by their decay/formation time. To study reaction mechanisms the time evolution of the transients, formed after laser excitation, is monitored. Often some quenchers as energy acceptors, radical traps, hydrogen donors, $O_2$, electron donors or acceptors are used. Adding a quencher to the solution will introduce a new mechanism for the deactivation of the transient produced after excitation.

| | | |
|---|---|---|
| GS $\xrightarrow{h\nu}$ T $\longrightarrow$ $P_r$ | without quencher | $k_{exp} = k_{dec}$ |
| GS $\xrightarrow{h\nu}$ T $\xrightarrow{Q}$ $P_r + P_Q$ | with quencher | $k_{exp} = k_{dec} + k_q[Q]$ |

**Scheme 4.** Change in decay rate constant with the addition of quencher. GS is the sample in ground state, Q is the quencher, T the transient species and $k_{dec}$, the decay kinetic constant of T (Cosa and Scaiano 2004).

The experimental decay rate constant ($k_{exp}$) changes in the presence of these quenchers and the linear dependence of $k_{exp}$ with quencher concentration yields the value for $k_q$, as

23

reported in Scheme 4. The nature of the observed transient can be assigned on the basis of a comparison of the obtained $k_q$ with literature values.

## 2.3 INDOLES

### 2.3.1 *Indomethacin*

Indomethacin (**1a**) is a nonsteroidal anti-inflammatory drug (NSAID) (Fig. 12). Approved by FDA in 1965, it acts inhibiting the production of prostaglandins. Indomethacin is metabolized in human body and several metabolites are found in plasma and urine. The main metabolites derive from *O*-demethylation and *N*-deacylation, in particular the demethylation followed by deacylation is the major metabolic process (Duggan et al. 1972). Indomethacin is widely used due to its antipyretic and analgesic properties, more potent than aspirin. It has been recently found in the environment, in particular in a Japan river (Hoshina et al. 2011).
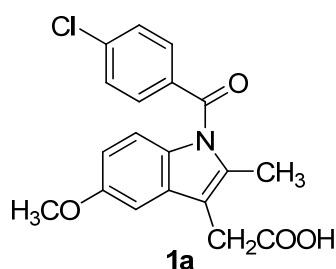


**Figure 12.** Indomethacin (**1a**, 1-(4-chlorobenzoyl)-5-methoxy-2-methyl-1*H*-indole-3-acetic acid).

Indomethacin is stable in neutral or slightly acid solution in the dark, but decomposes in strong alkaline solution (RxList). The drug, as crystalline solid, is photostable (Ekiz-Guecer and Reisch 1991), but it is photochemically labile in solution, especially in organic solvents (Dabestani et al. 1993; Weedon and Wong 1991). The photochemical reaction observed in organic solvents, using medium pressure mercury lamp, was decarboxylation of the acetic side chain that can be followed by oxidation (Dabestani et al. 1993; Weedon and Wong 1991). By sunlight irradiation in methanol no decarboxylation was observed and the obtained products were rationalized as deriving from an acyl radical (Wu et al. 1997). Conflicting data were reported for irradiation in aqueous solution with no photochemical activity in buffered aqueous solution (Moore and Chappuis 1988) in contrast to the observation of photodegradation to a complex mixture under aerobic and anaerobic conditions (Pawelczyk et al. 1977).

Indomethacin has in the molecular structure a *N*-benzoylindole and an acid group. It is slightly soluble in water and has a pKa of 4.5. The molecule exhibits absorption up to 400 nm with the maximum of the lowest energy band at 320 nm so that it is photosensitive in a wide range of light (Weedon and Wong 1991). Indomethacin, when excited at 300 nm, emits at long wavelengths (around 555 nm) with a large Stokes' shift highly depending on solvent (Weedon and Wong 1991). It is reported that *N*-benzoyl-indole derivatives fluoresce weakly and the energy of the emitting state and the quantum yield of fluorescence are strongly influenced by solvent polarity. This behavior was explained supposing the initial formation of a singlet excited state (non-emissive) that can relax to a dipolar singlet excited state through an intramolecular charge transfer from the indole to the benzoyl group. This excited state is weakly fluorescent (Disanayaka and Weedon 1987).

*Results*

In Fig. 13 the UV-Vis spectrum of indomethacin in aqueous solution is reported. Indomethacin exhibits absorption up to 400 nm with the maximum of the lowest energy band at 320 nm.
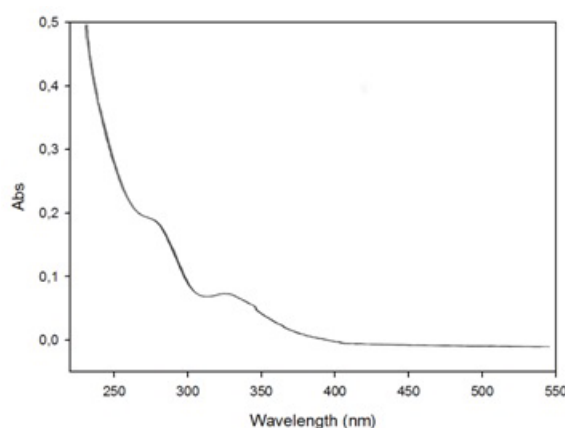


**Figure 13**. Indomethacin UV-Vis spectrum in $H_2O/CH_3CN$ 95:5(v/v) 1 x $10^{-5}$M.

Due to the low solubility in water, acetonitrile was used as co-solvent. In particular, kinetic experiments were carried out using drug solutions in water/acetonitrile 95:5 (v/v) at 1 x $10^{-5}$ M concentration. The kinetic constants and the half-life times were determined by exposing drug solutions in quartz tubes to UV-C and UV-B lamps as well as to sunlight (Table 1).

| Light source | $k$ (min$^{-1}$) | $t_{1/2}$ (min) |
|---|---|---|
| UV-C lamps | 0.055 | 12.6 |
| UV-B lamps | 0.0156 | 44 |
| Sunlight | $9.3 \times 10^{-4}$ | 744 |

**Table 1.** Kinetic constants ($k$) and the half-life time ($t_{1/2}$) of indomethacin photodegradation by different light sources.

A quantum yield of $1.5 \times 10^{-4}$ was determined under UV-B irradiation.

Drug solutions ($1 \times 10^{-5}$ M) in water/acetonitrile 95:5 (v/v) were irradiated by UV lamps (UV-C, UV-B) and sunlight and analysed by HPLC at selected times (Fig. 14). Chromatograms were similar although, in some cases, the peaks intensities were different, likely due to the different light source power and irradiation times.
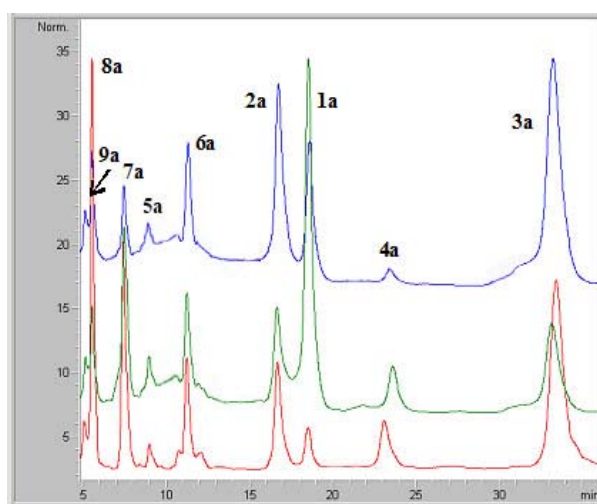


**Figure 14**. Representative HPLC profiles of irradiation mixtures of indomethacin in H$_2$O/CH$_3$CN (95:5 v/v, $1 \times 10^{-5}$ M) a) red: after 19 d of sunlight exposure, b) green: after 90 min of UV-B irradiation c) blue: After 30 min of UV-C irradiation.

Preparative irradiations of indomethacin ($1 \times 10^{-3}$ M; water-acetonitrile 1:1, v/v) were carried out using UV-C lamps and sunlight as light sources. The irradiation times were 4 h and 45 days, respectively.

HPLC analysis and chromatographic separation evidenced the formation of eight photoproducts. The photoproducts isolated are alcohol **2a**, aldehyde **3a**, acid **4a**, methylindole **5a**, anthranilic acids **6a** and **9a**, *p*-chlorobenzoic acid **7a** and NH-indole **8a** (Fig. 15). Aldehyde **3a** and 3-methylindole **5a** were previously isolated by irradiation of the drug in methanol (Weedon and Wong 1991). Photoproduct **8a** was described in

26

literature (Torisu et al. 2005), **7a** is commercially available while the other photoproducts (**2a**, **4a**, **6a** and **9a**) were new.
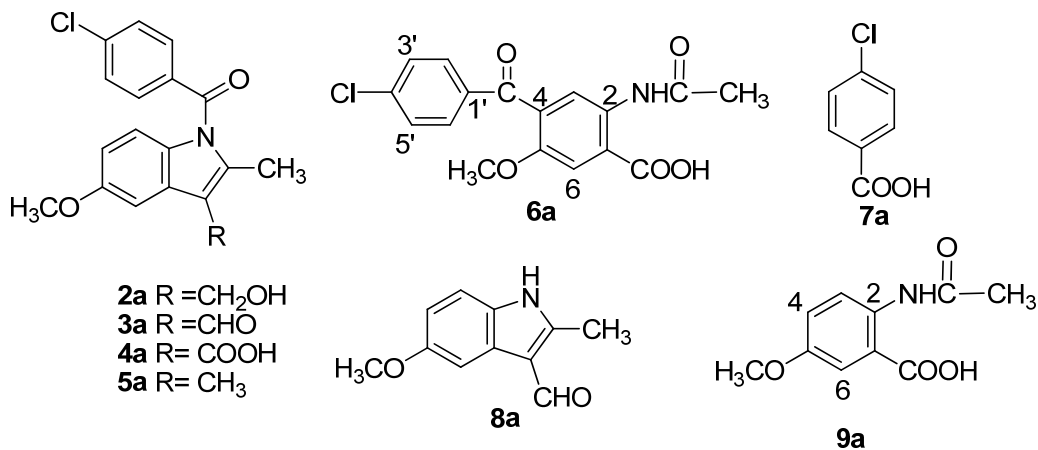


**Figure 15**. Photoproducts formed by indomethacin irradiation in aqueous solution.

The structure of photoproduct **2a** was confirmed by the presence in the mass spectrum of the molecular peak at 352 $m/z$ [M+Na]$^+$ and the peaks at 312 $m/z$ (corresponding to the loss of OH group) and at 139 $m/z$ (due to a $N$-chlorobenzoyl fragment). The NMR spectra of photoproduct **2a** are similar to those of indomethacin. Significant is the shift of the methylene signal at lower field, from δ 3.69 to δ 4.82. In the HSQC spectrum these protons give direct heterocorrelation with the carbon at δ 55.8. These values are typical of a –CH$_2$OH function.

The mass spectrum of photoproduct **4a** shows a molecular peak at 344 $m/z$ [M+H]$^+$, corresponding to molecular formula C$_{18}$H$_{14}$ClNO$_4$. In the $^1$H-NMR and $^{13}$C-NMR spectra the methylene (–CH$_2$–) signals are absent. In the HMBC experiment, the methyl singlet at δ 2.77 gives heterocorrelation ($J_4$) with the carbon at δ 170.3 typical of a carboxylic group (–COOH).

The mass spectrum of photoproduct **6a** shows the presence of molecular peaks at 348 $m/z$ [M+H]$^+$ and 370 $m/z$ [M+Na]$^+$, with the typical chlorine pattern, according to the molecular formula C$_{17}$H$_{14}$ClNO$_5$. $^1$H-NMR spectrum shows the presence of a singlet of methyl group at δ 2.15 , a signal at δ 3.72 of methoxy group protons and, in the range δ 8.51-7.48 , four signals corresponding to six aromatic protons. The $^{13}$C-NMR spectrum evidences two carbons at δ 175.1 and δ 175.0 , corresponding to a carboxylic carbon (–COOH) and an amidic carbon (–CONH–) respectively, and a carbonyl carbon (–CO–) at δ 199.0 . The HMBC spectrum shows the correlations of the carbonyl carbon with H-

27

2', H-4', H-3 and H-6 protons, as well as that of the amidic carbon with methyl protons and that of the carboxylic carbon with the H-6 proton (Fig. 16).
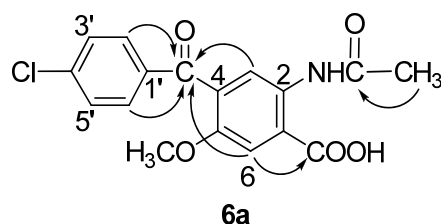


**Figure 16**. Some significant heterocorrelations observed in the HMBC spectrum of **6a**.

The structure of photoproduct **9a** was confirmed by the presence in the mass spectrum of the molecular peak at 232 $m/z$ $[M+Na]^+$ corresponding to the molecular formula $C_{10}H_{11}NO_4$. The $^1$H-NMR spectrum shows, as the $^1$H-NMR spectrum of **6a**, the presence of a singlet of a methyl group at δ 2.15, a signal at δ 3.79 of the methoxy protons. The $^1$H-NMR spectrum shows the presence of only three aromatic protons: two doublets at δ 8.37 and 7.62 corresponding to H-3 and H-6 respectively, and a double doublet at δ 6.96 (H-4). The proton H-4 correlates in COSY experiment with H-3 by a large $J_3$ ($J$ = 9.2 Hz) and with H-6 by a tighter $J_4$ ($J$ = 2.8 Hz). Characteristic signals in the $^{13}$C-NMR spectrum are the carboxylic carbon (–COOH) at δ 174.0 and amidic carbon (–CONH–) at δ 170.1. The HMBC spectrum shows the correlations of the carboxylic carbon with H-6 proton and that of the amidic carbon with methyl protons.

The photostability of some indomethacin photoproducts was also tested. Due to the presence of the same chromophore (*N*-chlorobenzoylindole) alcohol **2a**, aldehyde **3a** and 3-methylindole **5a** exhibit similar absorption bands as the drug and, hence, similar photoreactivity. Compounds **2a**, **3a**, **5a** and **8a** were irradiated in 1 x $10^{-4}$ M solutions (H$_2$O/ CH$_3$CN 95:5, v/v) by UV-C lamps. Photoproduct **5a** under irradiation is quickly degraded to give mainly products **6a** and **7a**. Compound **8a** is more photostable and its HPLC peak slowly decreased in time, and only compound **9a** was identified in very low amount. In Table 2 the percentage of conversion and the related photoproducts after 20 minutes of UV-C irradiation are reported.

| Compound[a] | Conversion (%)[b] | Photoproducts |
|:---:|:---:|:---:|
| **2a** | 40 | **3a, 6a, 7a** |
| **3a** | 75 | **4a, 7a, 8a** (trace), **9a** (trace) |
| **5a** | > 90 | **2a** (trace), **6a, 7a** |
| **8a** | 30 | **9a** (trace) |

**Table 2.** Percentage of conversion and the related photoproducts after UV-C irradiation of **2a**, **3a**, **5a** and **8a**. [a]1 x $10^{-4}$ M, $H_2O$/$CH_3CN$ 95:5, v/v. [b]After 20 min.

To better understand reaction pathways, irradiation experiments were performed in deaerated solutions. Drug solution (1 x $10^{-5}$ M) in water/acetonitrile 95:5 (v/v) was irradiated by UV-C lamps and analysed by HPLC after 30 minutes. In these conditions acid **4a**, anthranilic acids **6a** and **9a** are not formed.

*Mechanistic interpretation*

The main degradation products of indomethacin are alcohol **2a** and aldehyde **3a** found in all the irradiation mixtures (even in deaerated solutions) together with minor compounds **6a** and **7a**. Methylindole **5a** was detected in low amount. Acid **4a** forms in prolonged experiments (by UV-B and sunlight) and in oxygenated media, also anthranilic acids **6a** and **9a** were found only in oxygenated media. Analysis of products structures indicates that degradation of indomethacin involves:

a) decarboxylation of the acetic chain

b) fragmentation of the amide bond

c) oxidative cleavage of C2-C3 bond of the indole ring.

The proposed pathways for the photoinduced degradation of the drug are shown in Scheme 5. The main event is the decarboxylation reaction. On the basis of the photochemistry of structurally related arylacetic acids (Bosca et al. 2004; Bosca et al. 1990; Pitchumani and Madhavan 2004) and the photochemical behavior of indoles in water (McGimpsey and Goerner 1996; Sobolewski and Domcke 2000) it is plausible that an initial photoionization occurs leading to radical cation **10a**. Then, decarboxylation *via* a mesolytic cleavage (Pitchumani and Madhavan 2004) gives radical **11a**. This species adds oxygen affording the corresponding alcohol **2a** and/or aldehyde **3a** likely *via* a peroxide radical **12a** or, to a lesser extent, undergoes a hydrogen shift giving 3-methylindole **5a**.
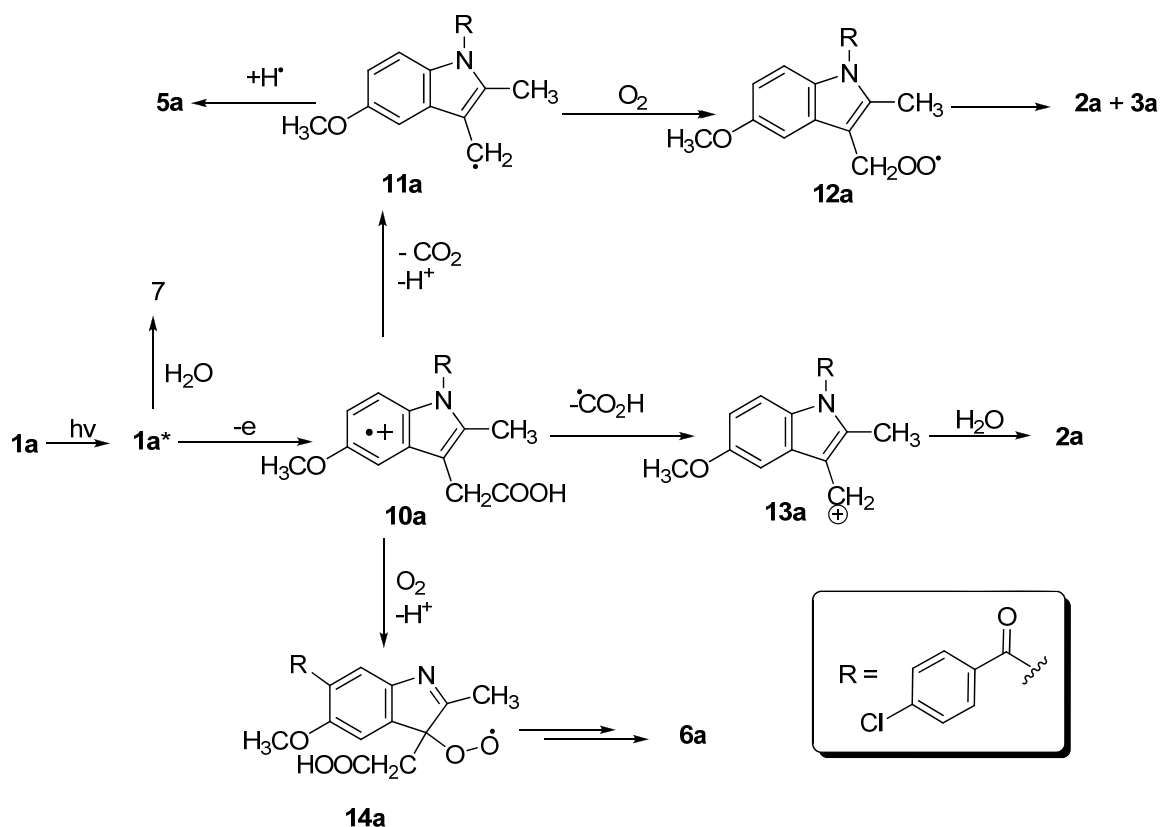
**Scheme 5**. Suggested mechanisms for the main phototransformation products of indomethacin in aqueous solution.

It is also possible that fragmentation of radical ion **10a** produces cation **13a** that can be trapped by the nucleophilic solvent (water) to give alcohol **2a**. This route should account for the finding of alcohol **2a** even in degassed solution. The mesolytic cleavage was previously suggested for naproxen photodegradation (Bosca et al. 1990). The presence in indomethacin of the electron-rich alkoxyarylindole system should promote this route as suggested for the role of alkoxynaphtalenic system in naproxen photodegradation (Bosca et al. 1990; Pitchumani and Madhavan 2004).

Formation of *N*-acyl anthranilic acid **6a** can be explained by the photochemical oxidative cleavage of C2-C3 bond, as reported for 2-, 3- and 2,3-dimethylindoles, through the intermediacy of peroxidic species (dioxetane or hydroperoxide) (Mudry and Frasca 1973). It is noteworthy that in anthranilic acid **6a** the *p*-clorobenzoyl group is at C-6. This substitution should be due to an electrophilic or radical reaction dictated by $OCH_3$ group, e.g. starting from radical ion **10a** (Fig. 18), rather than a photo-Fries rearrangement, as observed in other *N*-acylindoles, that involves C-7 or C-4 position (Oldroyd and Weedon 1991). On the other hand, previous studies on indomethacin didn't report the presence of these rearranged products in organic, even polar, solvents (Dabestani et al. 1993; Weedon and Wong 1991).

30

Photoinduced hydrolysis of the *N*-benzoyl function could be responsible for the finding of chlorobenzoic acid **7a** that can be formed by the drug as well as by all other *N*-acylatedindoles **2a-5a**. Control experiments showed that these compounds are recovered unchanged by keeping them in water solution in darkness, even after 10 days.

Compounds **4a**, **8a** and **9a** are minor products and could be originated as shown in Scheme 6.
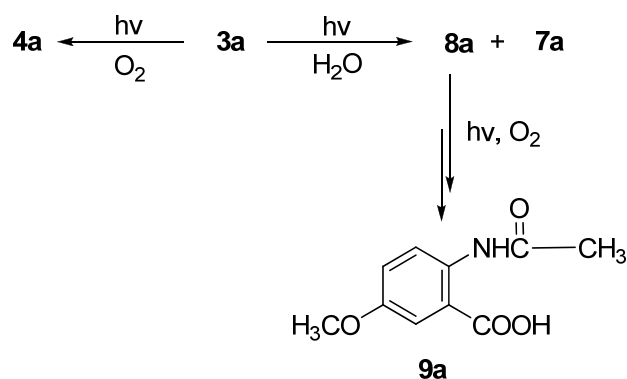


**Scheme 6**. Secondary photodegradation pathways.

*Conclusions*

Eight photoproducts were isolated by UV or solar irradiation of indomethacin in aqueous solution confirming the earliest observation of the drug photodegradation in water (under anaerobic and aerobic conditions) as a complex reaction (Pawelczyk et al. 1977). In addition to radical species, this investigation highlights the possible involvement of cationic species promoted by the ionization of the aryl portion prior to decarboxylation.

The photochemical oxidative cleavage of C2-C3 bond through the intermediacy of peroxidic species (dioxetane or hydroperoxide) was also observed, and this agrees with the tendency of indoles to give self-sensitized photooxygenation.

It is noteworthy that the photochemical behavior of indomethacin in water is quite different from that observed in organic solvents, even in methanol (Dabestani et al. 1993; Weedon and Wong 1991), and could be due to the peculiar role of water to favor photoionization reaction, to stabilize ionic intermediates and trap electrophilic species.

## 2.3.2 *Etodolac*

Etodolac (**1b**) is a nonsteroidal anti-inflammatory drug (NSAID) (Fig. 17), in particular it is a member of the pyranocarboxylic acid group. Approved by the U.S. Food and Drug Administration in 1991, it is used to treat mild to moderate pain, and helps to relieve symptoms of arthritis (osteoarthritis and rheumatoid arthritis). Etodolac is metabolized in the liver, and several metabolites, as hydroxylated-etodolac and etodolac glucuronide, were identified in human plasma and urine (Berendes and Blaschke 1996; Strickmann and Blaschke 2001).

Although etodolac is extensively metabolized in human body and only 1% is excrete unchanged in the urine and 16% in the feces, it has been recently detected in river water samples at a concentration of 0.3 ng/L (Hoshina et al. 2011).

Etodolac is mainly commercialized under the trademark name Lodine[®] in a racemic mixture of etodolac. It has an indole in the molecular structure, a pyran-like ring and an acid group. Etodolac is slightly soluble in water and has a pKa of 4.65.



**1b**
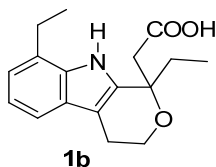
**Figure 17**. Etodolac (**1b**, (±)-1,8-diethyl-1,3,4,9-tetrahydropyrano-[3,4-β]indole-1-acetic acid).

Etodolac has been described as unstable in aqueous solutions at high temperature (75-95 °C) and at different pHs (Lee et al. 1988). It degrades in three products deriving from decarboxylation and ring opening. No data about photostability of etodolac are reported in literature.

*Results and discussion*

UV-Vis spectrum of etodolac (Fig. 18) shows an absorption band with a maximum at λ 225 nm ($\varepsilon = 4.26 \times 10^4$) and a shoulder around 272 nm ($\varepsilon = 8.29 \times 10^3$). pH does not influence the etodolac absorption spectrum.

The stability of the drug in the dark was tested at room temperature using $5 \times 10^{-5}$ M solutions ($H_2O/CH_3CN$ 9:1, v/v) at pH 4, 7 and 9, these pHs are usually considered environmentally relevant (Valenti et al. 2009). After 24h HPLC analyses of these solutions show no degradation of etodolac.

**Figure 18.** Etodolac UV-Vis spectra in $H_2O/CH_3CN$ 9:1(v/v) 5 x $10^{-5}$ M at different pHs.

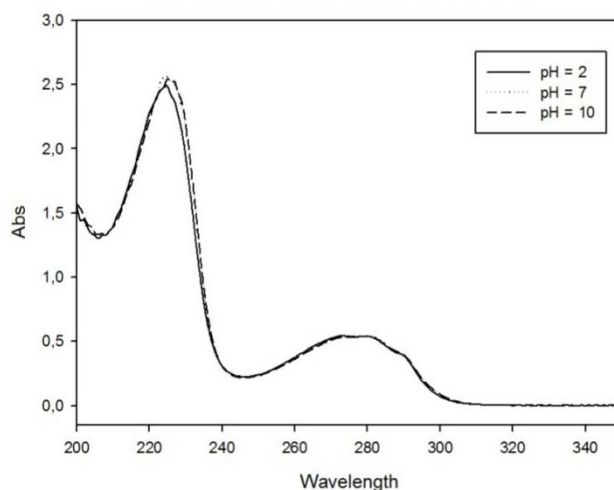An investigation on the photochemical behavior of etodolac in aqueous solutions using UV-B lamps and sunlight as irradiation sources were carried out. Etodolac solution (1 x $10^{-4}$ M) in $H_2O/CH_3CN$ 9:1 (v/v) was irradiated in quartz tubes, using UV-B lamps. Drug degradation was monitored by HPLC analyzing the irradiation solutions at specific time intervals. Under these conditions the kinetic data and the quantum yield were determined and are reported in Table 3.

|  | Etodolac (**1b**) |
|---|---|
| $R$ (M s$^{-1}$) | (1.12 ± 0.05) x $10^{-6}$ |
| $k$ (s$^{-1}$) | (1.80 ± 0.01) x $10^{-2}$ |
| t$_{1/2}$ (s) | 38.6 |
| $\Phi$ | 1.17 x $10^{-8}$ |

**Table 3**. Photodegradation rate (R), kinetic constant ($k$), half-life time (t$_{1/2}$) and quantum yield ($\Phi$) of etodolac determined under UV-B irradiation ($H_2O/CH_3CN$ 9:1 (v/v), 1 x $10^{-4}$ M).

Etodolac in these conditions was degraded quickly.

In order to isolate and characterize the photoproducts a concentrated drug solution was irradiated for one hour. $^{1}$H-NMR analysis of the irradiation mixture shows the presence of etodolac and one main photoproduct in ca. 1:1.3 molar ratio. Chromatographic separation led to the isolation of photoproduct **2b**, that was fully characterized by spectroscopic techniques and mass spectrometry. The molecular structure assigned to photoproduct **2b** is reported in Fig. 19.
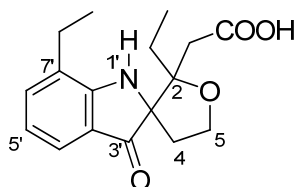
**Figure 19**. Etodolac photoproduct **2b**.

The mass spectrum shows molecular peaks at 304 *m/z* [M+H]$^+$ and 326 *m/z* [M+Na]$^+$, and the peak at 286 *m/z* corresponding to the loss of hydroxyl group (-OH). $^{13}$C-NMR analysis shows the presence of a signal at δ 181.2 due to the ketone function and a signal at δ 60.8 assigned to the spiro carbon. HMBC spectrum evidences correlations of H-4 protons with C-3, C-5 and with the carbonyl carbon. The methylene protons of the acetic acid function, in the HMBC experiment, give heterocorrelation with the C-2 quaternary carbon and the carboxylic carbon, with C-3 spiro carbon and carbonyl carbon C-3'.

Formation of spiro compounds from indoles was previously observed and the related intermediates evidenced (Cermola et al. 2007; Mateo et al. 1996). According to these data, a plausible route for **2b** is reported in Scheme 7. The drug should undergo oxygen attack to C2-C3 bond leading to hydroperoxide **4b**; the latter in aqueous solution should give the corresponding alcohol **3b**, and this, in the presence of a weak acid (all species have a carboxylic group) should rearrange to photoproduct **2b**.
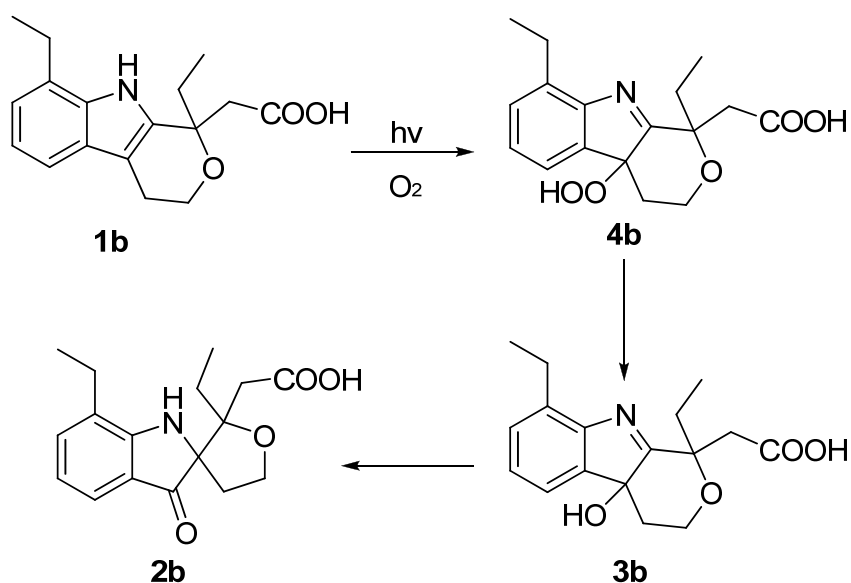


**Scheme 7**. Suggested formation pathway for spiro compound **2b**.

In order to confirm the mechanistic hypothesis and to evidence possible intermediates, irradiations of etodolac in aqueous solution at different times were carried out. ^{1}H-NMR analysis of the irradiation mixture (after 10 min) showed the presence of etodolac, compound **2b** and another photoproduct in ca 1:0.17:0.23 molar ratio, respectively. Analysis by LC-MS of the mixture (after 10 min) exhibited the presence of **1b**, **2b** and another product with peak $[M+H]^+$ at 304 $m/z$ that could be attributable to compound **3b** (Fig. 20). Another peak with $[M+H]^+ = 320$ $m/z$ was also present in very low amounts. Both compounds were not recovered by chromatography due to instability and/or very low amounts.



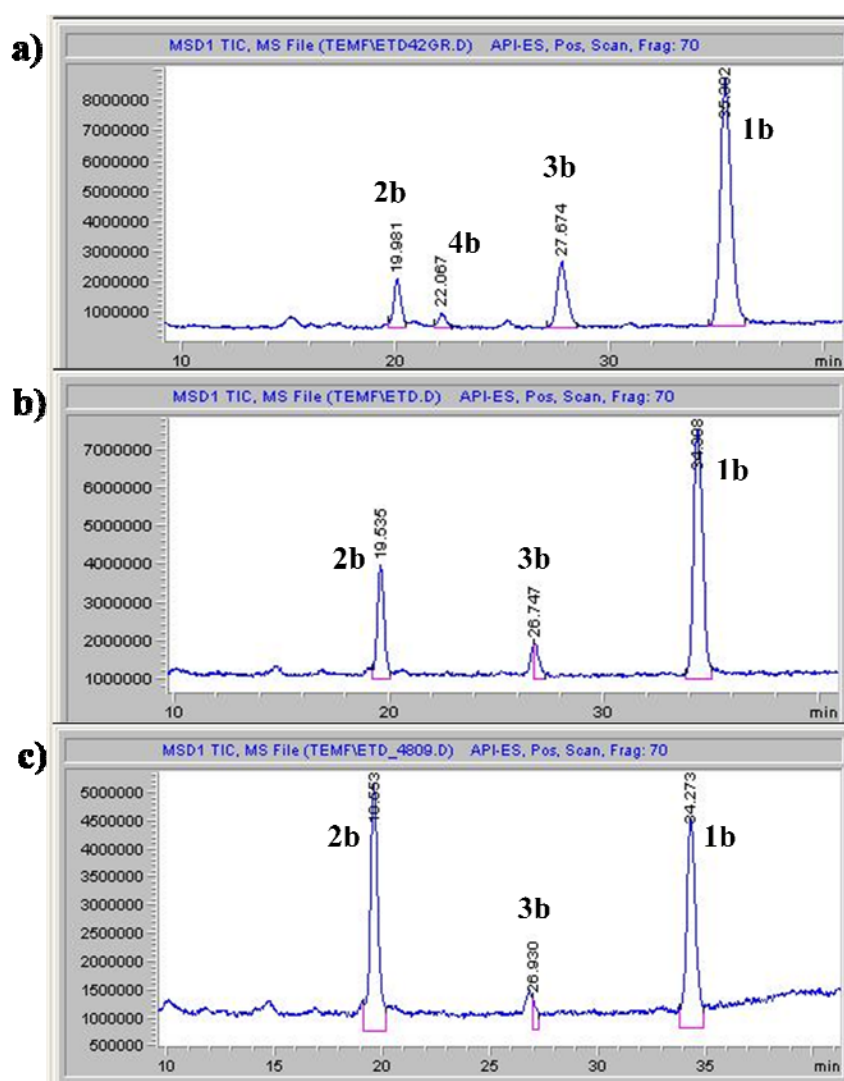**Figure 20**. LC-MS profiles of the irradiation mixture of etodolac in $H_2O/CH_3CN$ (9:1 v/v, 1 x $10^{-3}$ M) after: a) 10 min, b) 20 min, c) 60 min by UV-B irradiation.

The LC-MS analysis at longer irradiation times (20 and 60 minutes) showed the decrease of intermediates **3b** and **4b** and the increase of photoproduct **2b**.

In order to demonstrate that the oxygenated products derive from atmospheric oxygen attack to etodolac and to exclude the involvement of water, irradiation experiments were performed in water/acetonitrile 9:1 (v/v) under argon atmosphere and in aerated solution of drug in acetonitrile. In the first case, the drug was recovered almost unchanged even after one hour. In acetonitrile, HPLC and ^{1}H-NMR analyses of the irradiation mixture showed the presence of the same products as in water/acetonitrile, confirming that water isn't involved in products formation.

Aqueous solution of etodolac ($5 \times 10^{-5}$ M) was exposed to sunlight and analysed at fixed time intervals by HPLC. Under these conditions etodolac was degraded with half-life time around one day. HPLC analysis, as for UV-B irradiation, showed the presence of etodolac **1b**, photoproducts **2b**, and intermediates **3b** and **4b**.

*Conclusion*

The formation of etodolac photoproducts can be explained on the basis of photooxidative processes. According to literature data on indole photoreactivity (Cermola et al. 2007; Iesce et al. 2005), etodolac undergoes oxygen addition to the double bound of the pyrrole ring leading to oxygenated products. These data confirm the tendency of this heterocycle, especially when condensed to an aromatic ring, as in indoles, to generate radical oxygenated species.

## 2.4 CARBAMATE

### 2.4.1 *Rivastigmine*

Rivastigmine (**1c**) is a relatively new drug (Fig. 21). It was introduced in EU in 1998 and in USA in 2000. Rivastigmine hydrogen tartrate is commercialized as Exelon®; it is used for the treatment of mild to moderate Alzheimer's disease in adults and for symptomatic treatment of severe dementia in patients with idiopathic Parkinson's disease (Bar-On et al. 2002). Rivastigmine is a cholinesterase inhibitor of the carbamate type and acts on the central nervous system, due to the presence of carbamate function that is the active site of the molecule (Mustazza et al. 2002; Yao and Li 2008). Rivastigmine is mainly metabolized through the renal system, *via* esterase-mediated hydrolysis of the carbamate moiety. The main metabolite is (*S*)-3-(1-dimethylaminoethyl) phenol (**1c'**) (see Fig. 28), known as NAP 226-90 (Rao et al. 2005).



**1c**
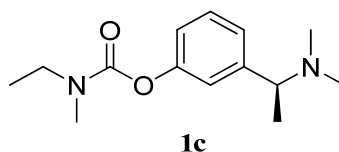
**Figure 21**. Rivastigmine (**1c**, (*S*)-3-[(1-dimethylamino)ethyl]phenyl *N*-ethyl-*N*-methyl carbamate).

Few studies are reported in literature about stability and photostability of the drug. This have been mainly focused on analytical methods for rivastigmine detection (Salem et al. 2010) or determination of optical purity (Wang et al. 2006). A work (Rao et al. 2005) describes the behavior of rivastigmine hydrogen tartrate bulk drug under forced degradation conditions [0.5 N hydrochloric acid, 0.5 N sodium hydroxide, 3% hydrogen peroxide, heat (60 °C), and UV light (254 nm)]. Drug degradation has been observed only under basic conditions yielding, after 48 h, trace amount of human metabolite (*S*)-3-(1-dimethylaminoethyl) phenol.

*Results*

Rivastigmine has a benzylamine and a carbamic function and has a pKa of 8.85. The absorption spectrum of rivastigmine in water shows a band centred at 260 nm with a shoulder at 270 nm and a weak tail extending to λ > 290 nm (Fig. 22).
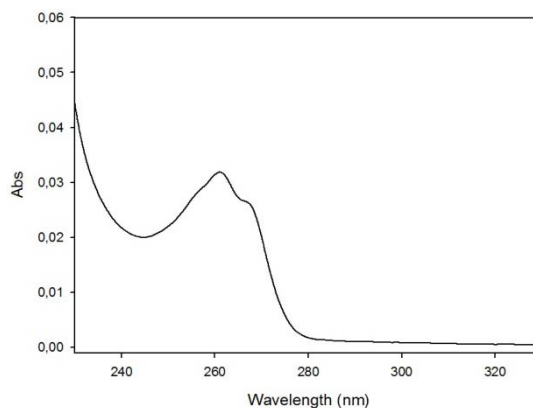
**Figure 22**. Rivastigmine UV-Vis spectrum in water, $5 \times 10^{-5}$M.

Firstly, the drug stability was checked in aqueous solution in the dark. It was stable after 48 h, even when tested in acidic (pH 4) and alkaline (pH 9) solutions. These pH ranges are milder than those previously employed (Rao et al. 2005) and are usually considered environmentally relevant (Valenti et al. 2009).

Kinetic experiments were made irradiating a dilute water solution of rivastigmine ($5 \times 10^{-5}$ M) in a pyrex photoreactor with UV-B light. Under these conditions rivastigmine exhibits a half-life time of 177.5 h and a polychromatic quantum yield of $2.61 \times 10^{-3}$ (Table 4).

|  | Rivastigmine (**1c**) |
|---|---|
| $R$ (M s$^{-1}$) | $(4.91 \pm 0.01) \times 10^{-11}$ |
| $k$ (s$^{-1}$) | $(1.08 \pm 0.02) \times 10^{-6}$ |
| $t_{1/2}$ (h) | 177.5 |
| $\Phi$ | $2.61 \times 10^{-3}$ |

**Table 4**. Photodegradation rate (R), kinetic constant ($k$), half-life time ($t_{1/2}$) and quantum yield ($\Phi$) of **1c** under UV-B irradiation in water ($5 \times 10^{-5}$ M).

A $1 \times 10^{-5}$M solution of the drug in water was exposed to sunlight in quartz tubes in Naples in September–October 2010. HPLC analysis showed that after 12 days rivastigmine decreased by approximately 50% and converted to two photoproducts: ketone **2c** and, in small amount, alcohol **3c** (Fig. 23).
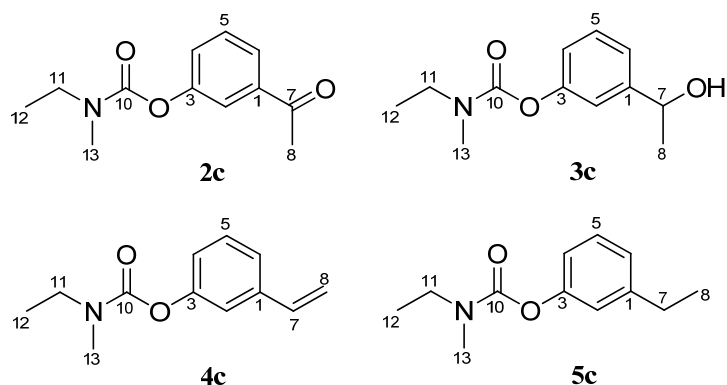
**Figure 23**. Photoproducts formed by rivastigmine irradiation.

Preparative experiments using 1 x 10$^{-3}$ M solutions of the drug by UV-B lamps led to the isolation of products **2c** and **3c** (Fig. 23). In addition, chromatography afforded a fraction consisting of two products in very small amounts that were then identified as alkene **4c** and alkane **5c** (Fig. 23).

For products studies and with the aim of verifying the role of water and oxygen in the drug photodegradation, UV-B irradiation experiments were carried out in different solvents (acetonitrile, methanol, methanol/acetonitrile 9:1 v/v) and in the presence and absence of oxygen. Table 5 reports product distribution after 1 h of irradiation. The product percentages were deduced by $^1$H-NMR by integration of isolated characteristic signals.

| Solvent | Condition | Yield (%) | | | | | |
|---|---|---|---|---|---|---|---|
| | | **1c** | **2c** | **3c** | **4c** | **5c** | **6c** |
| H$_2$O/CH$_3$CN 9:1 (v/v) | In air | 70 | 20 | 10 | Trace | Trace | - |
| | Under argon | 70 | 20 | 10 | Trace | Trace | - |
| CH$_3$CN | In air | < 5 | 95 | - | - | - | - |
| | Under argon | 90 | - | - | 5 | 5 | - |
| CH$_3$OH | In air | < 95 | 5 | - | Trace | Trace | Trace |
| | Under argon | > 95 | - | - | Trace | Trace | < 5 |
| CH$_3$OH/CH$_3$CN 9:1 (v/v) | In air | < 90 | 10 | - | Trace | Trace | - |
| | Under argon | < 80 | - | - | 10 | 10 | Trace |

**Table 5**. Product distribution after 1 h of UV-B irradiation of rivastigmine solutions (1 x 10$^{-3}$ M) under different conditions.

As shown in Table 5, in all solvents ketone derivative **2c** is the main photoproduct, in water even under deareated conditions. Vinyl **4c** and ethyl **5c** derivatives are secondary products. Alcohol derivative **3c** is present only in water while in methanol ether **6c** was found (Fig. 23).
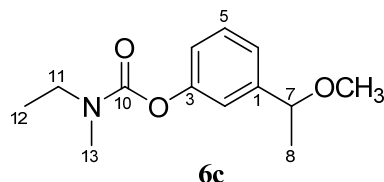


**Figure 23**. Photoproduct formed by rivastigmine irradiation in methanol.

Products **2c**, **3c** and **6c** were fully characterized. Arylalkene **4c** and arylalkane **5c** were recovered as a 1:1 mixture in small amounts, therefore only ^{1}H-NMR data could be obtained and refer to this mixture.

The mass spectrum of photoproduct **2c** shows the presence of the molecular peak at 221 $m/z$ [M]$^{+\bullet}$, a peak at 177 $m/z$ corresponding to the loss of $CH_3CO$ and peaks at 68 and 58 $m/z$ due to amidic fragment and $N$-methyl-$N$-ethyl fragment, respectively. According to the structure, in the ^{1}H-NMR spectrum H-8 methyl protons resonate as a singlet at δ 2.60 and, in the HMBC experiment, give heterocorrelation with the quaternary carbon C-1 and with carbonyl carbon C-7 (Fig. 24). The latter gives a signal, in the ^{13}C-NMR spectrum, at δ 197.2 , characteristic of a conjugated carbonyl group.
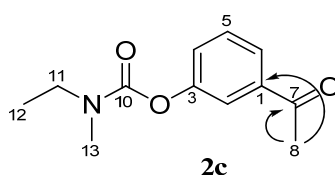


**Figure 24**. Some significant heterocorrelations observed in the HMBC spectrum of **2c**.

Compound **3c** in the EI-MS spectrum has its molecular ion peak at $m/z$ 223 [M]$^{+\bullet}$ and peaks at $m/z$ 86 (due to the fragment [$C_3H_8NCO$]$^+$) and at $m/z$ 58 (due to the [$CH_3CH_2NCH_3$]$^+$ fragment). The ^{1}H-NMR spectrum shows a doublet at δ 1.48 corresponding to H-8 methyl protons and a quartet at δ 4.88 due to H-7 proton. In the HMQC spectrum this proton gives direct heterocorrelation with C-7 carbon at δ 70.0, typical of an alcohol function.

The structure of photoproduct **6c** was confirmed by the presence in the mass spectrum of the molecular peak at 237 *m/z* [M]$^{+\bullet}$ and the peak at 206 *m/z* corresponding to the loss of methoxy group. The singlet at δ 3.23 of OCH$_3$ group in the $^1$H-NMR, and the signals of C-7 carbon at δ 79.3 and of methoxy carbon at δ 56.6 in the $^{13}$C-NMR spectrum are in agreement with the proposed structure of compound **6c**.

In the $^1$H-NMR spectrum of 1:1 mixture of **4c** and **5c**, significant signals of alkene **4c** are the double doublet at δ 6.68 corresponding to H-7 and the two doublets due to H-8 protons. Selected $^1$H-NMR signals for alkane **5c** are the triplet at δ 1.23 and the quadruplet at δ 2.65 corresponding to H-7 and H-8 protons, respectively.

*Mechanistic interpretation*

All products isolated retain the carbamate moiety, while they present a new function instead of -N(Me)$_2$ function (Fig. 23). Hence, despite the presence in the drug of two functions, carbamate and benzylamine, only the latter is involved in the formation of the photoproducts. In particular, the primary photochemical event is the cleavage of the benzyl-nitrogen sigma bond. This breakdown pattern is also observed in the mass spectrum of rivastigmine that exhibits a base peak at *m/z* 206 [M−NMe$_2$]$^+$ (Pommier and Frigola 2003). As reported for various benzylic compounds (Fleming and Pincock 1999; Turro et al. 2010), the photochemical cleavage may occur homolytically and/or heterolytically from the excited state S$_1$. In the case of rivastigmine, a value of 434 kJ mol$^{-1}$ for the transition energy S$_0$→ S$_1$ was estimated from the intersection between normalized emission and excitation spectra (Fig. 25).
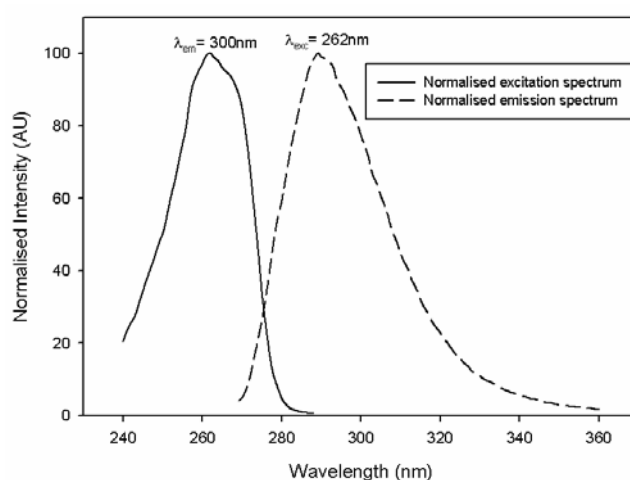


**Figure 25**. Normalized fluorescence spectra (emission and excitation) of rivastigmine aqueous solution at 295 ± 2 K.

A plausible interpretation of the photochemical events from excited **1c** is depicted in Scheme 8.
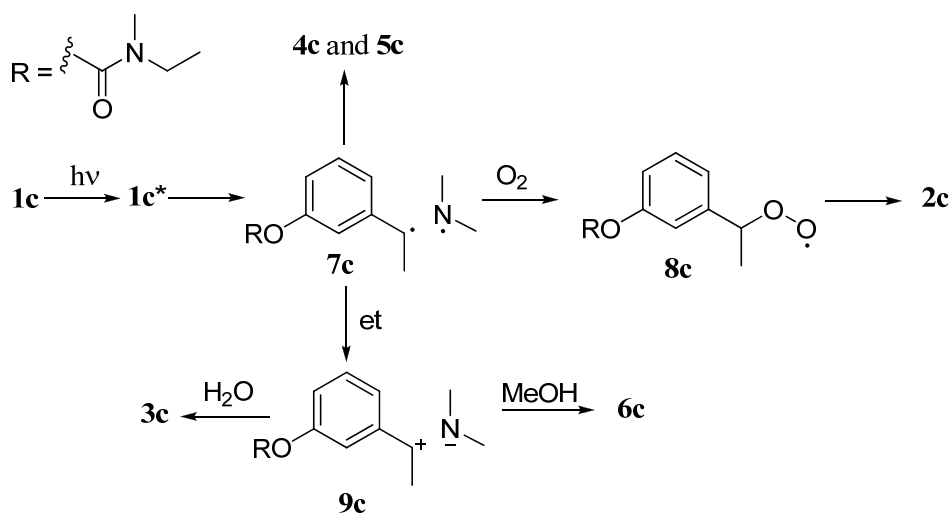


**Scheme 8**. Suggested phototransformation pathways.

If the cleavage occurs homolytically a radical pair **7c** is formed, and by oxygen trapping it leads to ketone **2c** *via* peroxidic species **8c**. As minor route a disproportion occurs affording alkene **4c** and alkane **5c**. Radical pair **7c** can also convert to an ionic pair *via* an electron-transfer with the formation of the well stabilized benzylic cation **9c**. This process is supported by the presence of benzyl alcohol **3c** in aqueous media and benzyl ether **6c** in methanol deriving from the nucleophilic solvent trapping of the positive charged species (Fleming and Pincock 1999). The benzylic carbocation formation could be partly favoured by the presence of the oxygen-substituent in meta position of the aromatic ring. Indeed, in the photochemically excited state, meta-alkoxy groups are known to be particularly efficient in the stabilization of a developing positive charge at a benzylic site (Pincock and Wedge 1994). Under aqueous conditions it is also possible that the drug undergoes a photoionization leading to radical cation **10c** that could decay to **2c** *via* reaction with dioxygen species ($O_2$, $O_2^{\bullet-}$) or, in the absence of oxygen, *via* hydrolysis of iminium ion **11c**, as reported in Scheme 9.
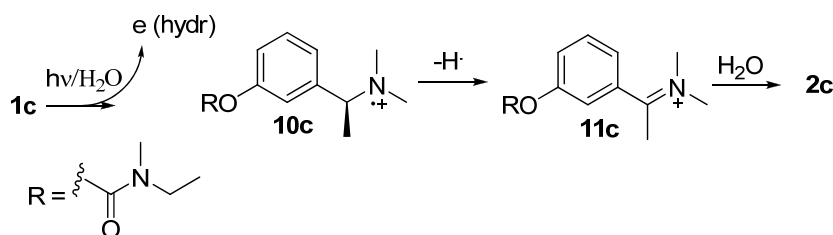


**Scheme 9**. Photoionization of rivastigmine in water.

This hypothesis accounts for the findings of ketone **2c** in deaerated aqueous conditions. It is reported that the photochemical single electron-transfer reaction (SET) of amines can be promoted by ketones (Cohen and Stein 1971; Yoon et al. 2004). In fact, we observed that the photodegradation rate of rivastigmine increased (i) in time as well as ketone **2c** was formed and (ii) in the presence of increasing concentrations of **2c**, suggesting that ketone **2c** itself could act as a photosensitizer. The tendency of the drug to give a radical cation *via* SET-promoted photochemical reaction (Scheme 10) was confirmed using a well-known electron-transfer sensitizer as 9,10-anthraquinone (Galadi and Julliard 1996). Irradiation at 360 nm of a water/acetonitrile solution of rivastigmine in the presence of this compound converted the drug to ketone **2c** within 20 min, while no trace was detected in the blank experiment.
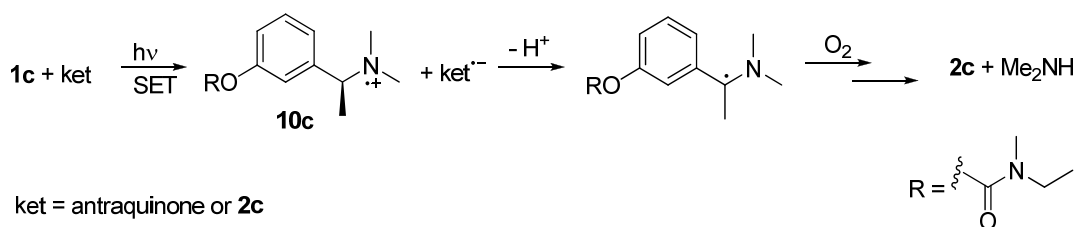


**Scheme 10**. Single electron-transfer (SET) of rivastigmine in the presence of the aromatic ketones.

*Laser flash photolysis (LFP) studies*

In order to support our mechanistic hypotheses transient absorption spectroscopy experiments were performed. Fig. 26 shows the transient absorption spectra upon LFP excitation (266 nm) of rivastigmine (1.66 mM) in pure water and acetonitrile immediately after the laser pulse (0.2 µs) at 295 K in open cuvettes.
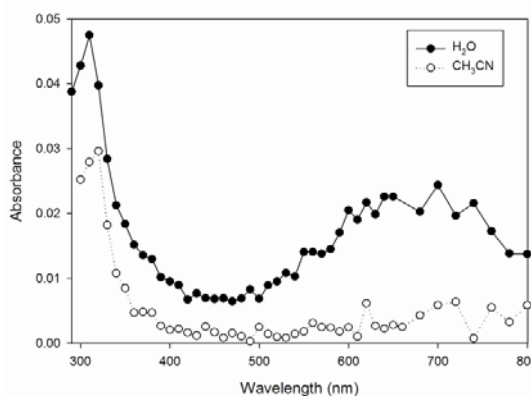


**Figure 26**. Transient absorption spectra obtained after 266 nm excitation of 1.66 mM rivastigmine in water (filled circles) and acetonitrile (empty circles) solutions at pH 6.0 and T = 295 ± 2 K.

For the absorption band centred at 310 nm, present in both cases, a fast decay of a first species (probably due to the triplet state) and formation and consequent decay of a long lived transient were observed. From the trace at 310 nm it is possible to see the parallel decay and growth from two unrelated transients having different rate constants. From the fit of the second species absorption *vs* time decay a correlation between the pseudo-first order decay and the water/acetonitrile percentage was obtained ranging from $(3.24 \pm 0.01) \times 10^5$ (100% water) up to $(6.18 \pm 0.06) \times 10^6$ (100% acetonitrile) (Fig. 27).
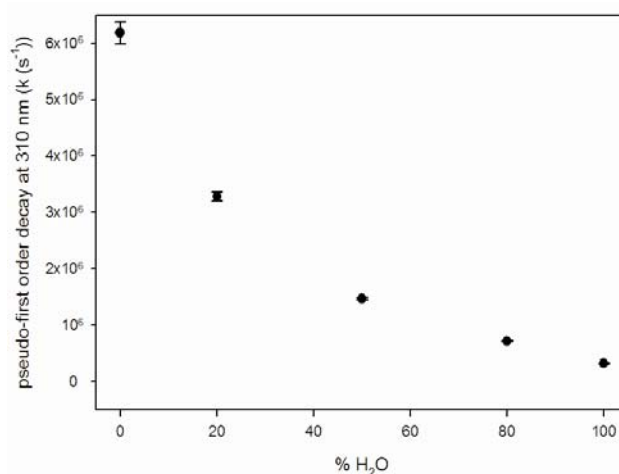


**Figure 27**. Correlation between the pseudo-first order decay of one transient observed at 310 nm and the water/acetonitrile percentage.

The methyl-benzyl radicals typical absorption band is reported in the range 315–320 nm (Claridge and Fischer 1983; Vialaton and Richard 2000). Thus, it is reasonable to attribute this signal to the formation of the resonance-stabilized benzylic radical **7c**. Isolation of typical radical-derived products as alkene **4c** and alkane **5c** supports this assignment. The second absorption band, centred at 700 nm and detected only in water, could be attributed to the presence of the solvated electron (Jou and Freeman 1977). This supports the proposed mechanism reported in Scheme 9 despite the absence of the absorption band of radical cation **10c**. In an attempt to evidence the formation of this intermediate we tried to selectively form it *via* electron transfer from rivastigmine to the triplet excited chloranyl at 355 nm (Johnston and Schepp 1993). Under such conditions it was possible to discern only the band at 450 nm due to the chloranil radical anion, but no transient relative to radical cation **10c** was observed. It is probable that this species is not detectable owing to its low absorption and/or short life-time.

*Phototransformation of 3-(1-dimethylaminoethyl)phenol*

Rivastigmine under irradiation undergoes β-cleavage of the C-N bond. Despite the presence in the drug of two photolabile functions, carbamate and benzylamine, only the latter is directly involved in the formation of the photoproducts. In order to verify the role of the carbamic group on the photoreactivity of rivastigmine, in particular on the β-cleavage of benzylamine moiety, the photochemical behavior of racemic (±)-3-(1-dimethylaminoethyl)phenol (**1c'**) was investigated (Fig. 28). As above reported, the (*S*)-enantiomer is the main human metabolite of rivastigmine (Rao et al. 2005).



**1c'**
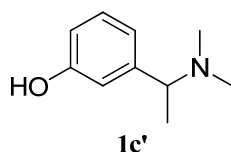
**Figure 28**. Compound **1c'**, (±)-3-(1-dimethylaminoethyl)phenol.

Fig. 29 reports the UV spectrum of **1c'**: this shows an absorption band with maximum centred at 275 nm ($\varepsilon = 4.97 \times 10^3$ L mol$^{-1}$ cm$^{-1}$) with a tail extending to $\lambda > 300$ nm.
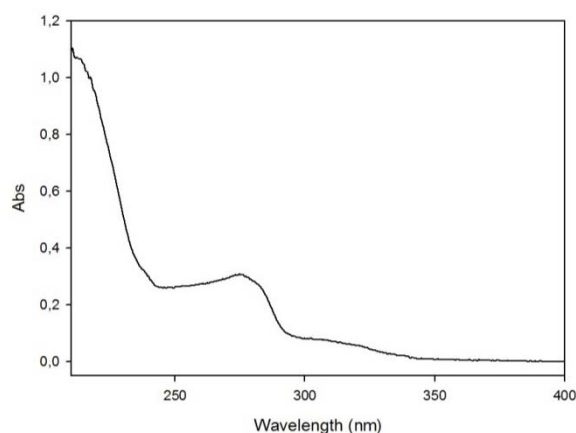


**Figure 29**. UV-Vis spectrum of **1c'** in $H_2O/CH_3CN$ (9:1 v/v), $5 \times 10^{-5}$ M.

Solutions of compound **1c'** in $H_2O/CH_3CN$ 9:1(v/v) at different concentrations (1 x $10^{-3}$ M and $5 \times 10^{-5}$ M) were irradiated in quartz tubes, using UV-B lamps. Under these conditions, the kinetic constants and the half-life times were determined (Table 6). The half-time in concentrated solution is of 173 seconds, much smaller than that calculated for rivastigmine.

|  | 1c' | |
|---|---|---|
|  | $1 \times 10^{-3}$ M | $5 \times 10^{-5}$ M |
| $R$(M s$^{-1}$) | $(2.81 \pm 0.05) \times 10^{-6}$ | $(2.50 \pm 0.03) \times 10^{-6}$ |
| $k$ (s$^{-1}$) | $3.98 \times 10^{-3} \pm 0.04 \times 10^{-4}$ | $(5.96 \pm 0.01) \times 10^{-3}$ |
| t$_{1/2}$ (s) | 173 | 115 |
| Φ | $2.55 \times 10^{-3}$ | |

**Table 6**. Photodegradation rate (R), kinetic constant ($k$), half-life time (t$_{1/2}$) and quantum yield (Φ) of **1c'** determined under UV-B irradiation.

Irradiation of a $1 \times 10^{-3}$ M solution in H$_2$O/CH$_3$CN 9:1(v/v) was carried out by UV-B lamps. After 1 h HPLC and NMR analyses showed that **1c'** was completely degraded and only one photoproduct was formed. To this product that was isolated by chromatography and fully characterized structure **2c'** was assigned (Fig. 30).
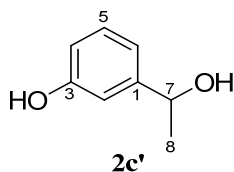


**Figure 30**. Photoproduct **2c'**, 3-(1-hydroxyethyl) phenol.

The $^1$H-NMR spectrum of compound **2c'** shows a quartet at δ 4.74 corresponding to H-7, a doublet at δ 1.41 due to H-8 methyl protons and three signals in the range δ 7.14 - 6.65 corresponding to four aromatic protons. In the $^1$H-NMR spectrum it is significant the absence of signals due to the protons of N(Me)$_2$ group.

Product structure indicates that compound **1c'** undergoes β-cleavage of the benzyl-nitrogen sigma bond as observed for rivastigmine. In particular, the presence of benzyl alcohol **2c'**, as the only photoproduct, suggests that the cleavage leads rapidly to benzylic cation **3c'** (Scheme 11), and this latter undergoes nucleophilic solvent attack by water to give alcohol **2c'**. No traces of other products were evidenced spectroscopically nor by chromatography, even in degassed solutions.
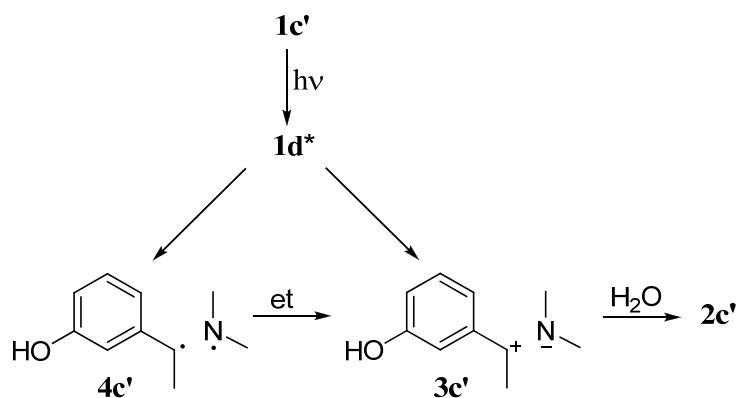
**Scheme 11**. Suggested phototransformation pathway.

*Conclusions*

The photodegradation in water of rivastigmine and phenol **1c'** involves the tertiary amino site with departure of Me$_2$N-group. While rivastigmine affords radical- and, ion-derived products the phenol derivative **1c'** gives only one an ion-derived product, likely due to the higher stabilization of the intermediate ion pair by meta-OH substituent. Indeed, in the photochemically excited state, meta-alkoxy groups are known to be particularly efficient in the stabilization of a developing positive charge at a benzylic site (Pincock and Wedge 1994). The deactivating effect of a carbamate group could account for longer degradation time of rivastigmine than that of phenol **1c'**.

The conversion of rivastigmine that is slow by direct irradiation with UV-B light or sunlight is promoted by ketones or photoelectron-transfer sensitizers such as anthraquinone.

## 2.4.2 *Loratidine*

Loratidine **1d** is an antihistaminic drug used to treat allergies (Fig. 31). Approved by the FDA (Food and Drug Administration) in 1993 it is commercialized by Schering-Plough. Loratidine is a selective inverse agonist of peripheral H$_1$-receptors. It is mainly metabolized through the hepatic system. The main metabolite is desloratidine, deriving from the loss of carbamate moiety. Also desloratidine is a biologically active compound, and is commercialized as antihistaminic drug. Loratidine is excreted unchanged in the urine for 41% and in the feces 43% of drug dose (Ramanathan et al. 2007). It has been recently detected in Spanish river samples in a concentration range of 17.1-3.96 ng/L (Lopez-Serna et al. 2012).

Loratidine has been described as photolabile under UV-C irradiation, but no data have been reported on photoproducts identification (Abounassif et al. 2005).



**1d**
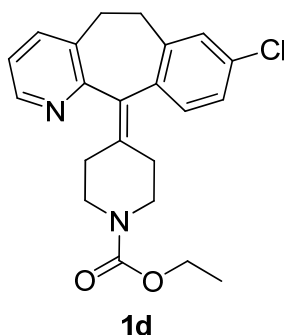
**Figure 31**. Loratidine (**1d**, ethyl 4-(8-chloro-5,6-dihydro-11*H*-benzo[5,6]cyclohepta[1,2 -b]pyridin-11-ylidene)-1-piperidinecarboxylate).

*Results and discussion*

Loratidine has in the molecular structure a tricyclic system, a piperidine ring and a carbamic function. Its UV spectrum shows an absorption band at λ 247 nm with a tail up to 300 nm (Fig. 32).
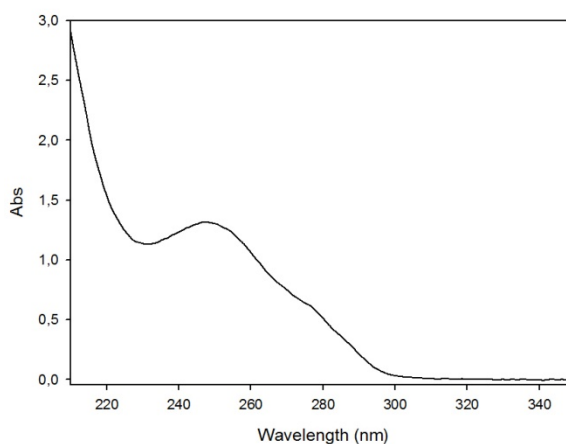


**Figure 32**. Loratidine UV-Vis spectrum in $H_2O/CH_3CN$ 9:1(v/v), 1 x $10^{-4}$ M.

The drug was found to be stable after 48 h in the dark in aqueous solution (1 x $10^{-4}$ M, $H_2O/CH_3CN$ 9:1 v/v) at pH 4, 7 and 9.

Loratidine irradiations were carried out in $H_2O/CH_3CN$ 9:1(v/v) solutions (1 x $10^{-4}$ M) using UV-B lamps as irradiation sources and drug changes were monitored by HPLC at specific time intervals. The kinetic constant and the quantum yield determined under these conditions are reported in Table 7.

|  | Loratidine (**1d**) |
|---|---|
| $R$(M s$^{-1}$) | $(3.18 \pm 0.05) \times 10^{-7}$ |
| $k$ (s$^{-1}$) | $(5.04 \pm 0.07) \times 10^{-3}$ |
| $t_{1/2}$ (s) | 137.4 |
| $\Phi$ | $5.89 \times 10^{-4}$ |

**Table 7.** Photodegradation rate (R), kinetic constant ($k$), half-life time ($t_{1/2}$) and quantum yield ($\Phi$) of loratidine determined under UV-B irradiation ($H_2O/CH_3CN$ 9:1 v/v, $1 \times 10^{-4}$ M).

HPLC analysis of irradiation mixture showed the formation of two photoproducts already after 2 min (Fig. 33).
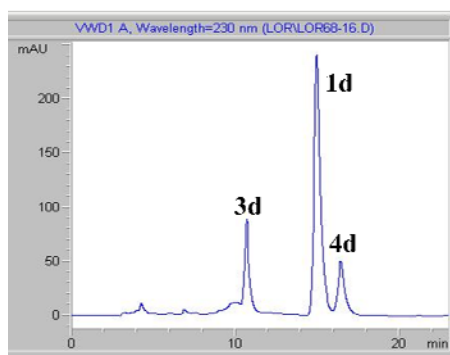


**Figure 33**. HPLC profile of irradiation mixture of loratidine in $H_2O/CH_3CN$ (9:1 v/v, $1 \times 10^{-4}$ M) after 2 min of UV-B irradiation.

The same HPLC profile was observed when a similar solution of loratidine was exposed to sunlight in quartz tubes in Naples in February 2013. As expected degradation was slower and HPLC analysis showed that drug concentration decreased by approximately 50% after 2 days.

In order to isolate and characterize the photoproducts a concentrated drug solution ($1 \times 10^{-3}$ M, $H_2O/CH_3CN$ 75:25 v/v) was irradiated. After 60 min the chromatographic separation of irradiation mixture gave three photoproducts (Fig. 34). Structures **2d**, **3d**, **4d** were deduced by spectroscopic techniques and mass spectrometry.
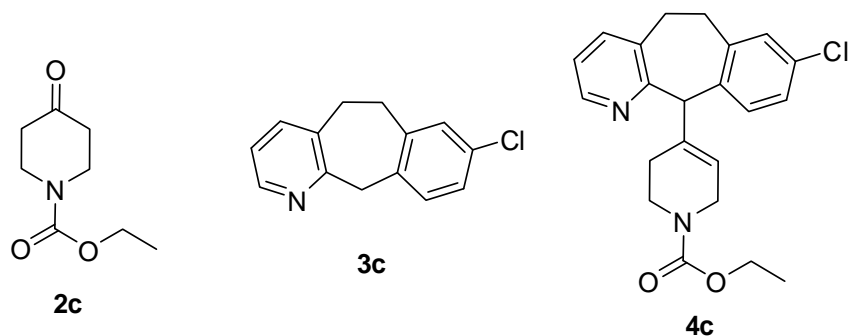
**Figure 34**. Loratidine photoproducts.

Compound **2d** was not observed by HPLC analysis since it is transparent at the selected wavelength (254 nm) of detector. Its presence was observed in GC-MS and ^{1}H-NMR analyses. Fig 35 reports the GC-MS chromatogram of the irradiation mixture after 6 min that evidences the presence of all isolated photoproducts.
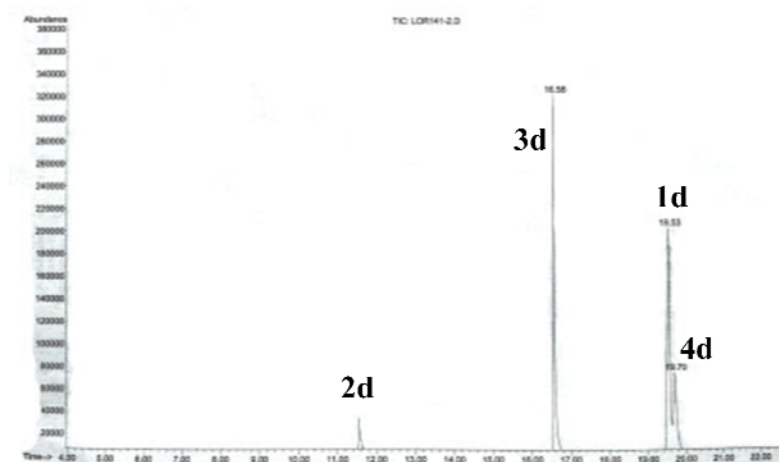


**Figure 35**. GC-MS profile of irradiation mixture of loratidine in  $H_2O/CH_3CN$ (75:25 v/v, 1 x $10^{-3}$ M) after 6 min of UV-B irradiation.

Compound **2d** is commercially available and was identified by its mass spectrum and by comparison of its NMR spectra with those of an authentic sample.

The structure of photoproduct **3d** was confirmed by the presence in the mass spectrum of the molecular peak at 229 *m/z* $[M]^{+\bullet}$ corresponding to the molecular formula $C_{14}H_{12}ClN_2$.^{1}H-NMR spectrum shows the presence of six aromatic protons in δ range 8.38-7.13, of signals at δ 4.56 and at δ 3.20 due to di-benzylic methylene (H-11) and to benzylic methylenes (H-5, H-6), respectively.

The mass spectrum of photoproduct **4d** shows a molecular peak at 382 *m/z* $[M]^{+\bullet}$ corresponding to the molecular formula $C_{22}H_{23}ClN_2O_2$, hence it is a loratidine isomer. The ^{1}H-NMR spectrum shows significant differences only in the aliphatic proton range.

50

In particular, two signals at δ 4.86 and at δ 4.8, due to H-11 and H-3' respectively, are observed. The shift of the double bond produces, in the $^{13}$C-NMR spectrum, the disappearance of the singlet carbon signal at δ 133.3 and the appearance of a doublet carbon signal at δ 121.1.

In order to understand the role of water and oxygen in the photoproducts formation, UV-B irradiation experiments were performed in $CH_3CN$ and in $H_2O/CH_3CN$ under inert atmosphere. When the irradiation was carried out in acetonitrile, compounds **2d** and **3d** were not observed, and only photoproduct **4d** was formed. All photoproducts (**2d-4d**) were instead found in $H_2O/CH_3CN$ 75:25 (v/v) under argon atmosphere.

The formation of compounds **2d** and **3d** was observed only in aqueous solution, hence they probably derive from water attack to the photoexcited loratidine. Photoproduct **4d** was observed under all irradiation conditions. It derives from 1,3-hydrogen shift, probably *via* a radical pair (Scheme 12). The radical recombination can give loratidine or its isomer **4d** (Turro et al. 2010).
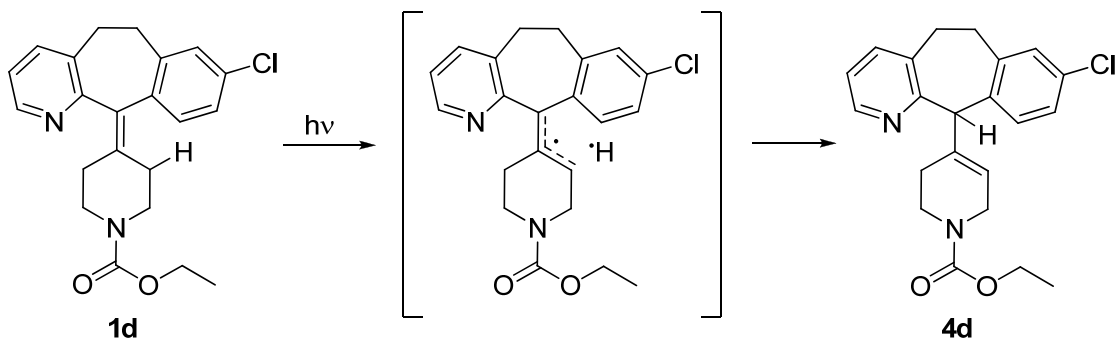


**Scheme 12**. Suggested formation pathway for compound **4d**.

*Conclusion*

Loratidine is rapidly transformed either under UV-B or by sunlight exposure. The reactive site is the double bond while the carbamate moiety is unreactive. It could be interesting to carry out a detailed mechanistic study on photoproducts formation, in particular with the help of techniques able to observe excited states and intermediates, such as the laser flash photolysis, as well as extending to simple model compounds.

### 2.4.3 *Chlorpropham*

Chlorpropham (**1e**) was registered in the United States in 1962 as a pre-emergence and post-emergence herbicide and as a plant growth regulator. It is used as a sprouting inhibitor for ware potatoes and sucker control agent in tobacco (Metcalf 1971; Tomlin 2001). Due to the extensive use it has been found in surface water (Eke 1996) and in groundwater at concentration up to 1.6 µg/L (Mehnert et al. 1995). Residue levels of the herbicide have been found even in the processed potato products (Lentza-Rizos and Balokas 2001). U.S. EPA has assessed the dietary risk posed by chlorpropham and has estimated that the acute dietary exposure must be lower than 2.5 mg/kg/day (US EPA 1996).

Chlorpropham is enough resistant to hydrolysis and oxidation. The photoreactivity of the pesticide is known. In water it gives isopropyl 3-hydroxycarbanilate by replacement of chlorine by a hydroxyl moiety using different irradiation sources (Boule et al. 2002; David et al. 1998; Guzik 1978). Our attention has been focused to kinetics and determination of quantum yield.

*Results*

The UV spectrum of the herbicide, shown in Fig. 36, presents absorption bands with maximum centred at 238 and 279 nm. The molar absorption coefficients were determined: $\varepsilon_{238} = 4.28 \times 10^3 \text{ M}^{-1} \text{ cm}^{-1}$ and $\varepsilon_{279} = 2.10 \times 10^2 \text{ M}^{-1} \text{ cm}^{-1}$.
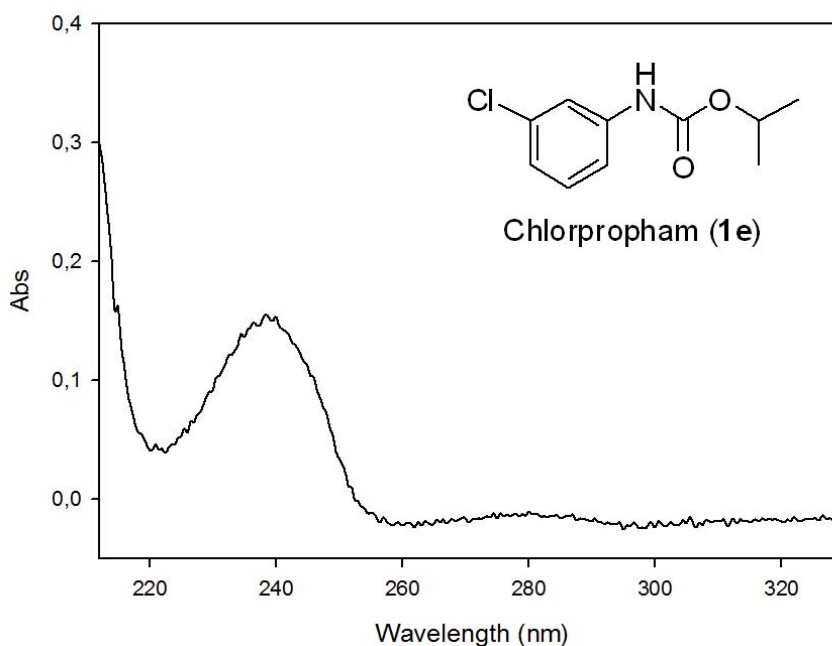


**Figure 36**. Chlorpropham (**1e**, isopropyl 3-chlorophenylcarbamate) and its UV-Vis spectrum in $H_2O/CH_3CN$ (9:1 v/v), $5 \times 10^{-5}$M.

Kinetics experiments were carried out irradiating chlorpropham in quartz tubes with UV-B light in aqueous solution (5 x $10^{-5}$ M, $H_2O/CH_3CN$ 9:1 v/v) and the changes were monitored by HPLC. Table 8 reports the kinetic data and quantum yield.

|  | Chlorpropham (**1e**) |
|---|---|
| $R$ (M s$^{-1}$) | $(1.15 \pm 0.01)$ x $10^{-8}$ |
| $k$ (s$^{-1}$) | $(2.95 \pm 0.18)$ x $10^{-4}$ |
| $t_{1/2}$ (s) | $2.34$ x $10^{3}$ |
| $t_{1/2}$ (min) | 39.0 |
| $\Phi$ | $4.89$ x $10^{-4}$ |

**Table 8.** Photodegradation rate (R), kinetic constant ($k$), half-life time ($t_{1/2}$) and quantum yield ($\Phi$) of **1e** under UV-B irradiation (5 x $10^{-5}$ M, $H_2O/CH_3CN$ 9:1 v/v).

HPLC analysis of the irradiation mixture evidenced the disappearance of the pesticide together with the formation of one detectable photoproduct that was identified as the dechlorinated **2e** by comparison of its retention time with that of a sample obtained by preparative experiments (Fig. 37).
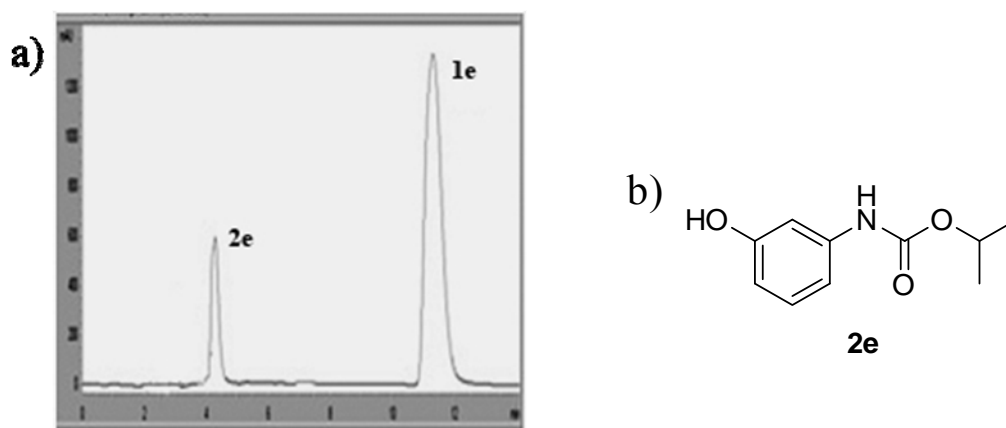


**Figure 37**. a) HPLC profile of irradiation mixture of chlorpropham(**1e**) in $H_2O/CH_3CN$ (9:1 v/v, 5 x $10^{-5}$ M) after 15 min of UV-B. b) Photoproduct **2e**.

Chlorpropham solution (5 x $10^{-5}$ M) in $H_2O/CH_3CN$ (99:1 v/v) was also exposed to sunlight in closed quartz tubes in July-August 2012 in Naples and was analysed by HPLC after 10, 30 and 60 days. As expected, degradation of the herbicide by sunlight was slower than by UVB lamps. After 60 days, careful analysis (by HPLC and $^1$H-NMR) of the mixture showed the presence of chlorpropham and of photoproduct **2e**.

In order to isolate the photoproduct a concentrated herbicide solution, (1 x 10$^{-3}$ M) in H$_2$O/CH$_3$CN 9:1 (v/v), was irradiated by UV-B lamps for one hour. Chromatography of the irradiation mixture led to isolation of unreacted chlorpropham **1e**, hydroxycarbanilate **2e** (Guzik 1978) and another product, in very small amounts, to which structure **3e** was assigned by spectroscopic means (Scheme 13). In particular, its mass spectrum shows the absence of isotopic chlorine peaks and a peak at 236 *m/z* indicating the presence of another nitrogen. Moreover in the proton spectrum a typical singlet at δ 2.16 associated to a methyl linked to a carbonyl group and the heterocorrelation, in the HMBC spectrum, between these methyl protons and a quaternary low-field signal at δ 163.6 indicate the substitution of chlorine with -NHCOCH$_3$.
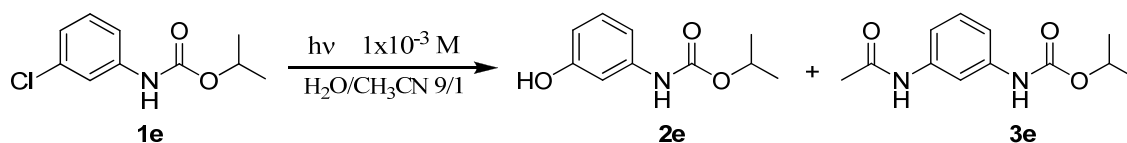


**Scheme 13**. Irradiation of chlorpropham (1 x 10$^{-3}$ M) in H$_2$O/CH$_3$CN 9:1 by UV-B.

Formation of acetamides has been sometime observed in the irradiation of halocompounds in aqueous acetonitrile and is known as photo-Ritter reaction (Bi et al. 2010). Hence, to better understand the formation pathway of photoproduct **3e**, and to verify the role of acetonitrile in chlorpropham photodegradation UV-B irradiation experiments were carried out using different amounts of acetonitrile. Table 9 reports the products distribution after 1 h irradiation; products percentages were deduced by ^{1}H-NMR by integration of characteristic signals.

| Solvent | Yield (%) | | |
|---|---|---|---|
| | **1e** | **2e** | **3e** |
| H$_2$O/CH$_3$CN 99:1 (v/v) | - | 100 | - |
| H$_2$O/CH$_3$CN 9:1 (v/v) | 10 | 83 | 7 |
| H$_2$O/CH$_3$CN 1:1 (v/v) | 61 | 29 | 10 |
| CH$_3$CN | 94 | - | 6 |

**Table 9**. Product distribution after 1 h of UV-B irradiation of chlorpropham (1 x 10$^{-3}$ M) in different solutions.

The results (Table 9) evidence the determinant role of acetonitrile in the formation of acetamide **3e**. According to photo-Ritter reaction, increasing acetonitrile increases product **3e** yield and when irradiation was carried out using 100% of acetonitrile only **3e** was formed.

Furthermore the photostability of the major photoproduct **2e** was also tested. A solution of **2e** in $H_2O/CH_3CN$ (9:1 v/v, 1 x $10^{-3}$ M) was irradiated in quartz tubes with UV-B lamps and analysed by HPLC and $^1$H-NMR at selected times. After 4h analyses showed no degradation.

*Mechanistic interpretation*

Formation of phenol **2e** from chlorpropham is due to a nucleophilic photosubstitution of the chlorine with water, one of the most frequent photoreaction of halogenated aromatic compounds in aqueous solvents (Boule et al. 2002; Schutt and Bunce 2004). As reported in literature, this nucleophilic photosubstitution takes place through a $S_{NR}+Ar^*$ mechanism and the first step of the reaction is the formation of radical cation **4e** by photoionization (Schutt and Bunce 2004). This process is favoured by aqueous medium. Indeed, increasing the water content in the reaction medium the phototransformation rate increases (Table 9). Radical cation **4e** may undergo a nucleophilic attack from water yielding phenol **2e**. Trapping of the radical cation by acetonitrile and subsequent hydrolysis gives acetamide **3e** (Scheme 14) according to photo-Ritter reaction (Bi et al. 2010).
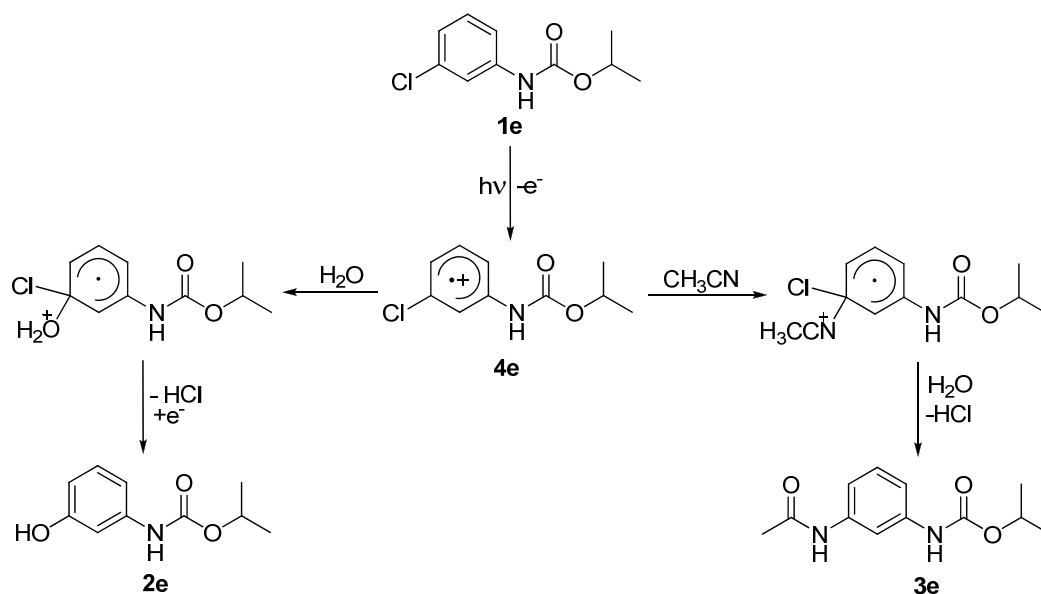


**Scheme 14**. Phototransformation mechanisms of chlorpropham.

The carbamic function in compound **1e** as well as in **2e** is photostable, and doesn't undergo photocleavage under UV-B irradiation. As expected, chlorpropham in water undergoes photosolvolysis leading to the formation of dechlorinated phenol **2e** *via* a radical cation intermediate. Moreover, when acetonitrile is used in the reaction medium acetamide **3e** is also formed and derives from the nucleophilic trapping of the radical cation (**4e**) by acetonitrile.

## 2.4.4 *Phenisopham*

Phenisopham (**1f**) is a pesticide currently in use in Europe. It is a selective contact herbicide, absorbed by the foliage, it is a member of the carbamate pesticides family. Phenisopham is generally used in combination with other herbicides, in particular it is used in post-emergence control of broad-leaved weeds in cotton (Griveau et al. 2009). Stability and photolysis of phenisopham has not been investigated so far.

*Results*

The phenisopham UV spectrum shows an absorption band centred at 234 nm ($\varepsilon_{234}$ = 3.53 x $10^3$ $M^{-1}$ $cm^{-1}$) and a band at 273 nm ($\varepsilon_{273}$ = 1.64 x $10^2$ $M^{-1}$ $cm^{-1}$) (Fig. 38). Although weak, the lowest energy band extends up to $\lambda$ > 290 nm in the ultraviolet range of solar radiation indicating that the pesticide can absorb solar light.
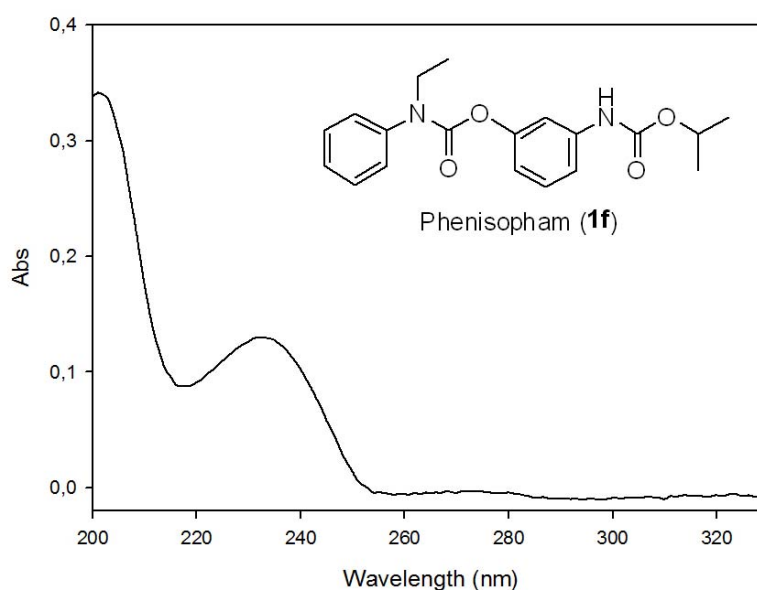


**Figure 38**. Phenisopham (**1f**, 3-[[(1-methylethoxy)carbonyl]amino]phenyl *N*-ethyl-*N*-phenylcarbamate) and its UV-Vis spectrum in $H_2O/CH_3CN$ (9:1), 5 x $10^{-5}$M.

Phenisopham is slightly soluble in water, then acetonitrile was chosen as co-solvent to obtain clear solutions. Control experiments in aqueous solution in the dark evidenced that it was recovered unchanged after 48 h, even when tested in acidic (pH 4) and alkaline (pH 9) solutions.

The kinetic data (Table 10) were determined irradiating a herbicide solution  (5 x $10^{-5}$ M, $H_2O/CH_3CN$ 9:1 v/v) in quartz tubes by UV-B light.

| | Phenisopham (**1f**) |
|---|---|
| $R$ (M s$^{-1}$) | $(1.16 \pm 0.01)$ x $10^{-8}$ |
| $k$ (s$^{-1}$) | $(2.11 \pm 0.01)$ x $10^{-4}$ |
| $t_{1/2}$ (s) | 3.30 x $10^3$ |
| $t_{1/2}$ (min) | 55.0 |
| $\Phi$ | 3.94 x $10^{-4}$ |

**Table 10.** Photodegradation rate (R), kinetic constant ($k$), half-life time ($t_{1/2}$) and quantum yield ($\Phi$) of **1f** under UV-B irradiation (5 x $10^{-5}$ M, $H_2O/CH_3CN$ 9:1 v/v).

HPLC analysis of the irradiation mixture after 30 min evidenced the presence of five peaks in addition to that of starting **1f** (Fig. 39). They were assigned to phenol **2f** and amides **4f-6f** by comparing their retention times with those of samples that were isolated by preparative experiments and fully characterized (Fig. 40). Identification of aniline **3f** was made comparing its HPLC retention time with that of a commercially available standard compound.
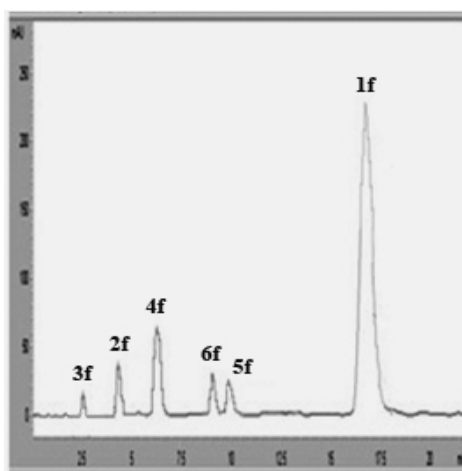


**Figure 39**. HPLC profile of irradiation mixture of phenisopham (**1f**) in $H_2O/CH_3CN$ (9:1 v/v, 5 x $10^{-5}$ M) after 30 min of UV-B.

To have environmental information about photodegradation of phenisopham, herbicide solutions (5 x $10^{-5}$ M) in $H_2O/CH_3CN$ (99:1 v/v) were exposed to sunlight in closed quartz tubes in July-August 2012 in Naples and were analysed by HPLC after 10, 30 and 60 days. Careful HPLC and $^1$H-NMR analyses showed the slow degradation of the herbicide and the formation of its photoproducts, in small amounts.

Preparative experiments (1 x $10^{-3}$ M solution; water-acetonitrile 7:3, v/v) were carried out using UV-B lamps. A conversion of 35% was obtained after 2 h of irradiation. Repeated chromatographies gave unreacted herbicide and four photoproducts, *o*-hydroxybenzamides **4f** and **5f**, *p*-hydroxybenzamide **6f** and phenol **2f**. Due to its small amounts aniline **3f** was not isolated (Fig. 40). It was identified in the crude irradiation mixture by comparison of the HPLC retention time and by characteristic $^1$H-NMR signals with those of an authentic sample.
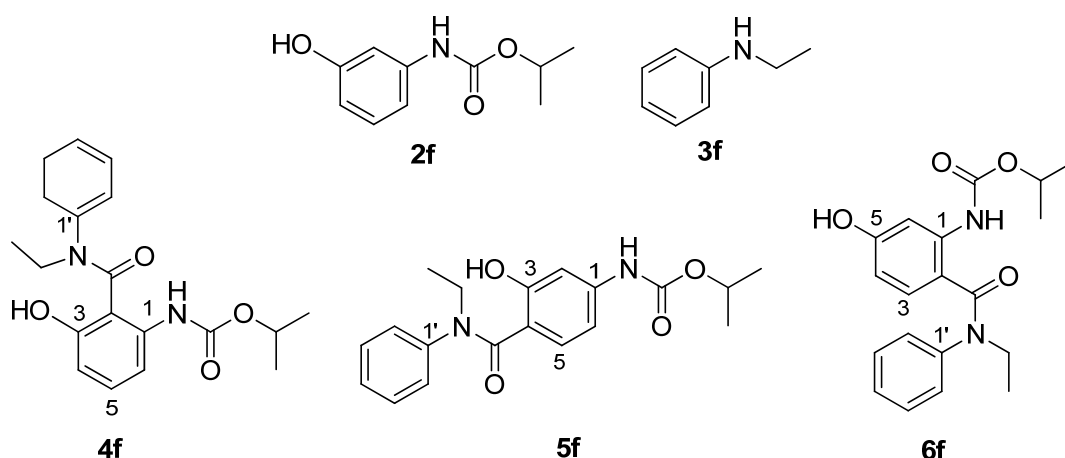


**Figure 40**. Photoproducts formed by phenisopham irradiation in aqueous solution.

Photoproduct **2f** was also found in the irradiation of chlorpropham, and is known (Guzik 1978). The other photoproducts (**4f**, **5f** and **6f**) were new.

The mass spectrum of **4f** shows the molecular peak at 342 *m/z* [M]$^{+\bullet}$ corresponding to the molecular formula $C_{19}H_{22}N_2O_4$, confirming that **4f** is an isomer of parent compound **1f**. In the IR spectrum two bands are present at 3562 cm$^{-1}$ and 3418 cm$^{-1}$ due to O-H and N-H bond stretchings. $^1$H-NMR shows a doublet at δ 6.50 corresponding to H-4 proton, in orto to hydroxyl group, that couples, in the $^1$H-$^1$H COSY experiment, with H-5 proton at δ 7.07. In the HMBC experiment, the isopropyl protons at δ 4.96 give heterocorrelation with the carbamate carbon at δ 154.6 and the methylene protons give

heterocorrelations with the amidic carbon at δ 168.0 and quaternary carbon C-1' at δ 141.1 (Fig. 41).
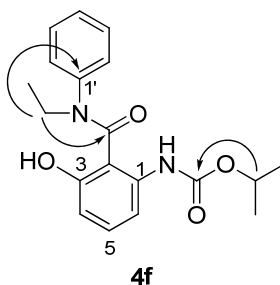


**Figure 41**. Some significant heterocorrelations observed in the HMBC spectrum of **4f**.

The structure of compound **5f** was confirmed by the presence in the mass spectrum of the molecular peak at 342 *m/z* [M]$^{+\bullet}$, and by spectroscopic analysis. In the IR spectrum two bands are present at 3628 cm$^{-1}$ and 3424 cm$^{-1}$ corresponding to O-H and N-H bond stretchings. $^1$H-NMR shows two doublets at δ 7.10 and 6.54 corresponding to H-6 and H-5 protons, respectively. H-2 proton gives a signal at δ 6.86  typical of a proton in orto to hydroxyl group. In the $^{13}$C-NMR spectrum the signal of the amidic carbon is at δ 170.7; this carbon, in the HMBC experiment, gives heterocorrelation with H-5 proton and with methylene protons at δ 3.93.

As compounds **4f** and **5f**, compound **6f** in the EI-MS spectrum has the molecular peak at *m/z* 342 [M]$^{+\bullet}$ and in the IR spectrum shows the presence of NH and OH (3583 cm$^{-1}$, 3300 cm$^{-1}$). In the $^1$H-NMR a double doublet at δ 6.09  due to H-4, in $^1$H-$^1$H COSY experiment, is coupled with H-3 proton at δ 6.74  and with H-6 proton at δ 7.78. In the HMBC experiment the isopropyl signal (CH) is coupled with the carbamate carbon at δ 153.7. Moreover, the HMBC spectrum shows heterocorrelations of H-3 proton with the amidic carbon at δ 170.4  and with quaternary carbons C-1 and C-5 at δ 140.9 and δ 156.9, respectively. Another heterocorrelation is observed between methylene protons with amidic carbon, with C-1' at δ 143.9 and with CH$_3$ of the ethyl group at δ 13.4 (Fig. 42).



**6f**
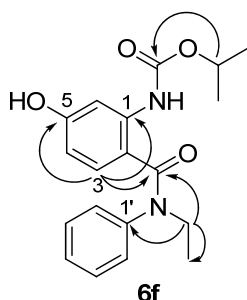
**Figure 42**. Some significant heterocorrelations observed in the HMBC spectrum of **6f**.

The photostability of compound **2f** (= **2e**) was already checked (see above). Solutions of **4f**, **5f** and **6f** in $H_2O/CH_3CN$ (8:2 v/v, $2 \times 10^{-4}$ M) were irradiated in open quartz tubes with UV-B lamps and analysed by ¹H-NMR. After 4 h no degradation for each compound was observed. Similar treatment for **3f** caused a complete degradation in a mixture of unidentified products.

*Mechanistic interpretation*

The main degradation product of phenisopham is *o*-hydroxybenzamide **4f**. Compounds **5f** and **6f** were found in similar amount, phenol **2f** and aniline **3f** were detected in low amounts. Analysis of products structures indicates that, as for chlorpropham, the *N*-aryl-*O*-alkyl carbamate function is unreactive. Instead the *N*-aryl-*O*-aryl carbamate group undergoes photoinduced O-CO bond cleavage leading to a radical pair. According to photo-Fries mechanism (Miranda and Galindo 2004; Turro et al. 2010), in-cage recombination in *ortho*- and/or *para*-position affords products **4f**, **5f** and **6f**, while the radical escape leads to the fragmentation products **2f** and **3f** (Scheme 15).
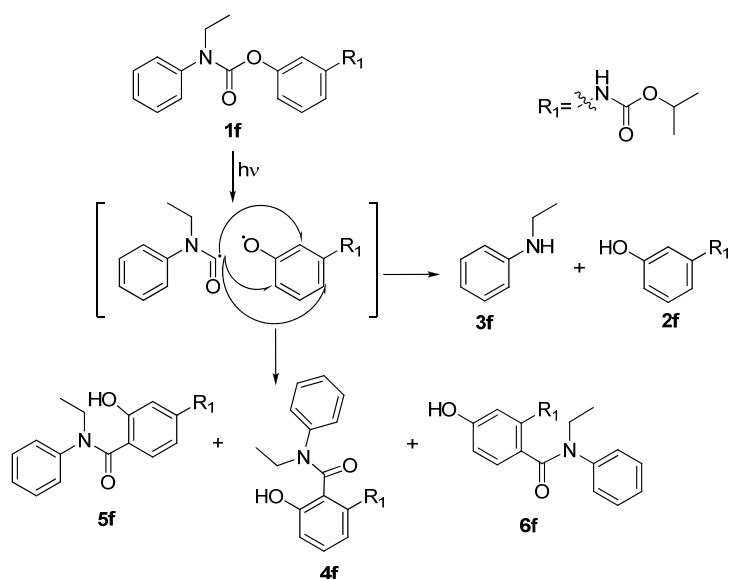


**Scheme 14**. Phototransformation mechanism of phenisopham.

*Conclusions*

Phenisopham undergoes photocleavage of the *N*-aryl-*O*-aryl carbamate bond. A radical mechanism occurs that leads via a photo-Fries rearrangement to the formation of hydroxybenzamides (**4f-6f**) and fragmentation products (**2f** and **3f**). The *N*-aryl-*O*-alkyl carbamate bond appears photostable even in amides **4f-6f**.

## 2.4.5 *Model carbamic compounds*

The data from irradiation of rivastigmine, chlorpropham and phenisopham indicate that the *N*-alkyl-*O*-aryl and *N*-aryl-*O*-alkyl carbamate moieties are photostable, while the photoinduced cleavage of a carbamic bond was observed only in phenisopham, for the diaryl substituted carbamate function.

In an attempt to understand the role of the substituents on nitrogen and oxygen of the carbamic group, model *N*-aryl-*O*-aryl substituted carbamates were synthesized and their photochemical behavior examined. Model compounds **1g-l** (Fig. 43) can be discerned by the presence and the different position of chlorine on the *N*-aryl group (function present in chlorpropham) and by the different substitution on nitrogen (function present in phenisopham).



| 1 | $R^1$ | $R^2$ | $R^3$ |
|---|---|---|---|
| **g** | H | Cl | H |
| **h** | Et | Cl | H |
| **i** | H | H | Cl |
| **j** | Et | H | Cl |
| **k** | H | H | H |
| **l** | Et | H | H |
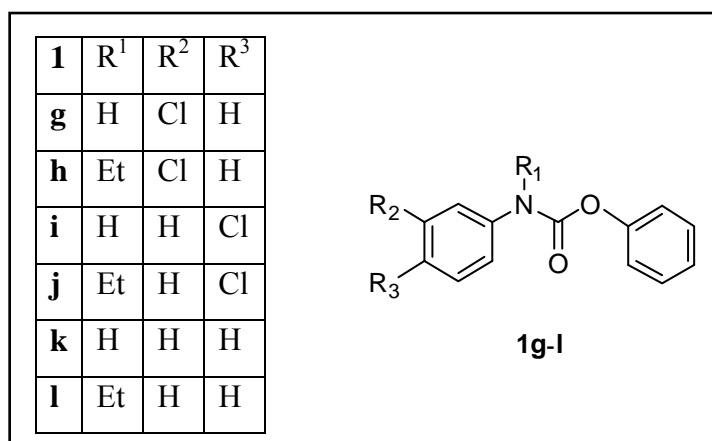
**Figure 43**. Model carbamic compounds **1g-l**.

*Synthesis*

Model compounds **1g-1l** were prepared in high yields by classical methods *via* reaction of phenyl chloroformate with the corresponding aniline (Scheme 15).
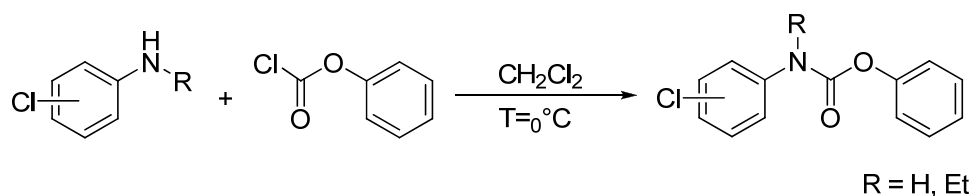


**Scheme 15**. Synthesis of model carbamic compounds **1g-l**.

In Fig. 44 the UV spectra of compounds **1g** and **1h** are reported. The *N*-monosubstituted carbamate **1g** has stronger absorption bands around 240 nm than the *N*-ethyl **1h**.
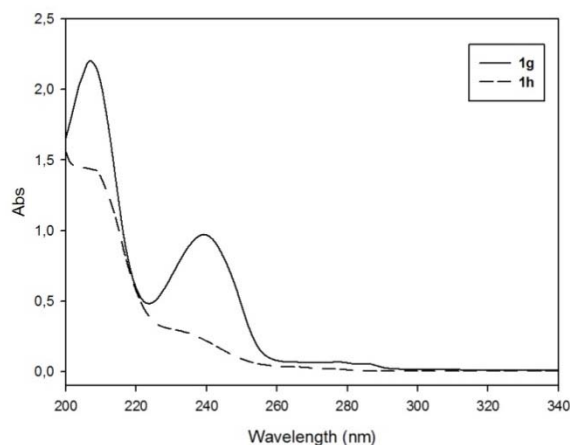
**Figure 44**. UV-Vis spectra of **1g** and **1h** in $H_2O/CH_3CN$ (1:1 v/v), 5 x $10^{-5}$M.

Similar trends are observed in the UV spectra for the other model compounds, in particular, *N*-ethyl derivatives **1g,i,k** show weaker absorptions, even in 280-300 nm range, than compounds **1h,j,l** (Fig. 45).
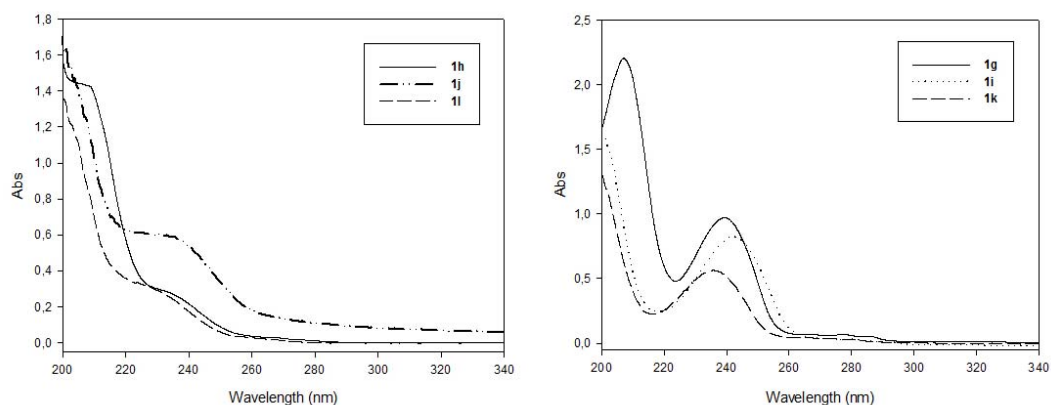


**Figure 45**. UV-Vis spectra of compound **1g-l** in $H_2O/CH_3CN$ (1:1 v/v), 5 x $10^{-5}$M.

*Irradiation experiments*

The photochemical behavior of the model compounds was investigated using UV-B lamps as light sources. The aqueous solutions used contained up to 50% of acetonitrile due to the low solubility of these compounds. Concentrated solutions (1 x $10^{-3}$ M) were necessary for isolating photoproducts. Irradiation was followed mainly by HPLC and in some cases also by TLC and NMR. Different irradiation times were used considering a conversion of ca. 20-40% of starting compound. The percentages of products were deduced by NMR spectra and confirmed by preparative TLC. Known products were identified by comparing spectral data with those reported and/or with those of authentic samples. Unknown compounds were spectroscopically characterized.

The irradiation of compounds **1g** and **1h** led to formation of phenols **2g,h** and acetamides **3g,h**. *N*-ethyl derivative **1h** required longer irradiation time (22% conversion after 14 h) than **1g** (30% after 2 h) (Scheme 16).
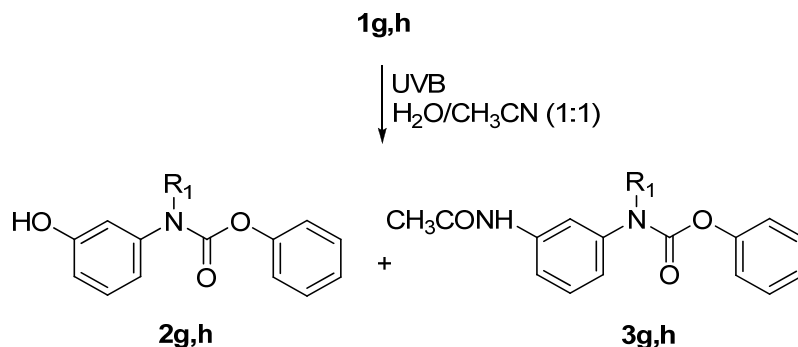


**Scheme 16**. Irradiation of compound **1g** ($R_1$=H): 2 h; **1g** (71%), **2g** (14%) and **3g** (15%). Irradiation of compound **1h** ($R_1$=Et): 14 h, **1h** (78%), **2h** (10%) and **3h** (12%).

Compounds **1g,h** behave exactly as chlorpropham. It was observed that, in the irradiation of **1g**, a decrease of acetonitrile amount from 50% to 30% led to a decreased amount of product **3g** (from 15 to 5%), and accelerated the conversion (30% after only 1 h). Compound **2g** was identified by comparison of its NMR spectrum with that reported in literature (Akita et al. 2005).

Compound **2h** in the EI-MS spectrum has its molecular ion peak at *m/z* 257 [M]$^{+\bullet}$ and a peak at *m/z* 164 due to loss of phenol fragment [M-C$_6$H$_4$OH]$^+$. $^1$H-NMR shows seven patterns of signals with almost identical chemical shifts in comparison with those of parent compound **1h**, except the chemical shifts of H-6 ($\delta$ 6.73 ), H-4 ($\delta$ 6.86 ) and H-2 ($\delta$ 6.78) protons that absorb at lower field, due to shielding effect of the hydroxyl group.

The mass spectrum of compound **3h** shows the absence of isotopic chlorine peaks and a peak at 298 *m/z* indicating the presence of another nitrogen. Moreover, in the proton spectrum a typical singlet at $\delta$ 2.12 associated to a methyl linked to a carbonyl group and in the $^{13}$C-NMR a quaternary low-field signal at $\delta$ 168.3 confirmed the substitution of chlorine with an acetamidic function (-NHCOCH$_3$).

In the irradiation of *p*-chloroderivative **1i** compounds **2i** and **3i** were recovered in small amounts, while compound **8i** was the main photoproduct; polymeric material was also recovered by chromatography (ca. 33%) (Scheme 17). Spectroscopic data of **8i** matched those of **1k**. Compounds **2i** and **3i** was identified by comparison of their proton NMR spectra with those of authentic samples. Conversion of *N*-ethyl derivative **1j** was slow.

After 10 h only 29% of **1j** was converted and the sole product identified was acetamide **3j** (Scheme 17).
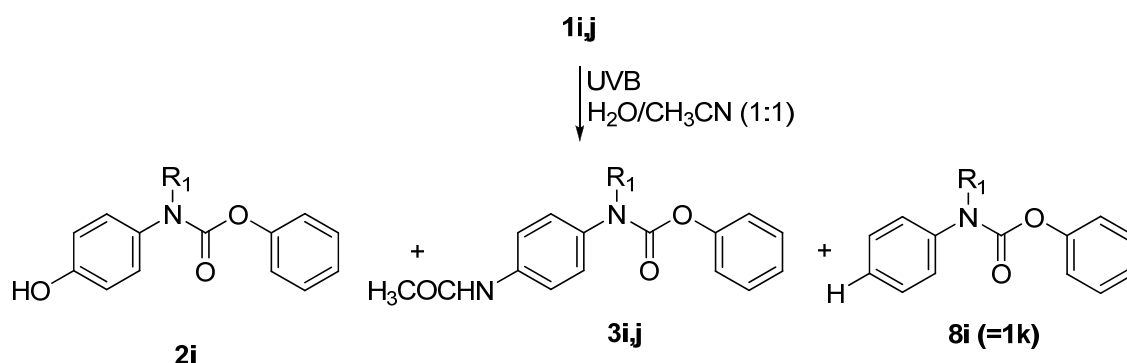


**Scheme 17**. Irradiation of compound **1i** (R[1]=H): 2 h; **1i** (10%), **2i** (8%), **3i** (15%) and **8i** (34%). Irradiation of compound **1j** (R[1]=Et): 10 h, **1j** (71%), **3j** (29%).

Structure of compound **3j** was assigned by its spectroscopic features. In particular, mass spectrum showed the absence of isotopic chlorine peaks and a peak at 298 *m/z* indicating the presence of another nitrogen. In the $^1$H-NMR spectrum there is a typical singlet at δ 2.16 associated to a methyl linked to a carbonyl group and the heterocorrelation, in the HMBC spectrum, between these methyl protons and a quaternary low-field signal at δ 172.2 indicates that chlorine was substituted by -NHCOCH$_3$ group.

Compounds **1k** and **1l** exhibited high photostability, **1k** even more than **1l**. Indeed, after 42 h of irradiation *N*-ethyl derivative **1l** was converted for 24% while **1k** for ca 5%. Separation of the irradiation mixture of **1l** led to products **4l** and **6l** in small amounts and to hydroxybenzoic acid **9** (Scheme 18).
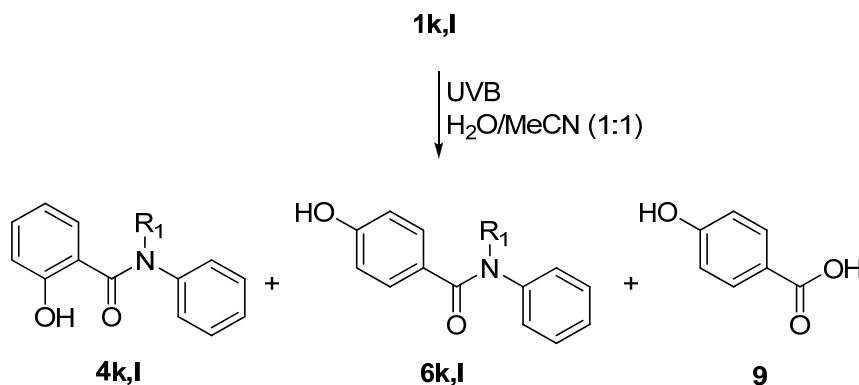


**Scheme 18**. Irradiation of compound **1k** (R[1]=H): 42 h; **1k** (>95%), **4k** (trace), **6k** (trace) and **9** (trace). Irradiation of compound **1l** (R[1]=Et): 42 h, **1l** (75%), **4l** (trace), **6l** (6%) and **9** (18%).

Careful NMR analysis showed that similar products were also present in chromatographic fractions from irradiation of **1k** (Scheme 17). Compounds **4k** and **6k** were identified by comparison of their proton NMR spectra with those reported in literature (Ma et al. 2012). Compounds **4l**, **6l**, and 4-hydroxybenzoic acid (**9**) were identified by comparison of their proton NMR spectra with those of authentic samples. Compounds **1k,l** were found more photostable than phenisopham although they gave similar photo-Fries products. The structural difference between compounds **1k,l** and the pesticide is the presence on the *O*-aryl group of an *N*-substituent. Hence, to verify the role of a similar substituent model compound **1m** was synthesized *via* reaction of phenylisocyanate with 3-hydroxyacetanilide (**7m**) (Scheme 19).
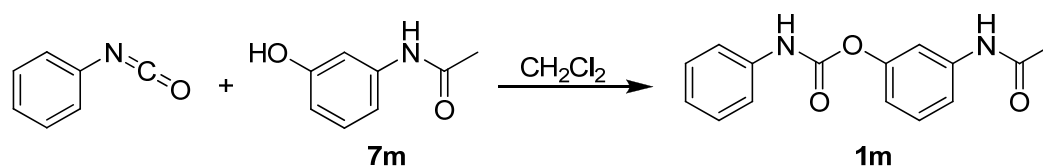


**Scheme 19**. Synthesis of model carbamic compound **1m**.

Fig. 46 reports the UV spectrum of model compound **1m**, it shows a strong absorption band around 240 nm.
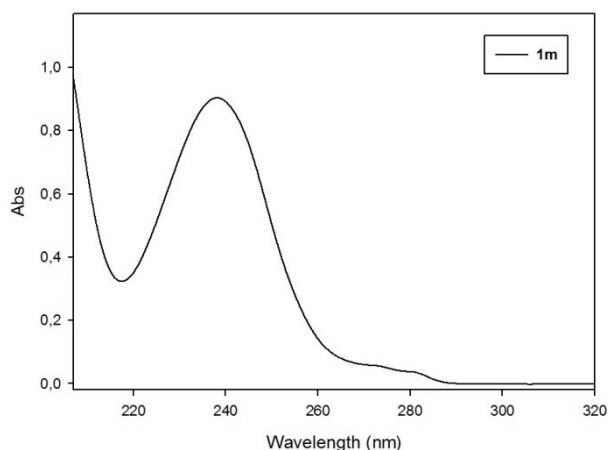


**Figure 46**. UV-Vis spectrum of **1m** in $H_2O/CH_3CN$ (1:1 v/v), 5 x $10^{-5}$M.

Conversion of **1m** was faster than **1k**. Indeed, after 42 h of irradiation, compound **1m** was transformed for ca 17 % (**1k** only ca 5%). Separation of the irradiation mixture led to isolation, in small amounts, of products **6m**, **7m**, and a mixture of **4m** and **5m** (Scheme 20).
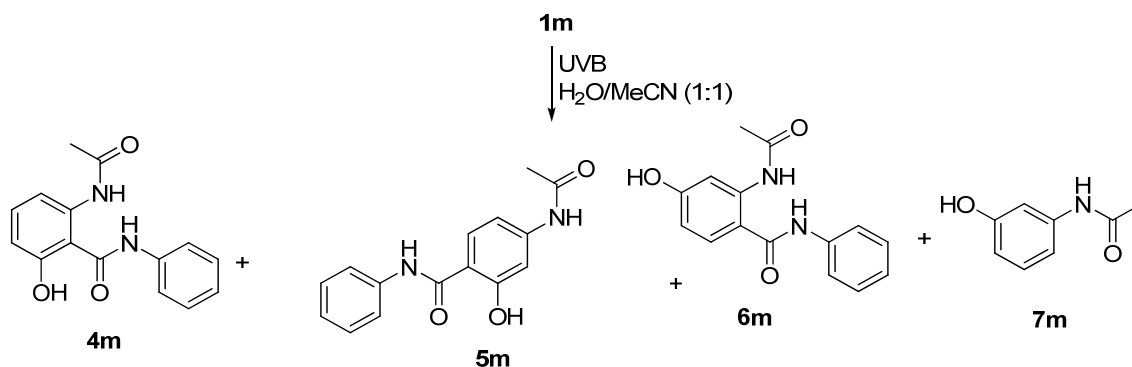
**Scheme 20**. Irradiation of compound **1m**: 42 h; **1m** (83%), **4m** (4%), **5m** (5%), **6m** (3%) and **7m** (5%).

*Mechanistic interpretation*

The results indicate that diaryl substitution on the carbamate function does not entail the bond breakage. Indeed, products by photoinduced carbamate cleavage are observed only in carbamates **1k**, **1l** and **1m**.

A summary of the reactions observed for the different compounds with a suggested description of the products routes is shown in Scheme 21.
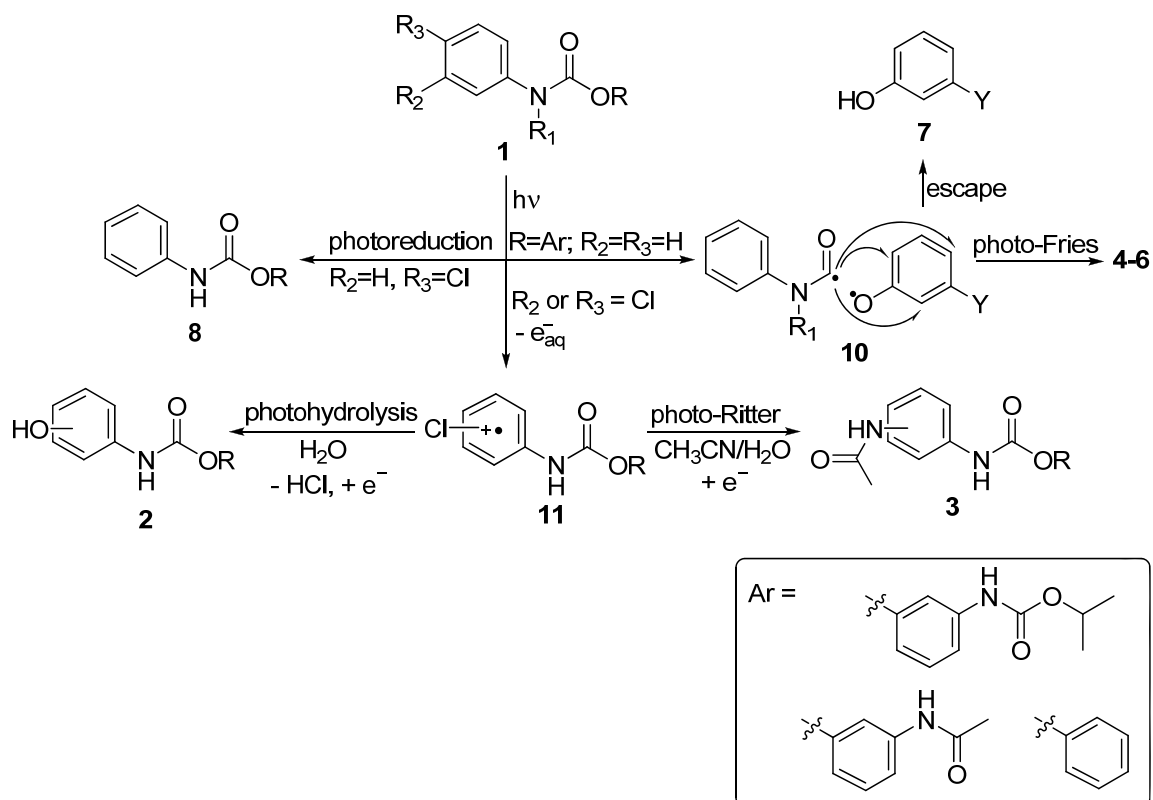


**Scheme 21**. Photodegradation pathways of carbamic compounds.

For compounds **1k**, **1l** and **1m** a photo-Fries rearrangement takes place. As reported in literature (Miranda and Galindo 2004; Turro et al. 2010), the rearrangement occurs through homolytic cleavage of the carbonyl-heteroatom single bond to give a caged radical pair **10**. In-cage recombination in *ortho-* and/or *para-*position affords the amides **4**, **5** and **6**, while radicals escape out of the cage leads to phenols and anilines (fragmentation products). Stabilization of radicals by substitution could account for the breakage less difficult in *N*-ethyl compound **1l** than **1k**. In the irradiation mixtures from **1g,h** *p*-hydroxybenzoic acid **9** is likely formed by hydrolysis of **6g,h** due to the long water contact for the prolonged irradiation (Scheme 21). In halogenated products **1g-j** the photoinduced carbamate cleavage is not observed. For these compounds the main photochemical event is the nucleophilic photosubstitution of chlorine with water yielding phenols **2**. Trapping of the radical cation intermediates by acetonitrile and subsequent hydrolysis gives products **3** *via* a photo-Ritter reaction. The presence of the substituent on the halogenated ring should play a determinant role since the $S_{NR}+Ar^*$ mechanism is favored in highly electron-rich aromatic molecules with low ionization potential (Turro et al. 2010). Photohydrolysis is the most frequent photoreaction of halogenated aromatic compounds in aqueous solvents and depends on the halogen position on the aromatic ring (Boule 1999; Schutt and Bunce 2004). Indeed, this reaction competes with photoreduction for *p*-chloroderivative **1i** that gives principally dehalogenated compound **8i**, as observed in similar cases (Soumillion and De Wolf 1981). *N*-ethyl derivatives **1h,j** degrade more slowly than the corresponding unsubstituted **1g,i** probably due to the different intensities of UV absorptions (Fig. 45). Indeed, *N*-ethyl compounds **1h,j** show weaker absorptions, even in the 280-300 nm range, than compounds **1g,i**.

In the dehalogenated derivatives the *N*-ethyl substitution has an opposite effect on degradation rate. This behavior could be explained on the basis of the different mechanism that involves carbamate cleavage. **1m** undergoes carbamate cleavage more quickly than **1k**, probably due to the presence of an activating $NH-CO-CH_3$ function on the *O*-aryl ring.


*Conclusion*

Investigation on model compounds evidences that the carbamate function is hardly photoreactive and that the *N*-aryl *O*-aryl substitution is not a sufficient condition to have a breaking of the carbamate bond. This breaking is completely overcome in the presence

of a chlorine on the aromatic ring. In the latter case substitution of halogen with nucleophilic solvents occurs. The presence of electron-donor substituents on the *O*-aromatic ring weakly favours the carbamate photocleavage.

*N*-substitution of the carbamate function does not affect the product formation but influences the degradation rate in different ways for the two classes of carbamate models due to radical stabilization or to a minor absorption of UV-B radiation.

# 3.0 INDIRECT PHOTOLYSIS

In the environment the direct phototransformation processes of xenobiotics may be overcome in the presence of other species that can compete in sunlight absorption and/or favour indirect photolysis processes. Indirect photolysis is an important degradation pathway for xenobiotics that don't exhibit significant absorption of sunlight ($\geq$ 290 nm) or are slowly degraded by direct photolysis.

In the environment indirect photolysis can be induced by naturally occurring compounds such as inorganic ions (nitrate and nitrite), transition metals (iron) and chromophoric dissolved organic matter (CDOM), for example humic substances. Under sun radiation these substances generate radical or oxidizing species such as molecular oxygen in a singlet electronic state ($^1O_2$), photoexcited organic matter ($^1CDOM^*$ and/or $^3CDOM^*$) and radical species such as $NO_2^{\bullet}$, halide ($Cl_2^{\bullet-}$, $Br_2^{\bullet-}$), carbonate ($CO_3^{\bullet-}$), hydroxyl ($HO^{\bullet}$) and peroxy ($RO^{\bullet}$, $ROO^{\bullet}$) (Leifer 1988; OECD 2000; Vaughan and Blough 1998; Vione et al. 2005). Chromophoric dissolved organic matter (CDOM), after excitation, may lead to the transformation of an organic pollutant (P) as well as to the formation of a variety of reactive species such as alkyl peroxy radicals and hydroxyl radical. Singlet oxygen may also be formed by excited CDOM (CDOM*) through energy transfer to ground-state oxygen ($^3O_2$) (Scheme 22) (Lam et al. 2003).
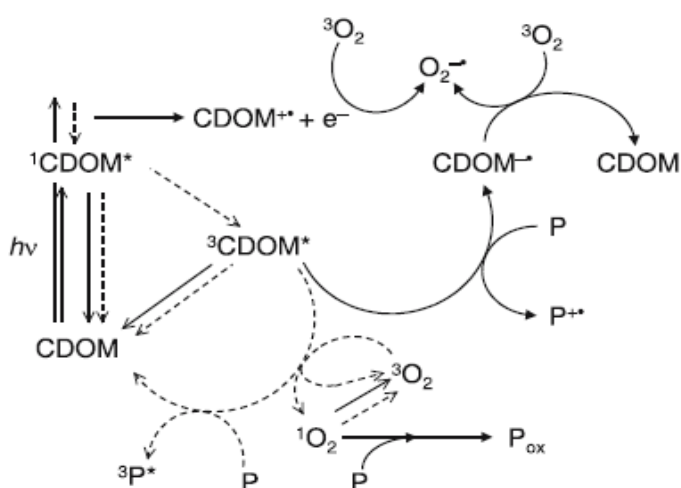


**Scheme 22**. Photoreactivity of CDOM.

It is well established that hydroxyl radical plays a significant role in the phototransformation of organic compounds in natural waters. $HO^{\bullet}$ is a strong and not selective oxidant (standard reduction potential of 1.8 V) and reacts with wide variety of

organic and inorganic compounds with a second-order rate constant nearly to diffusion-controlled rates ($> 10^9$ $M^{-1}$ $s^{-1}$) (Buxton et al. 1988). Hydroxyl radical is mainly reactive with electron-rich aromatic organic compounds due to its electrophilicity. It reacts with organic pollutants by electrophilic addition to a double bond, preferentially to the aromatic ring. Hydroxyl radical also reacts by H-abstraction from a carbon atom *via* a not selective reaction. In order to predict the environmental fate of pollutants it is therefore very important to know their reactivity toward photogenerated HO$^\bullet$.

Regarding the photochemical sources in the environment, nitrate ions are usually present in natural waters and their photolysis is a relevant source of hydroxyl radical in this medium. Under sunlight irradiation nitrate ions decompose to yield hydroxyl radicals (R2), nitrogen dioxide (R1), atomic oxygen at ground state and nitrite (R3). Nitrogen dioxide produces nitrate and nitrite, but it can also interact with organic compounds inducing nitration and nitrosation processes.
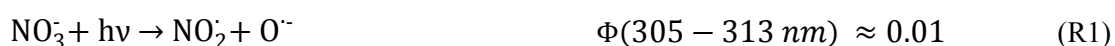
$$NO_3^- + h\nu \rightarrow NO_2^- + O^{\bullet-} \qquad\qquad \Phi(305-313\ nm) \approx 0.01 \qquad (R1)$$

$$O^{\bullet-} + H^+ \rightleftarrows HO^\bullet \qquad\qquad pK_a = 11.9 \qquad (R2)$$

$$NO_3^- + h\nu \rightarrow NO_2^- + O \qquad\qquad \Phi(305\ nm) \approx 0.001 \qquad (R3)$$

Nitrite is usually present in the environment at a lower concentration than nitrate (μM levels), but its higher molar absorptivity and photolysis quantum yield can make it an important HO$^\bullet$ environmental source. The excitation of nitrite ions by sunlight leads mainly to the formation of hydroxyl radical and NO$^\bullet$ according to the following reactions:

$$NO_2^- + h\nu \rightarrow NO^\bullet + O^{\bullet-} \qquad\qquad \Phi(355\ nm) = 0.025 \qquad (R4)$$

$$O^{\bullet-} + H^+ \rightleftarrows HO^\bullet \qquad\qquad pK_a = 11.9 \qquad (R5)$$

Nitrite ions have an intense absorption band in the visible spectrum around 355 nm (Fig. 47) and their photolysis is highly influenced by the irradiation wavelength. Indeed, the quantum yield of the process varies from about 0.07 near 300 nm to 0.025 at 355 nm and down to 0.015 at 371 nm. Differently from nitrate, nitrite is a source but also a sink

for the hydroxyl radical with a second order rate constant of $1.0 \times 10^{10}$ M$^{-1}$ s$^{-1}$ yielding nitrogen dioxide radical (NO$_2^\bullet$) (Vione et al. 2005).
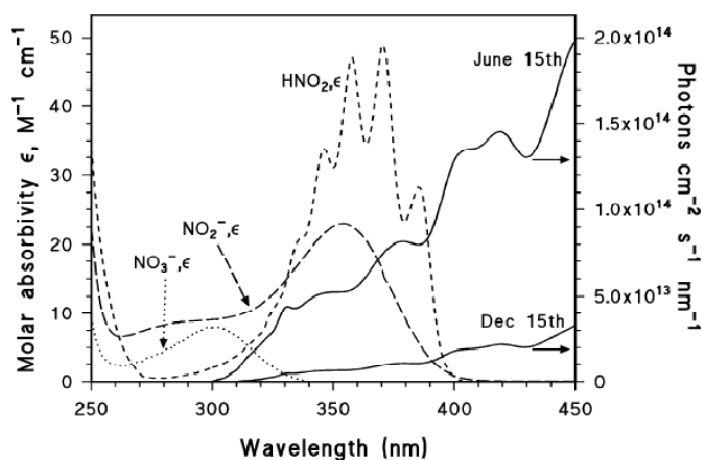


**Figure 47**. UV absorption spectra in molar absorptivity ε of nitrate, nitrite and nitrous acid. Spectral solar photon irradiance in Central Europe (15th June, 15th December) (Vione et al. 2005).

Another reactive species present in natural water is carbonate radical anion (CO$_3^{\bullet-}$), that is generated from the reaction of HO$^\bullet$ with carbonate or bicarbonate ions. Carbonate radicals may react with electron-rich compounds such as anilines and phenols and sulfur compounds. It has been reported that carbonate radicals are involved in the degradation of some sulfurated pesticides such as fenthion and thioanisole (Huang and Mabury 2000; Larson and Zepp 1988).

In this chapter we report the results concerning the indirect photolysis of two xenobiotics: rivastigmine (Riv, **1c**) and nicotine (Nic, **1n**). These studies were carried out in Clermont-Ferrand (France) in collaboration with the *Institut de Chimie de Clermont Ferrand (ICCF)* of the University Blaise Pascal. In particular, the formation rate (R$_{HO\bullet}^f$) of hydroxyl radical from irradiation of synthetic waters using different HO$^\bullet$ sources (*i.e.* H$_2$O$_2$, NO$_3^-$, NO$_2^-$) was determined. The transformation of xenobiotics was correlated with the hydroxyl radical formation and the second order rate constants between hydroxyl radical and xenobiotics ($k_{X, HO\bullet}$) were estimated. Moreover, three different kinds of natural waters (lake, river, rain) were collected, characterized and the R$_{HO\bullet}^f$ was measured. Subsequently, irradiations of rivastigmine, in these natural waters, were performed. The determination of second order rate constant for the reaction of a xenobiotic with HO$^\bullet$ is important to better understand and predict the environmental fate

71

of xenobiotics, moreover $k_{X, HO^\bullet}$ may be used to predict the oxidation rate of xenobiotic during treatments of polluted waters such as advanced oxidation processes (AOP's). Rivastigmine was chosen because its direct photolysis was previously investigated. Moreover, information about its behavior under indirect photolysis give a better insight into its environmental fate. Nicotine was chosen in collaboration with the research group of the *ICCF*. It is a biological active pollutant and it was often found in the environment (Valcárcel et al. 2011). Recently, the nicotine reactivity under simulated oxidation treatment, for example with hypochlorite, ozone and hydrogen peroxide was investigated (Bezares-Cruz et al. 2007; Nienow et al. 2009; Rodriguez et al. 2011; Sleiman et al. 2010; Zarrelli et al. 2012). To the best of our knowledge no study on nicotine photodegradation in water under environmental-like conditions is reported.

## 3.1 IRRADIATION EXPERIMENTS

Irradiations were carried out using a solar simulator in a thermostated cylindrical reactor (T = 15 ± 2°C), in order to limit thermal reactions. The reactor was located at one focal point of the lamp and was equipped on the top with a pyrex filter removing the wavelengths lower than ~285 nm. The emission spectrum of the Xenon lamp reaching the reactor surface was calculated to be 4.31 x $10^{19}$ photons cm$^{-2}$ s$^{-1}$ over the wavelength range 290-400 nm.

The aqueous solutions were prepared by mixing different concentrations of hydrogen peroxide (188μM, 376μM, 550μM 752μM), or nitrates (200μM, 400μM, 5mM) or nitrites (5.4μM, 10μM, 50μM, 100μM) to a constant concentration of xenobiotics (ranging from 25 to 45 μM). In order to follow the pollutant transformation, an aliquote of the solution was withdrawn at fixed interval times and analysed by UV-Vis spectroscopy and/or by HPLC techniques.

## 3.2 DETERMINATION OF THE REACTION RATES

The initial degradation rate of xenobiotics was determined monitoring the concentration evolution changing during irradiation. The time evolution of xenobiotics in the presence of photochemical sources of HO$^\bullet$ could be fitted with a pseudo-first order equation $C_0 = C_t e^{-kt}$ where $C_0$ was the initial xenobiotic concentration, $C_t$ the concentration at time $t$ and $k$ the pseudo-first order degradation rate constant. Concentration data were

plotted versus time and fitted using a linear equation. The initial degradation rate of xenobiotics is equal to the negative of the slope of the straight line. The error bands associated to the rate data represent 3σ, derived from the scattering of the experimental data around the fitting curves (intra-series variability).

The variation of xenobiotics concentration during irradiation was monitored by HPLC-UV.

## 3.3 DETECTION OF HYDROXYL RADICALS

Hydroxyl radical formation rate $R_{HO\bullet}^{f}$ (M s$^{-1}$) from irradiation of synthetic waters under solar simulated radiation was determined. Synthetic waters were made using, as HO$^{\bullet}$ sources, $H_2O_2$, $NO_3^{-}$ and $NO_2^{-}$ at different concentrations.

The hydroxyl radical formation rate ($R_{HO\bullet}^{f}$) was determined by using terephthalic acid (TA) as trapping molecule (Charbouillot et al. 2011). TA reacts with hydroxyl radical leading to the formation of 2-hydroxyterephthalic acid (TAOH), the yield ($Y_{TAOH}$) of reaction depends on the pH and temperature of the aqueous medium. At fixed temperature of 15°C the $Y_{TAOH}$ depends only on the pH:

$$Y_{TAOH} = (0.0248 \pm 0.0059)pH + (0.046 \pm 0.035) \qquad \text{(Eq. 11)}$$

The formation rate of TAOH ($R_{TAOH}^{f}$) depends on $Y_{TAOH}$ and on $R_{HO\bullet}^{f}$, according to the following relationship:

$$R_{TAOH}^{f} = \frac{Y_{TAOH}\, R_{HO\bullet}^{f}\, k_{TA,\,HO\bullet}[TA]}{k_{TA,\,HO\bullet}[TA] + k_{S,\,HO\bullet}[S]} \qquad \text{(Eq. 12)}$$

where S is the hydroxyl radical source, $k_{TA,\,HO\bullet}$ and $k_{S,\,HO\bullet}$ are the reaction rate constant of HO$^{\bullet}$ with TA and S, respectively. [TA] and [S] are the molar concentration of TA and S. Using high concentration of TA it is possible to hypothesize that all photogenerated HO$^{\bullet}$ are trapped by TA, and in this case $k_{S,\,HO\bullet}[S]$ may be neglected. The simplified equation is:

$$R_{TAOH}^{f} = Y_{TAOH}\, R_{HO\bullet}^{f} \qquad \text{(Eq. 13)}$$

73

From Eq.12 it is possible obtain the hydroxyl radical formation rate ($R_{HO^\bullet}^f$):

$$R_{HO^\bullet}^f = \frac{R_{TAOH}^f}{Y_{TAOH}}$$

(Eq. 14)

This method represents a simple and fast detection of photogenerated HO$^\bullet$ with a high sensitivity that allows us to detect down to 10 nM of HO$^\bullet$. The formation of TAOH was monitored by fluorescence (Scheme 23). An aliquot of irradiation solution was withdrawn and analysed by fluorescence at fixed intervals times. TAOH was quantified by using a calibration curve previously performed by using standard solution of TAOH. The initial formation rate of TAOH was determined reporting in a plot TAOH concentration *vs* time and fitting the data by linear regression. The slope of straight line is $R_{TAOH}^f$. The concentration of TA used during all experiments is between 500 μM and 1 mM in order to trap all photogenerated HO$^\bullet$.
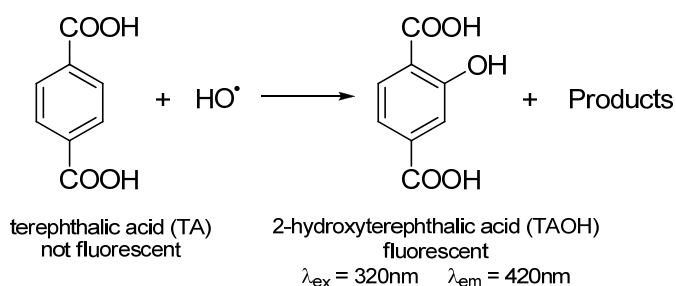


**Scheme 23**. TA reaction with hydroxyl radical.

Hydroxyl radical sources used in these experiments were hydrogen peroxide ($H_2O_2$), nitrate ($NO_3^-$) and nitrite ($NO_2^-$). Nitrate and nitrite are naturally present in surface waters, hydrogen peroxide is present only in cloud waters. Photolysis of $H_2O_2$ occurs at λ < 380 nm and produce two hydroxyl radicals:

$$H_2O_2 + h\nu \rightarrow 2HO^\bullet$$

(R6)

For each source, the $R_{HO^\bullet}^f$ was correlated to source concentration. There is a linear correlation between [S] and $R_{HO^\bullet}^f$, and the fit of data gives a straight line, whose slope is the formation kinetic constant of HO$^\bullet$ ($k_{HO^\bullet,S}^f$) (Fig. 48).

74
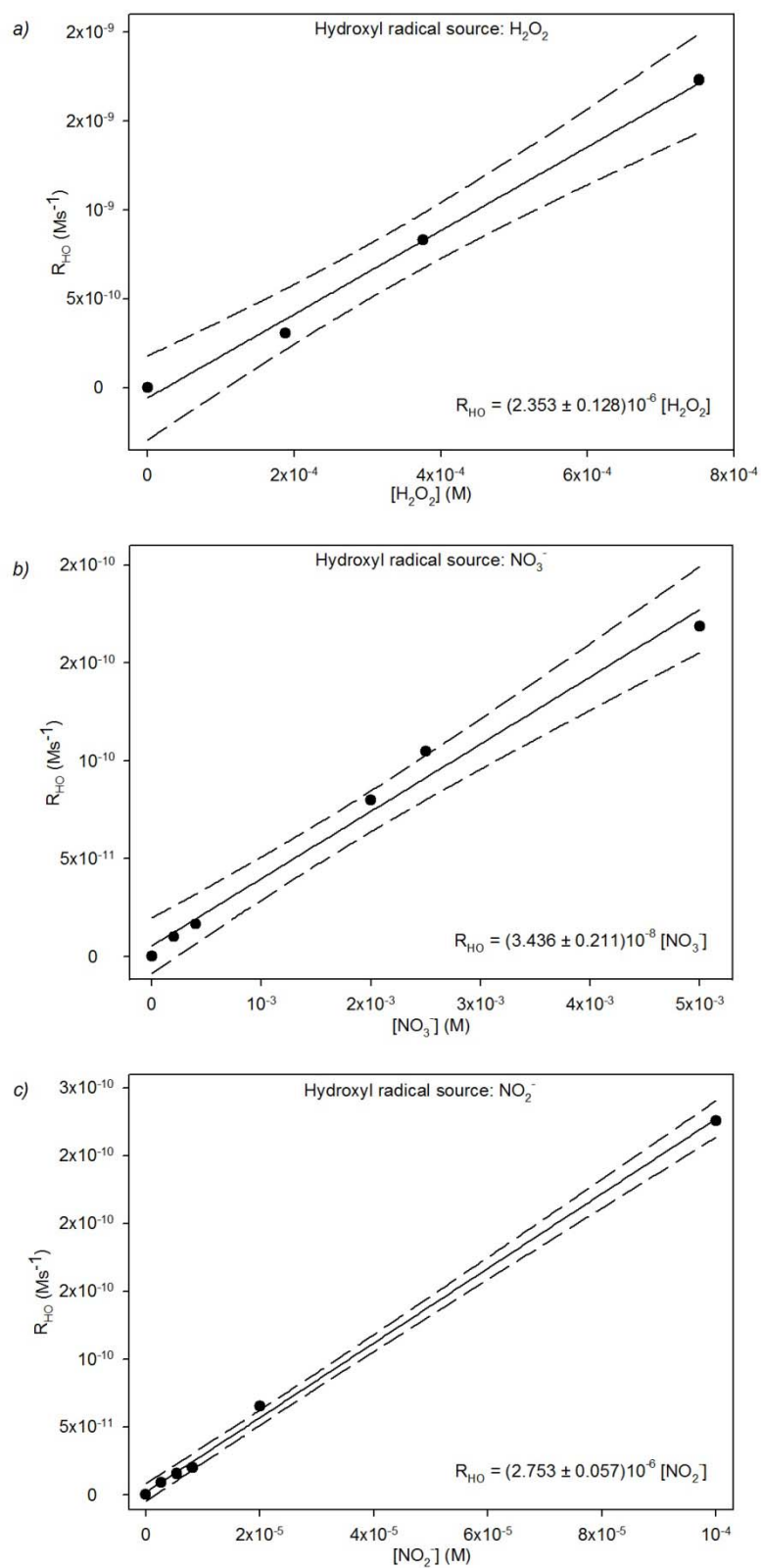
**Figure 48**. Linear correlation between the $R_{HO\bullet}^f$ and the molar concentration of hydroxyl radical source: a) $H_2O_2$, b) $NO_3^-$ and c) $NO_2^-$. The solid curve shows the linear regression fit of experimental data and dashed lines denote the 95% confidence interval of this fit.

The value of HO$^\bullet$ formation rate constant are reported in Table 11, and according to literature the highest value was found for nitrite photolysis.

| | H$_2$O$_2$ | NO$_3^-$ | NO$_2^-$ |
|---|---|---|---|
| $k^f_{HO^\bullet}$ (s$^{-1}$) | $(2.353 \pm 0.128)$ x $10^{-6}$ | $(3.436 \pm 0.211)$ x $10^{-8}$ | $(2.753 \pm 0.057)$ x $10^{-6}$ |

**Table 11**. The formation kinetic constants of HO$^\bullet$ determine for irradiation of hydrogen peroxide (H$_2$O$_2$), nitrate (NO$_3^-$) and nitrite (NO$_2^-$).

## 3.4 RIVASTIGMINE

The transformation of rivastigmine toward hydroxyl radical generated using different natural sources ($H_2O_2$, $NO_3^-$, $NO_2^-$) was investigated. The second order rate constant between hydroxyl radical and the drug was estimated.


*Determination of the second order rate constant of rivastigmine with hydroxyl radical*

The second order rate constant between hydroxyl radical and rivastigmine ($k_{Riv, HO^\bullet}$) was determined for the first time to the best of our knowledge. Competition kinetics was used to determined the initial depletion rate of rivastigmine in the presence of different concentrations of isopropanol (2Pr) , which is used as a competitor.

The degradation rate of rivastigmine, obtained by irradiation of solutions containing 45 µM of Riv, 380 µM of $H_2O_2$ and with addition of different isopropanol concentrations (ranging from 0 up to 1 mM), was determined. The following reactions were included in the kinetic data treatment reported below:


$$H_2O_2 + h\nu \rightarrow 2HO^\bullet \qquad\qquad\qquad [R_{HO^\bullet}^f] \qquad (R6)$$

$$Riv + HO^\bullet \rightarrow Products \qquad\qquad\qquad [k_{Riv, HO^\bullet}] \qquad (R7)$$

$$(CH_3)_2CHOH + HO^\bullet \rightarrow (CH_3)_2C^\bullet OH + H_2O \qquad [k_{2Pr, HO^\bullet}] \qquad (R8)$$

$$H_2O_2 + HO^\bullet \rightarrow H_2O + HO_2^\bullet \qquad\qquad [k_{H_2O_2, HO^\bullet}] \qquad (R9)$$
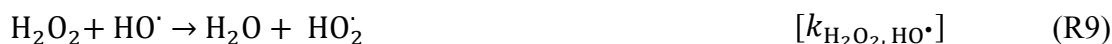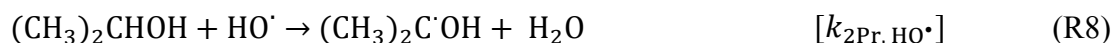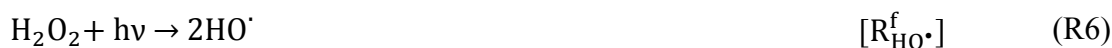

Initial degradation rate of rivastigmine was reported in a plot as a function of the isopropanol concentration and the experimental data were fitted using the following equation (Eq. 15):


$$R_{Riv}^d = \frac{R_{HO^\bullet}^f \, k_{Riv, HO^\bullet} \, [Riv]}{k_{Riv, HO^\bullet} \, [Riv] + k_{H_2O_2, HO^\bullet} \, [H_2O_2] + k_{2Pr, HO^\bullet} \, [2Pr]} \qquad (Eq.\ 15)$$


The data reported in Fig. 49 were fitted with an equation type: $y = \dfrac{a}{1 + bx}$ where $x$ is the concentration of isopropanol [2Pr] and:

$$a = \frac{R_{HO^\bullet}^f \; k_{Riv, HO^\bullet} \, [Riv]}{k_{Riv, HO^\bullet} \, [Riv] + k_{H_2O_2, HO^\bullet} \, [H_2O_2]} \qquad \text{(Eq. 16)}$$

$$b = \frac{k_{2Pr, HO^\bullet}}{k_{Riv, HO^\bullet} \, [Riv] + k_{H_2O_2, HO^\bullet} \, [H_2O_2]} \qquad \text{(Eq. 17)}$$

From the data fitted the second-order reaction rate constant between hydroxyl radical and rivastigmine was obtained:

$$k_{Riv, HO^\bullet} = \frac{\dfrac{k_{2Pr, HO^\bullet}}{b} - k_{H_2O_2, HO^\bullet} \, [H_2O_2]}{[Riv]} \qquad \text{(Eq. 18)}$$

The value found for the kinetic constant ($k_{Riv, HO^\bullet}$) was $(5.8 \pm 0.3) \times 10^9 \; M^{-1} \, s^{-1}$.
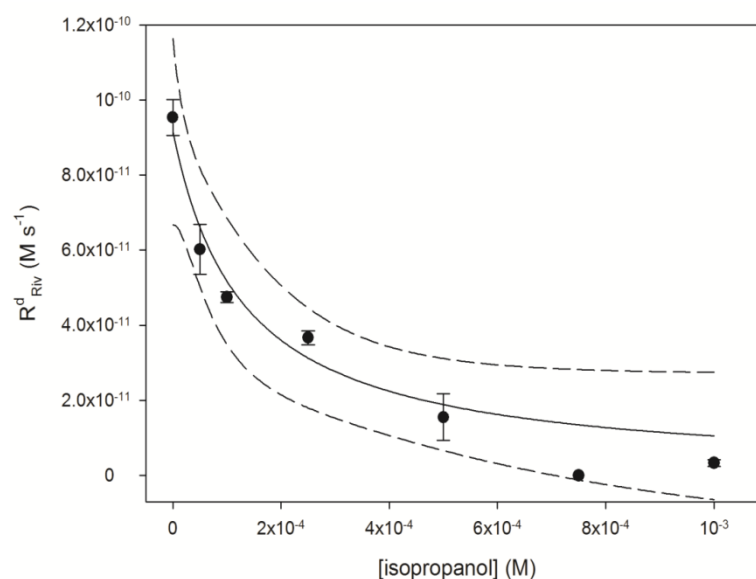


**Figure 49**. Initial degradation rate of rivastigmine under polychromatic irradiation of H$_2$O$_2$ 380 µM as a function of the isopropanol concentration. The solid curve shows the fit of experimental data with Eq. 15 and dashed lines denote the 95% confidence interval of this fit.

*Rivastigmine degradation in synthetic waters*

Rivastigmine (45 µM) was irradiated, by a solar simulator, in the presence of different amounts of hydrogen peroxide, nitrates and nitrites. The initial degradation rate of rivastigmine $R_{Riv}^d$ as a function of hydrogen peroxide, nitrate and nitrite concentration is reported in Fig. 50.

78
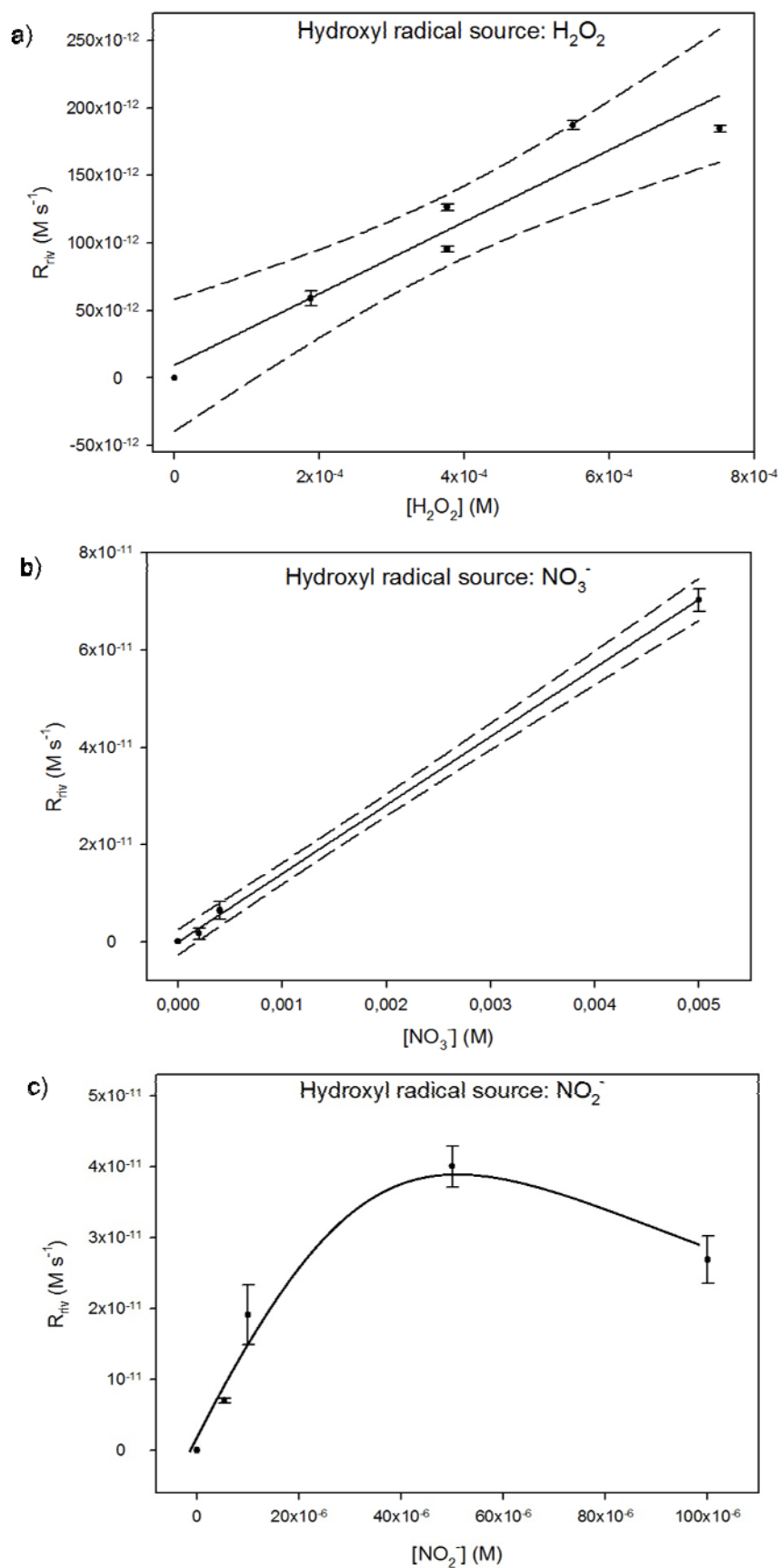
**Figure 50**. Initial degradation rate of rivastigmine as a function of the molar concentration of hydroxyl radical source: a) $H_2O_2$, b) $NO_3^-$ and c) $NO_2^-$. The solid curve shows the fit of experimental data and dashed lines denote the 95% confidence interval of this fit.

As expected, in the cases of hydrogen peroxide and nitrate as sources, the degradation rate of rivastigmine ($R_{Riv}^d$) increases by increasing the HO• source concentration. A different situation was observed with nitrite. Increasing nitrite concentration the rivastigmine degradation at first enhances and then decreases. This depletion could be explained considering the reactivity of nitrites toward hydroxyl radical with a second order rate constant of $k_{NO_2^-, HO•} = 1.0 \times 10^{10}$ M$^{-1}$ s$^{-1}$ (Mack and Bolton 1999).

In all irradiation mixtures there are other species, in addition to rivastigmine, that can react with hydroxyl radical. Using high concentration of HO• source, the latter can react with hydroxyl radical with a not negligible rate. For example, in the case of hydrogen peroxide a competition due to the reaction R9 (see above) could be expected. Taking into account the main species in solution it is possible to estimate the fraction of hydroxyl radical formation rate $R_{HO•,Riv}^f$ reacting with rivastigmine. Hydrogen peroxide reacts with HO• with a second order rate constant of $k_{H_2O_2, HO•} = 2.70 \times 10^7$ M$^{-1}$ s$^{-1}$ (Buxton et al. 1988). Considering the concentration of $H_2O_2$ and rivastigmine used during irradiation, and the kinetic constant of reaction R7 and $k_{Riv, HO•}$, it is possible to estimate the fraction of hydroxyl radical formation rate $R_{HO•,Riv}^f$ reacting with rivastigmine. Plotting the initial degradation rate of rivastigmine in function of $R_{HO•,Riv}^f$ it is possible to observe a linear correlation between the two rates (Fig. 51).
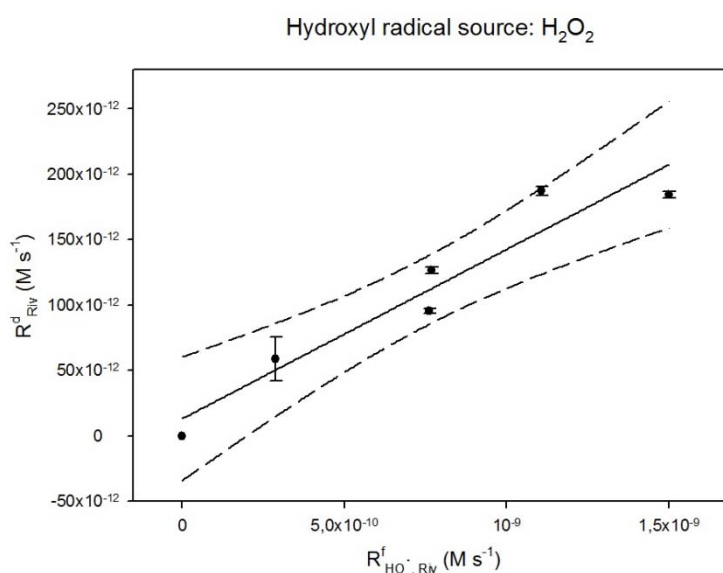


**Figure 51**. Linear correlation between $R_{Riv}^d$ and the fraction of hydroxyl radial formation rate $R_{HO•,Riv}^f$ reacting with rivastigmine, under irradiation of hydrogen peroxide solutions. The solid curve shows the linear fit of data and dashed lines denote the 95% confidence interval of this fit.

A similar procedure was used to evaluate the fraction of hydroxyl radical formation rate $R^f_{HO^\bullet,Riv}$ reacting with rivastigmine during irradiation in presence of nitrite. Also in this case a linear correlation was obtained between $R^d_{Riv}$ and $R^f_{HO^\bullet,Riv}$ (Fig. 52).
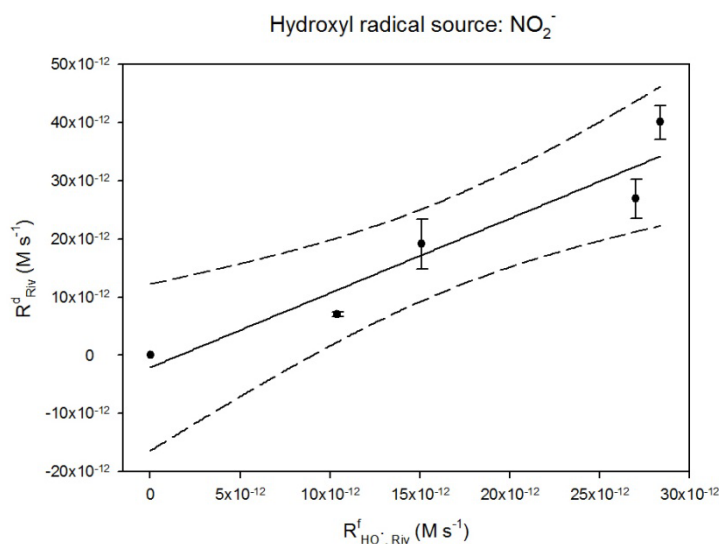


**Figure 52**. Linear correlation between $R^d_{Riv}$ and the fraction of hydroxyl radial formation rate $R^f_{HO^\bullet,Riv}$ reacting with rivastigmine, under irradiation of nitrite solutions. The solid curve shows the linear fit of data and dashed lines denote the 95% confidence interval of this fit.

The second order rate constant of nitrate with hydrogen peroxide is negligible and all hydroxyl radicals generated in solution react with rivastigmine giving a linear correlation of $R^d_{Riv}$ with $R^f_{HO^\bullet}$ reported in Fig. 53.
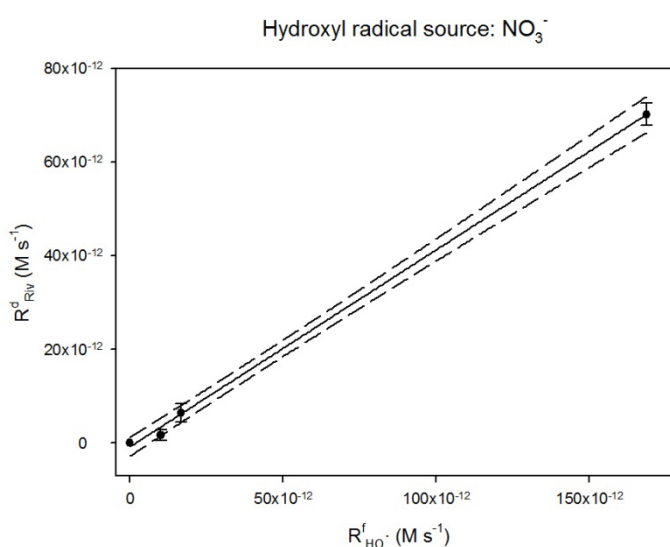


**Figure 53**. Linear correlation between the initial degradation rate of rivastigmine $R^d_{Riv}$ and hydroxyl radial formation rate $R^f_{HO^\bullet}$, under irradiation of nitrate solutions. The solid curve shows the linear fit of data and dashed lines denote the 95% confidence interval of this fit.

The slopes of the three straight lines are different (Figure 1, 2, 3); this implies that at the same value of $R^f_{HO^\bullet, Riv}$, the degradation rate of rivastigmine is different in function of the hydroxyl radical source used. In particular, the degradation rate is faster when nitrites are used, and it follows the trend: $R^d_{Riv}$ > with $NO_2^-$ > with $NO_3^-$ > with $H_2O_2$. The high degradation rate of rivastigmine, when nitrites or nitrates are used to generate hydroxyl radical, is probable due to collateral reactions of rivastigmine with reactive species produced during nitrite and nitrate photolysis such as $NO/NO_2$ radicals.

In order to confirm this hypothesis LC-MS analyses were carried out on the irradiation mixtures. Three experiments were conducted using three hydroxyl radical sources: hydrogen peroxide (experiment A), nitrates (experiment B) and nitrite. After 48 hours of irradiation the solutions were analysed. Three main reaction-type mechanisms were discerned and chemical structures of the nineteen identified products are proposed in Scheme 24 on the basis of their mass spectra. The main reaction, as expected in the presence of a $HO^\bullet$ precursor, is the hydroxylation of the aromatic ring leading to the formation of product **A1** while di- and tri- hydroxylated compounds (**A2** and **A3**) are successively generated. The alcohol (**A4**), ketone (**A5**) and vinyl (**A6**) derivatives could also be formed from direct photolysis *via* an homolytic and/or heterolytic cleavage of the N-C bond (Temussi et al. 2012). Hydroxylation of **A4** and **A5** leads to the formation of **A7** and **A8** found only in trace levels under adopted irradiation conditions. In the presence of nitrites and nitrates two species with *m/z* $[M+H]^+ = 280$ and 310 suggesting that nitration of the aromatic ring (**B1** and **B2**) could occur (Nelieu et al. 2004). Few products deriving from fragmentation were found in all experimental conditions. Moreover high mass values were found (*m/z* = 411, 429, 445 and 467) suggesting the formation of dimer molecules *via* radical recombination.
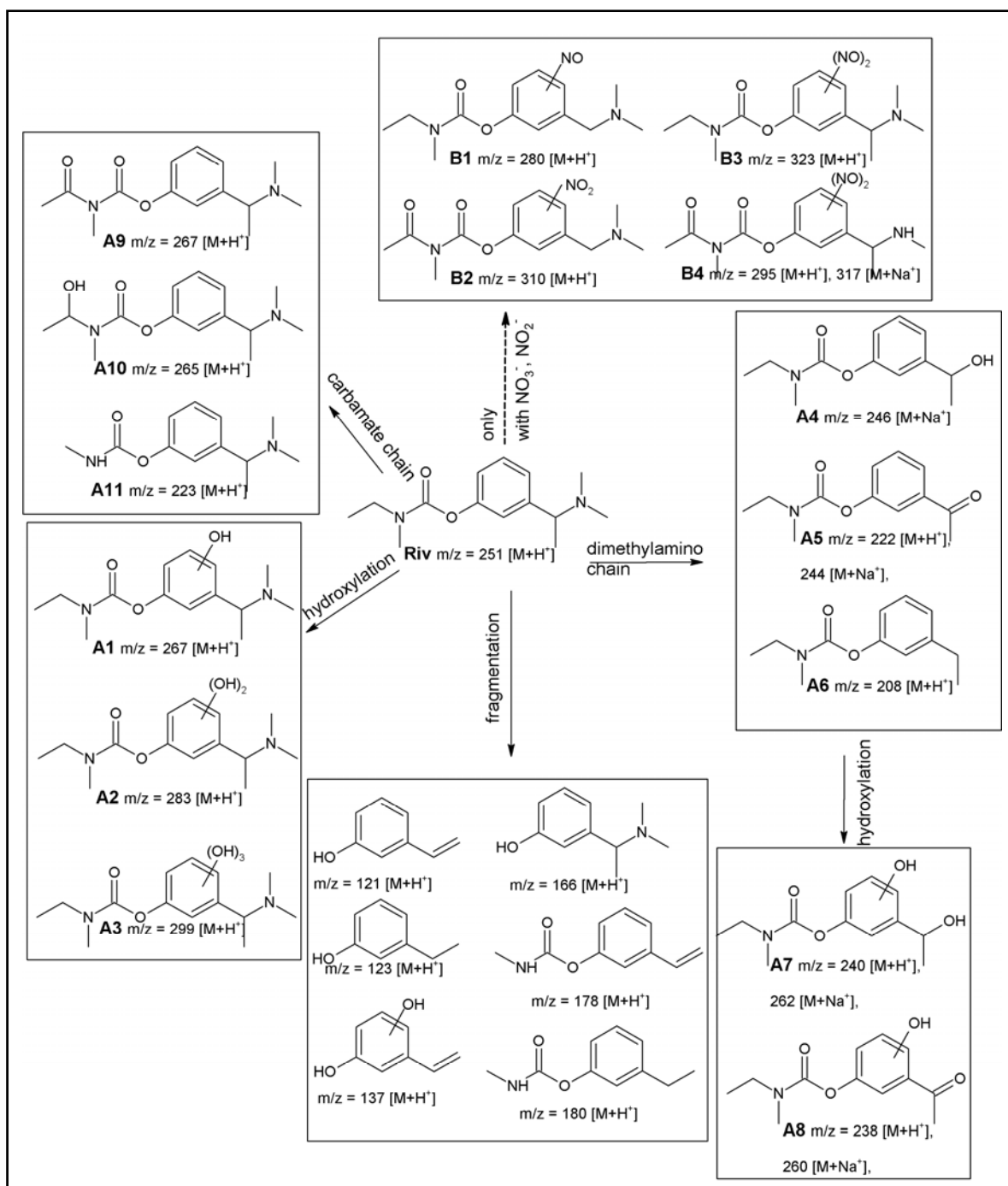
**Scheme 24.** Proposed structure and formation mechanisms for the main rivastigmine degradation products founded in the presence hydrogen peroxide, nitrites and nitrates as photochemical sources of hydroxyl radical under polychromatic irradiation.

*Rivastigmine degradation in natural waters*

Three samples of natural waters (lake, river and rain) were collected and analysed in order to perform hydroxyl radical measurement and rivastigmine degradation studies. River water and lake water were collected from Artiere river and Chambon lake respectively, both located in the Puy de Dôme region, France. Artiere river passes

through Clermont-Ferrand agglomeration, Chambon lake is in the massif of Dore mountains at 877 m above sea level. Rain water was collected on the 1st November 2011 at south of Clermont-Ferrand. Absorption spectra of the three natural waters and overlap with adopted irradiation spectrum are shown in Fig. 54.
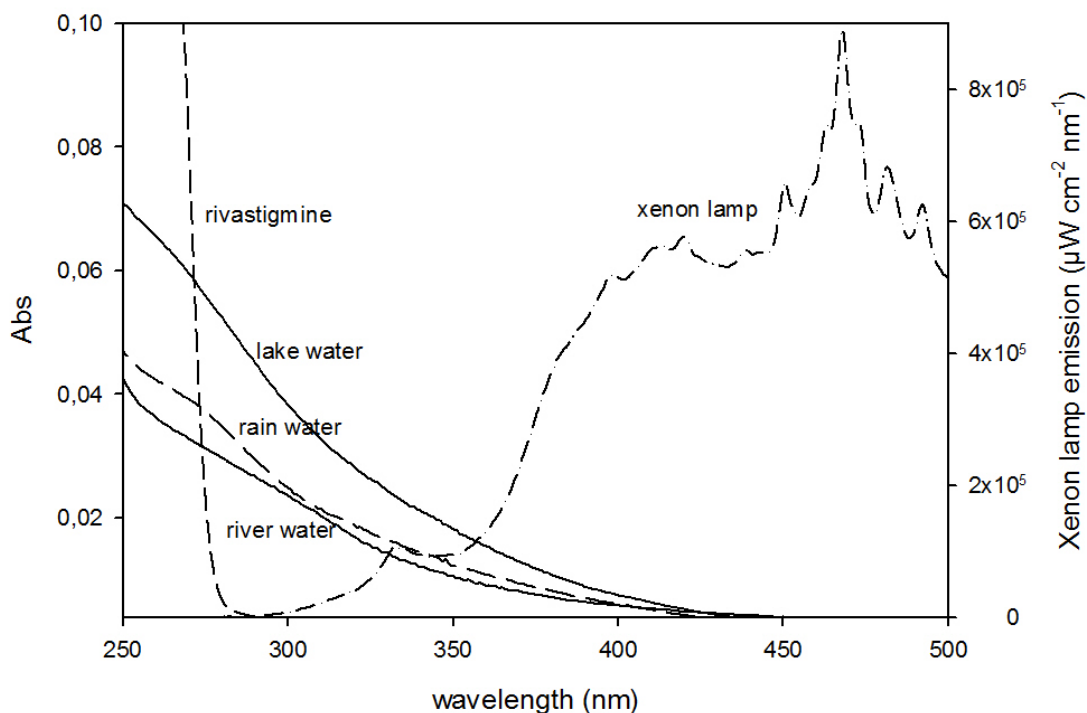


**Figure 54**. Emission spectrum reaching the solution and absorption spectra of natural waters (lake, river, rain) and of rivastigmine.

For each natural water the pH was measured and the inorganic ions concentration were determined by ion chromatography analyses. Total organic carbon (TOC) and $HCO_3^-/CO_3^{2-}$ were quantified by TOC. The theoretical hydroxyl radical formation rate was estimated by considering only $NO_2^-$ and $NO_3^-$ as photochemical sources. The hydroxyl radical formation rate was determined irradiating natural waters by solar simulator, using TA as molecular trapping (see above). All results are reported in Table 12.

| | Rain water | Lake water | River water |
|---|---|---|---|
| $NO_3^-$ (M) | $7.49 \times 10^{-6}$ | $3.53 \times 10^{-6}$ | $2.31 \times 10^{-4}$ |
| $NO_2^-$ (M) | $1.15 \times 10^{-6}$ | / | $7.30 \times 10^{-6}$ |
| $SO_4^{2-}$ (M) | $3.98 \times 10^{-6}$ | $5.09 \times 10^{-5}$ | $3.75 \times 10^{-4}$ |
| $Cl^-$ (M) | $4.99 \times 10^{-5}$ | $1.97 \times 10^{-4}$ | $3.47 \times 10^{-3}$ |
| $HCO_3^-/CO_3^{2-}$ (M) | 2.0 | 9.32 | 61.23 |
| TOC (mg/L) | 2.45 | 2.01 | 2.70 |
| pH | 7.2 | 6.6 | 7.9 |
| $R^f_{HO^\bullet \text{ measured}}$ (M s$^{-1}$)[a] | $(6.42 \pm 0.53) \times 10^{-12}$ | $(5.45 \pm 0.08) \times 10^{-12}$ | $(3.55 \pm 0.02) \times 10^{-11}$ |
| $R^f_{HO^\bullet \text{ predicted}}$ (M s$^{-1}$)[b] | $3.42 \times 10^{-12}$ | $1.21 \times 10^{-13}$ | $2.80 \times 10^{-11}$ |
| % HO$^\bullet$ formation from $NO_3^-$ [c] | 4.0 | 2.2 | 22.4 |
| % HO$^\bullet$ formation from $NO_2^-$ [c] | 49.3 | / | 56.6 |
| % HO$^\bullet$ formation from other [d] | 46.7 | 97.8 | 21.2 |
| $R^d_{Riv}$ (M s$^{-1}$) | $(2.47 \pm 1.20) \times 10^{-12}$ | $(2.83 \pm 1.63) \times 10^{-12}$ | $(1.02 \pm 0.05) \times 10^{-11}$ |

**Table 12**: Concentrations of nitrite, nitrate, $HCO_3^-/CO_3^{2-}$ and Total organic carbon (TOC) of natural waters used during rivastigmine experiments. [a] HO$^\bullet$ formation rate obtained by using 1mM of terephthalic acid as trapping molecule. [b] Theoretical HO$^\bullet$ formation rate estimated by considering only $NO_2^-$ and $NO_3^-$ as photochemical sources. [c] contribution to the hydroxyl radicals attributed to $NO_2^-$ and $NO_3^-$. [d] contribution to the hydroxyl radicals obtained by difference from know sources.

In lake water, where only nitrates were quantified in low concentration, the formation rate of HO$^\bullet$ measured under polychromatic radiation is very low ($R^f_{HO^\bullet} = 5.45 \times 10^{-12}$ M s$^{-1}$). The rain water contains both nitrate and nitrite in a concentration range of $10^{-6} - 10^{-5}$ M and $R^f_{HO^\bullet}$ measured is comparable to that obtained with the lake water ($R^f_{HO^\bullet} = 6.42 \times 10^{-12}$ M s$^{-1}$). For rain and lake waters about 47 and 98 % of hydroxyl radicals are produced by other photochemical sources such as free iron, iron-complexes or CDOM. River water presents a high concentration of nitrate, probably due to use of fertilizers (e.g. ammonium nitrate) in nearby agriculture fields and a not negligible concentration of nitrite. Due to the high nitrate and nitrite concentration, the formation rate of HO$^\bullet$

measured in this water results to be 6-7 times higher than in lake and rain ($R_{HO\bullet}^{f}$ = 3.55 x $10^{-11}$ M s$^{-1}$). In fact, nitrites and nitrates contribution to hydroxyl radicals formation for about 57 and 22 % of the total in river water. Hydroxyl radical formation rates ($R_{OH}^{f}$) measured in lake and rain water are similar to previously reported values for surface waters (Albinet et al. 2010; Vione et al. 2010).

Furthermore, irradiation of rivastigmine in these natural waters (lake, river and rain) was performed. According to the very low formation rate of HO$^{\bullet}$, in lake and rain waters, rivastigmine didn't undergo degradation. In river water a degradation rate of (1.02 ± 0.02) x $10^{-11}$ M s$^{-1}$ was measured.

An estimate of degradation rate of rivastigmine in river water can be predicted on the basis of $R_{HO\bullet}^{f}$ measured ($R_{HO\bullet}^{f}$ = 3.55 x $10^{-11}$ M s$^{-1}$) using the linear correlations between $R_{Riv}^{d}$ and $R_{HO\bullet}^{f}$ obtained previously (see plots in Fig. 51-53). The predicted degradation rate of rivastigmine calculated by the correlation obtained using $H_2O_2$ as hydroxyl radical source is 2.92 x $10^{-12}$ M s$^{-1}$. As expected from previously data, in this case the degradation rate is underestimated, because this value probably represents the rivastigmine degradation rate due just to the reaction with hydroxyl radical. The predicted degradation rate of rivastigmine calculated by the correlation obtained using $NO_2^{-}$ and $NO_3^{-}$ as hydroxyl radical source are 2.88 x $10^{-11}$ M s$^{-1}$ and 9.48 x $10^{-12}$ M s$^{-1}$, respectively. The values calculated in this way are close to experimental value of $R_{Riv}^{d}$ measured in river water. The matching between predicted $R_{Riv}^{d}$ and real value measured in river water was obtained only for one water sample and to be generalized it should be applied to more samples, but this is a good starting point to evaluate the environmental fate of xenobiotics.

## 3.5 NICOTINE

Nicotine (**1n**, Fig. 55) is an alkaloid found in the flowering plants family of Solanaceae, it is toxic by inhalation, ingestion, and skin contact and a lethal oral dose of ~40-60 mg for man was stated (Benowitz 1998). Nicotine is especially known because it is one of the major pharmacoactive ingredients in tobacco and it is daily consumed by a wide number of world's population, an annual global consumption of at ~5 x $10^4$ tons was estimated (Buerge et al. 2008). In the past it was widely used as insecticide for its antiherbivore chemical function. In the last years, U.S. EPA has accepted the cancellation of nicotine pesticides from the pesticide list, and in 2014 these pesticides will not be available for sale (US EPA 2009).
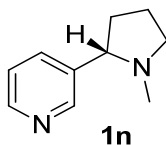


**Figure 55**. Nicotine (**1n**, (*S*)-3-(1-methylpyrrolidin-2-yl)pyridine).

In the last period a particular attention was focused on the nicotine presence in the environmental compartments. In particular, from an atmospheric point of view the possible formation of indoor aerosol from nicotine heterogeneous chemistry has been recently shown (Petrick et al. 2011; Sleiman et al. 2010). Nevertheless nicotine is able to reach surface waters during tobacco processing and manufacturing tobacco products and concentrations of few ng $L^{-1}$ have been measured in untreated and drinking waters (US EPA 2008). Recently, nicotine has been found in main rivers of Madrid Region in a concentration range of 0.3μg/L – 1.9μg/L, higher than those previously reported (Huerta-Fontela et al. 2008; Valcárcel et al. 2011).

The indirect photolysis of nicotine in typical conditions used in treatment of polluted waters was studied. Nicotine under ultraviolet light irradiation (254 nm) combined with high concentration of chemical oxidant (hydrogen peroxide) undergo rapid photochemical reactions. Studies about indirect photolysis of nicotine in environmental aquatic conditions aren't reported in literature so far.

Nicotine ($pk_{a1}$ = 3.37 ± 0.02, $pk_{a2}$ = 8.07 ± 0.02) (Nienow et al. 2009) in water may be present as neutral, monoprotonated or diprotonated form, depending on pH. In the pH range 4.7-7.7 monoprotonated nicotine is the principal species; UV-visible spectra at different pHs were recorded to check eventual variations in this range. The absorption

87

spectra of nicotine in aqueous solution at different pHs (pH = 4.7 and 7.7) and emission spectrum of the lamp used (solar simulator) are shown in Fig. 56.
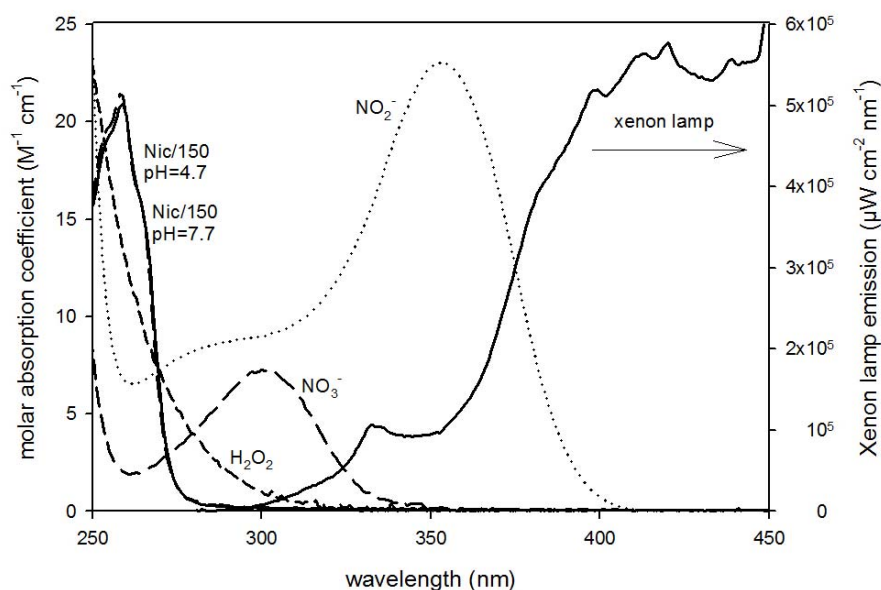


**Figure 56**. Emission spectrum reaching the solution and molar absorption coefficients of the aqueous nicotine (at pH 4.7 and 7.7), nitrate, nitrite and $H_2O_2$.

The indirect photolysis of nicotine under environmental-like conditions was investigated. The transformation of nicotine toward hydroxyl radical was studied, in particular, the second order kinetic constant of nicotine with hydroxyl radical was determined and irradiation in synthetic containing different hydroxyl radical sources ($H_2O_2$, $NO_3^-$, $NO_2^-$), was carried out.

The stability of alkaloid in aqueous solution was checked under dark conditions and no significant degradation was observed after 1 month.

*Nicotine degradation in synthetic waters*

The reactivity of nicotine with photogenerated hydroxyl radical from natural constituents of natural waters (such nitrates and nitrites) was studied.

A preliminary irradiation in pure milli-Q water was performed using 30 μM concentration of nicotine. An UV-Vis spectrum after 22.5 h of irradiation showed no significant degradation of nicotine; from HPLC analysis a very slow degradation rate of nicotine was calculated ($R_{Nic}^d$ = 5.04 x $10^{-12}$ M $s^{-1}$). In order to assess its reactivity with HO•, a solution of $H_2O_2$ (700 μM) and nicotine (30 μM) was irradiated; variation of nicotine concentration was checked by UV-Vis spectra. After 8 h it is possible to

88

observe an effect of the hydroxyl radical on the nicotine degradation. Solution spectra at different irradiation times showed a new absorption band formation and a diminution of nicotine band (Fig. 57).
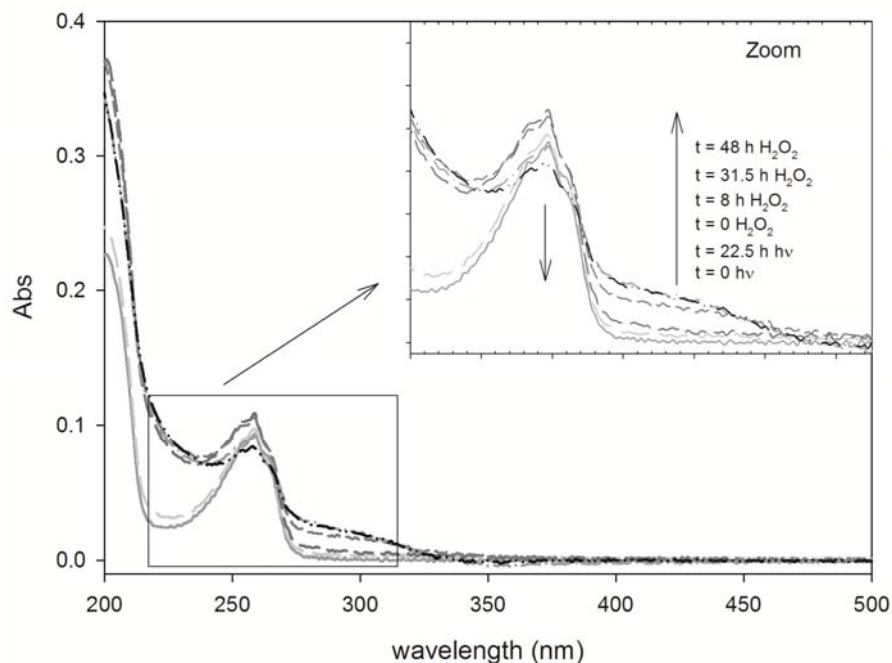


**Figure 57.** UV-Vis spectra of nicotine solution (30 µM) in pure milli-Q water before irradiation and after 22.5 h of irradiation, and spectra at different irradiation times of nicotine (30 µM) and $H_2O_2$ (700 µM) solution. A zoom of spectra is also reported to highlight the new absorption band formation and nicotine degradation.

Starting from these preliminary experiments, irradiations of nicotine in aqueous solutions with different concentrations of $H_2O_2$ were carried out.

Increasing the $H_2O_2$ concentration and $HO^\bullet$ formation rate a linear correlation of the nicotine degradation rate was observed (Fig. 58). In the plot the degradation rate of nicotine is reported in function of the hydrogen peroxide concentration. The data were fitted by linear regression.
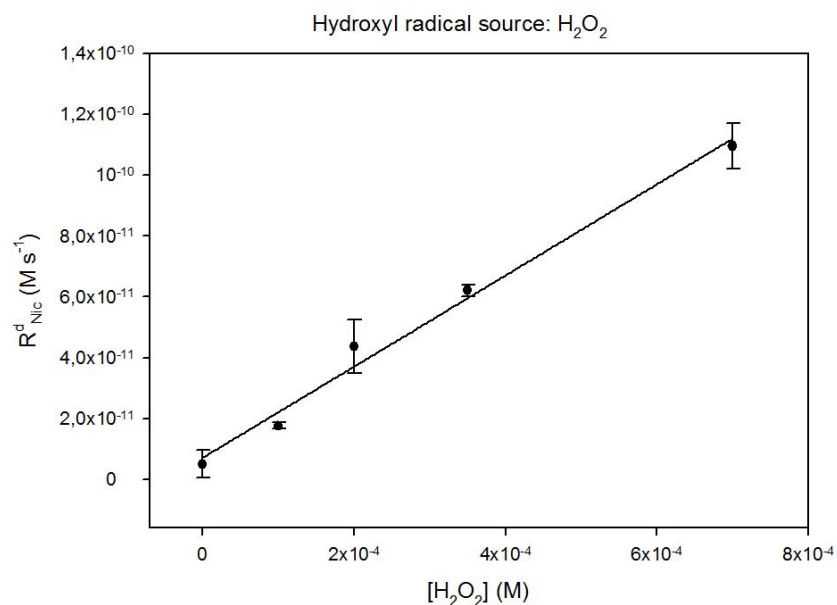
**Figure 58.** Initial degradation rate of nicotine as a function of the molar concentration of $H_2O_2$. The solid curve shows the fit of experimental data and dashed lines denote the 95% confidence interval of this fit.

Analogue experiments were made using nitrates as hydroxyl radical source. Also in this case a linear correlation between degradation rate of nicotine and nitrate concentration was found (Fig. 59).
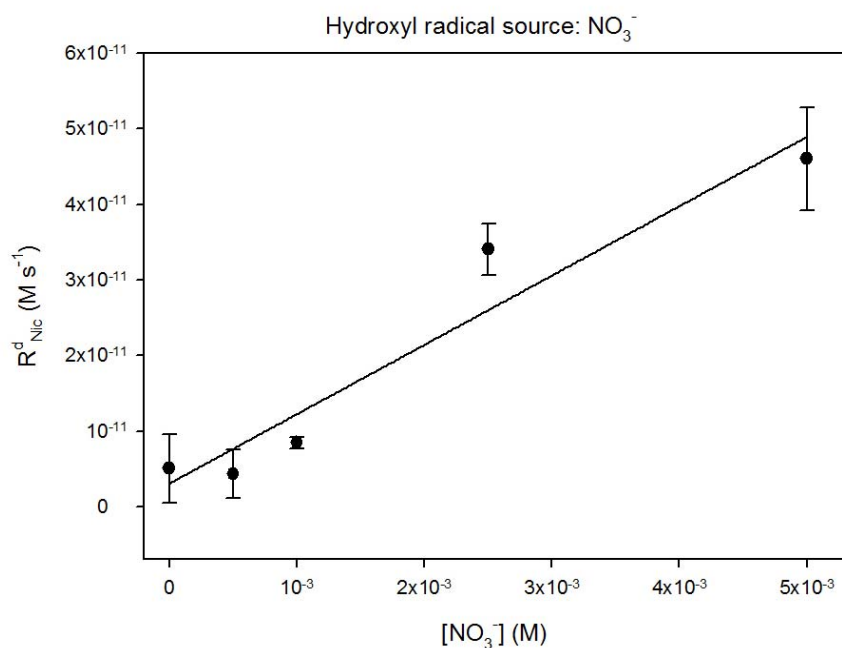


**Figure 59.** Initial degradation rate of nicotine as a function of the molar concentration of $NO_3^-$. The solid curve shows the fit of experimental data and dashed lines denote the 95% confidence interval of this fit.

Irradiation of nicotine in the presence of nitrites, at different concentration, was carried out. As observed for rivastigmine, when the nitrite concentration is 10 μM or 25 μM there is a linear increase of $R_{Nic}^d$, according to an increase of hydroxyl radical formation rate, but when nitrite concentration (50 μM) is greater than nicotine concentration a no-linear correlation between $[NO_2^-]$ and $R_{Nic}^d$ is observed (Fig. 60). In this case there is a decrease of nicotine degradation rate with the increase of nitrite concentration probably because $NO_2^-$ react with photogenerated hydroxyl radicals *via* a complex system (Mack and Bolton 1999).
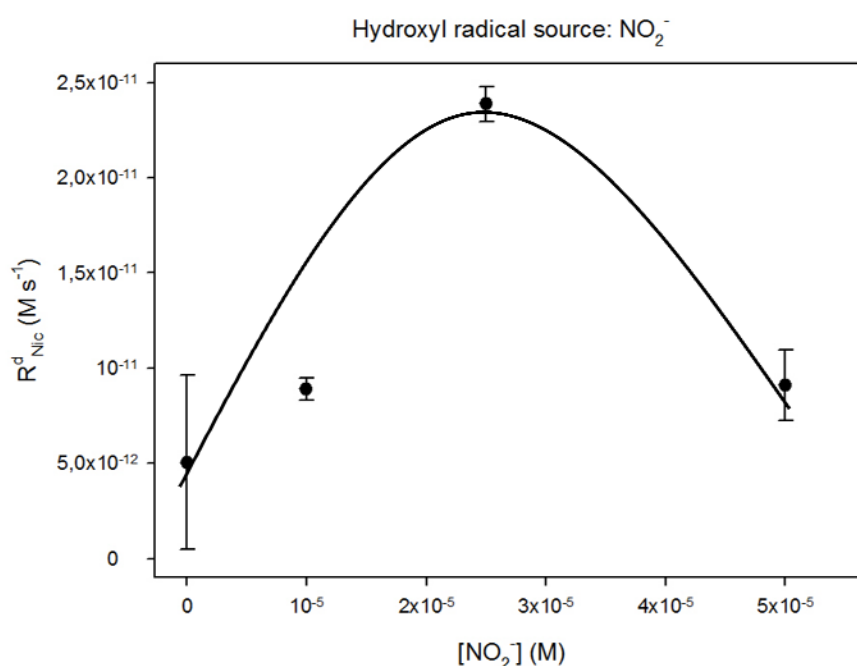


**Figure 60.** Initial degradation rate of nicotine as a function of the molar concentration of $NO_2^-$. The solid curve shows the fit of experimental data.

Also when hydrogen peroxide is used as hydroxyl radical source, a competition due to the reaction R9 could be expected. As reported for rivastigmine above, taking into account the main species in solution and the main reactions that involve the hydroxyl radical it is possible to estimate the fraction of hydroxyl radical formation rate $R_{HO^\bullet,Nic}^f$ reacting with nicotine.

For each hydroxyl radical source $R_{HO^\bullet,Nic}^f$ were plotted *vs* $R_{Nic}^d$ and the data were fitted (Fig. 61). In all cases a straight line was obtained, showing a linear correlation between the initial degradation rate of nicotine and the fraction of hydroxyl radial formation rate that may react with the alkaloid.
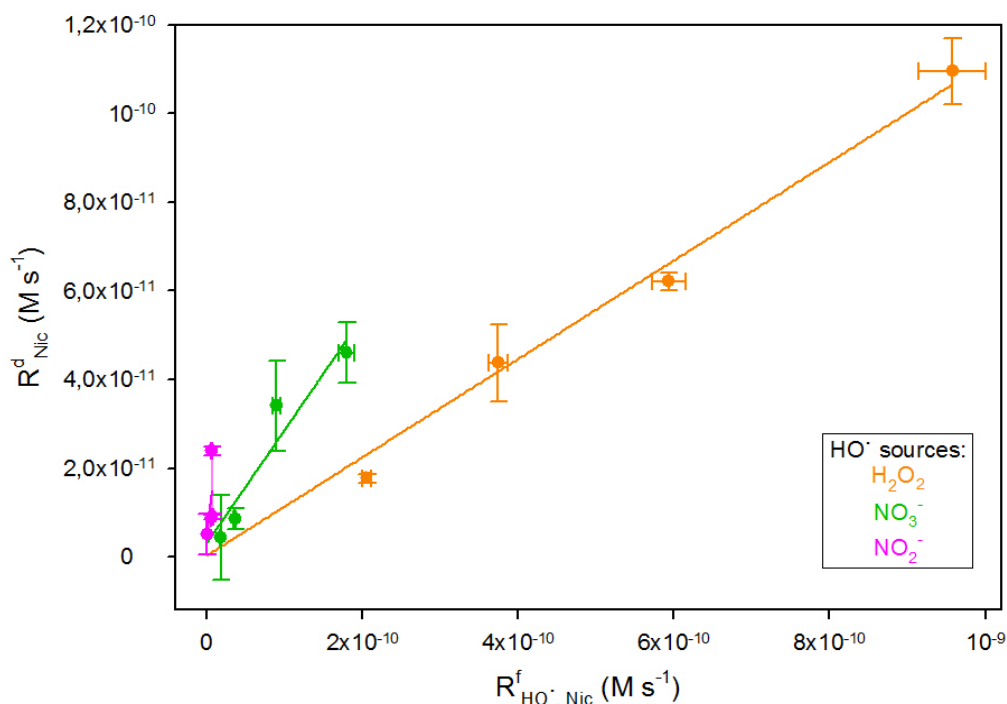
**Figure 61**. Linear correlation between the initial degradation rate of nicotine $R_{Nic}^{d}$ and the fraction of hydroxyl radial formation rate $R_{HO^\bullet,Nic}^{f}$ reacting with nicotine. The photochemical sources are: hydrogen peroxyde (orange) nitrites (pink) and nitrates (green).

As observed for rivastigmine, at the same value of $R_{HO^\bullet,Nic}^{f}$, the degradation rate of rivastigmine is different in function of hydroxyl radical source used. The slopes of the three straight lines are different (Fig. 61), in particular, the slope increases according to the order: nitrite > nitrate > hydrogen peroxide, when $NO_2^-$, $NO_3^-$ and $H_2O_2$ are the photochemical hydroxyl radical sources.

The faster degradation rate of nicotine, when nitrites or nitrates are used to generate hydroxyl radical, implies that the nicotine degradation is due not only to the reaction with the hydroxyl radical, but also to other reactions, probably with reactive nitrogen species formed during photolysis of nitrite and nitrate, such as $NO^\bullet$ or $NO_2^\bullet$.

*Determination of the second order rate constant of nicotine with hydroxyl radical*

The second order rate constant between hydroxyl radical and nicotine ($k_{Nic, HO^\bullet}$) was estimated by a method of competition kinetics. In this method nicotine competes for $HO^\bullet$, in a mixture, with a reference compound, whose reactivity toward the $HO^\bullet$, under the identical conditions, is known. Assuming negligible the direct photolysis of nicotine and TA, and assuming that the reactions of $HO^\bullet$ with nicotine (Nic) and with TA lead to

their irreversible transformation, the rate constants for the reaction between HO· and two compounds are evaluated using the following equation:

$$\ln\left(\frac{[\text{Nic}]_0}{[\text{Nic}]_t}\right) = \frac{k_{\text{Nic, HO}^\bullet}}{k_{\text{TA, HO}^\bullet}} \ln\left(\frac{[\text{TA}]_0}{[\text{TA}]_t}\right)$$

(Eq. 19)

where $[\text{Nic}]_0$ and $[\text{TA}]_0$ are molar concentrations before irradiation, $[\text{Nic}]_t$ and $[\text{TA}]_t$ are molar concentrations at time $t$ of irradiation, $k_{\text{Nic, HO}^\bullet}$ and $k_{\text{TA, HO}^\bullet}$ are the second-order rate constants for the reaction of HO· with nicotine and TA, respectively. A plot of $\ln([\text{Nic}]_0/([\text{Nic}]_t)$ *vs* $\ln([\text{TA}]_0/([\text{TA}]_t)$ give, by data fit (linear regression), a straight line, whose slope is the ratio of rate constants $k_{\text{Nic, HO}^\bullet}/k_{\text{TA, HO}^\bullet}$ (Fig. 62).
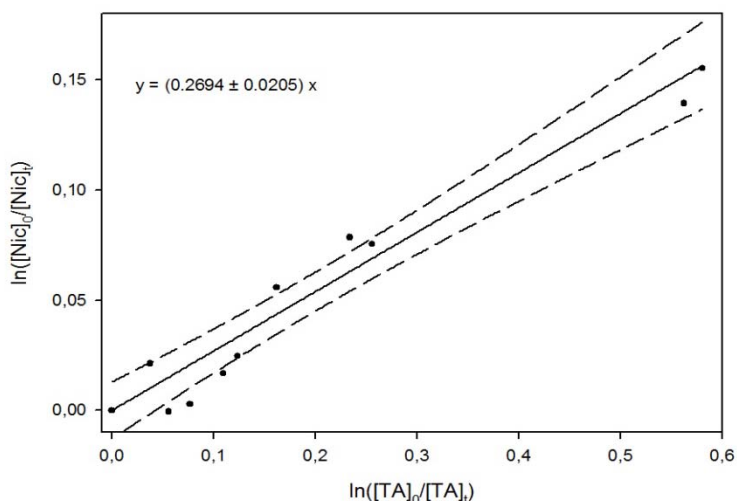


**Figure 62**. The solid curve shows the fit of experimental data with Eq. 19 and dashed lines denote the 95% confidence interval of this fit.

Knowing $k_{\text{TA, HO}^\bullet}$, it was possible to obtain the rate constant between hydroxyl radical and nicotine ($k_{\text{Nic, HO}^\bullet}$) from the slope of the plot. The value found is: $k_{\text{Nic, HO}^\bullet} = (1.08 \pm 0.08) \times 10^9\,\text{M}^{-1}\,\text{s}^{-1}$. The reactions included in the kinetic treatment of data reported are the following:

$$H_2O_2 + h\nu \rightarrow 2HO^\bullet \qquad\qquad [R^f_{HO^\bullet}] \qquad (R6)$$

$$H_2O_2 + HO^\bullet \rightarrow H_2O + HO_2^\bullet \qquad\qquad [k_{H_2O_2,\,HO^\bullet}] \qquad (R9)$$

$$Nic + HO^\bullet \rightarrow Products \qquad\qquad [k_{Nic,\,HO^\bullet}] \qquad (R10)$$

$$TA + HO^\bullet \rightarrow TAOH + Products \qquad\qquad [k_{TA,\,HO^\bullet}] \qquad (R11)$$

## 3.6 CONCLUSIONS

The degradation of two xenobiotics, rivastigmine and nicotine, was investigated toward different photochemical sources of hydroxyl radical and the second order kinetic constants with $HO^\bullet$ were determined.

The results showed that the degradation rate of these two xenobiotics depends on the $HO^\bullet$ source. Faster degradation was observed when nitrates and nitrites are used and such trend could be attributed to secondary reactions between xenobiotics and species formed during irradiation of $NO_3^-$ and $NO_2^-$ (i.e. NOx radicals). The formation of nitroderivatives by irradiation of xenobiotics in presence of nitrite and nitrate was previously observed (Shankar et al. 2007) and the formation of NO- and $NO_2$-phenyl substituted compounds was explained by reaction with $NO^\bullet$ and $NO_2^\bullet$ radicals produced by photolysis of nitrite and nitrate (Nelieu et al. 2004). These reactions are relevant, in fact, the photonitration has been observed in natural waters and nitroderivatives of pesticides have been found in the environment (Chiron et al. 2007). Photonitration leads in many cases to the formation of compounds that are environmentally more persistent and more toxic than parent molecules (Chiron et al. 2009; Suzuki et al. 1982). Nitrocompounds, in fact, are recognized as highly mutagenic/carcinogenic compounds (Clonfero 1997; Suzuki et al. 1982).

For rivastigmine an evaluation of photoproducts formed under indirect photolysis was carried out. The chemical structures of the main products generated *via* oxidation of Riv were suggested and hydroxylation, dimethylamino and carbamate chains degradation as well as nitration were identified as possible pathways to explain the degradation products formation. Moreover the irradiation of rivastigmine in three natural waters has underlined a key role of indirect degradation in natural media when direct photolysis is negligible.

To have a rough estimation of the environmental degradation rate of these xenobiotics, it is necessary to study the reactivity of these compounds toward reactive nitrogen species that may be present in natural waters. Moreover, it would be very important to understand the interaction of such molecules with other natural occurring species and study the stability and toxicity of their environmental metabolites.

These results give a better insight into the environmental fate of these xenobiotics. Moreover, the studies on the indirect photolysis of pollutants in water are often used to assess of xenobiotics phototransformation in atmosphere, where the indirect photolysis is one of the main phototransformation processes.

# 4.0 PHOTOTRANSFORMATION IN SOIL

The pollutants phototransformation in soil is very complex and it is difficult to be reproduced in laboratory scale experiments. Nevertheless, an investigation on transformation processes in simple model soils may evidence some of the factors that influence these processes, allowing to rationalize the photochemical behavior of xenobiotics in soil.

Soil is a very complex environmental compartment. It is a heterogeneous system formed by organic and inorganic compounds, gases and water. The main components are silicates, alumina silicate, humic substances, metal oxides and carbonates. Soils of different geographical regions have different structures and different properties due to the presence of microorganisms, content of water, pH, etc.

The transformation of pollutants in soil involves complex phenomena, such as adsorption, desorption, diffusion, biotic and abiotic reactions, hence it is difficult to estimate the environmental impact of a given pollutant in soil (Steger-Hartmann et al. 1997). All these processes in certain cases entail a total degradation of the pollutant, in others induce the formation of environmental metabolites. The photochemical processes have been recognized as abiotic transformation routes that can contribute to the degradation of pollutants in soils (González and San Román 2005). They generally lead to products that can be more easily degraded by biotic processes. Phototransformation in soil may take place through the direct solar light absorption by the xenobiotic, or may involve photoinduced transformations mediated by soil components. In the latter case the xenobiotic photodegradation is enhanced.

In order to have an overall estimate of the environmental fate of a xenobiotic investigation on the photodegradation in soil should also be carried out. A correlation between degradation patterns observed in model soils and the phototransformation of xenobiotics in aqueous solutions may be interesting to highlight the influence of the medium in photochemical reactions.

This study deals with a preliminary laboratory investigation on the influence of soil on the behavior of some xenobiotics considering model sterilized soils of different composition and using as light source lamps generating radiation belonging to the solar spectrum. The soils used contained common components as silicates and oxides. The role of light as well as water content was also considered.

The substances studied included the categories of drugs and pesticides: rivastigmine (**1c**), loratidine (**1d**), ethynilestradiol (**1o**) and carboxin (**1p**). All compounds absorb in

the UVB region.

Direct photolysis of rivastigmine (**1c**) and loratidine (**1d**) (Fig. 63) was described in chapter 2, for rivastigmine indirect photolysis was also described (chapter 3). Hence, investigation in soil appeared interesting in order to assess their photochemical behavior under different environmental-like conditions.
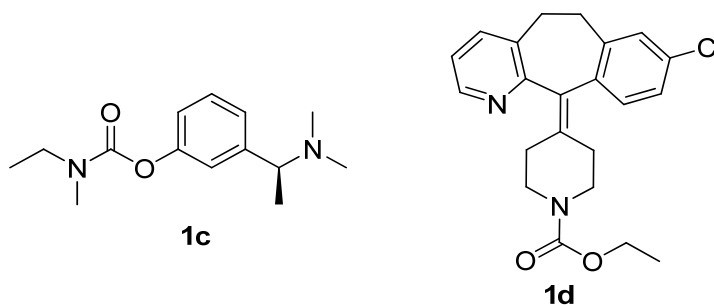


**Figure 63**. Rivastigmine (**1c**) and loratidine (**1d**).

Ethinylestradiol (**1o**) is a synthetic estrogen used primarily in birth control pills (Fig. 64). It is persistent even during the treatment with activated sludge, with removal efficiencies around 50% (Janex-Habibi et al. 2009). It has been found in high concentrations (ng L$^{-1}$) in major rivers in northern Italy (Calamari et al. 2003). It has been observed that the environmental concentrations of ethinylestradiol are capable of interfering with the normal reproductive functions of acquatic organisms compromising their life (Shved et al. 2008). The drug is poorly photoreactive. Liu et al. report that it can be destroyed by UV-light ($\lambda$ = 254 nm) radiation but no photochemical degradation was observed under sunlight (Liu et al. 2003). Jurgens et al. highlight the resistant to bio- and photodegradation of the drug (Jurgens et al. 2002) while other authors describe ethinylestradiol photodegradation in natural waters under sunlight irradiation (Matamoros et al. 2009; Zuo et al. 2006). We decide to carry out phototransformation experiments of ethinylestradiol in soil with the aim to verify the possible role of photosensitized processes in soil that could enhance the drug degradation.
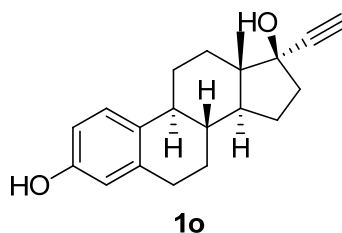


**Figure 64**. 17α-Ethinylestradiol (**1o**, (8*R*,9*S*,13*S*,14*S*,17*R*)-17-ethynyl-13-methyl-7,8,9,11,12,14,15,16-octahydro-6H-cyclopenta[a]phenanthrene-3,17-diol).

Carboxin, also known as Vitavax (ExToxNet 1996), is a systemic anilide fungicide inhibiting the mitochondrial function, used to control plant diseases caused by Basidiomycetes (Agnihotri 1986) (Fig. 65). The chemical and photochemical reactivity of carboxin has been extensively studied under various conditions. Carboxin (**1p**) has been found photosensitive even under sunlight exposure and undergoes phototransformations both in organic solvents (Iesce et al. 2002) and in water (DellaGreca et al. 2004b) giving mainly its sulfoxide (**2p**). The latter is also produced by microorganisms together with the corresponding sulfone (Balasubramanya and Patil 1980). Recent studies have demonstrated that it undergoes oxidation and a hydrolytic ring-opening in wet soils in the dark (Isidori et al. 2012). Therefore, the pesticide was chosen as substrate in the soil phototransformation experiments to compare the results with literature data and contribute to rationalize its environmental behavior.



**1p**
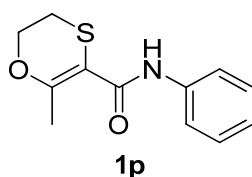
**Figure 65**. Carboxin (**1p,** 5,6-dihydro-2-methyl-N-phenyl-1,4-oxathiin-3-carboxamide).

## 4.1 PHOTOTRANSFORMATION EXPERIMENTS

Irradiation experiments were carried out on three synthetic soils: sandy soil (SS), bentonitic soil (BS) and kaolinitic soil (KS). These model soils have similar composition, with different amount of each constituent, as described below (Table 13). They were prepared according to the procedure suggested by Lo and Yang (Lo and Yang 1999). The xenobiotic solution was mixed to each soil, and the resulting mixture kept under stirring in order to encourage the uniform distribution of the xenobiotic in the soil. After solvent evaporation the solid mixture, distributed on a plate to obtain a thin soil layer, was irradiated by different light sources (solar simulator or UV-B lamps). The xenobiotic and its products were then extracted from soil with organic solvents and the extraction mixture analysed by NMR and separated by chromatography. Experiments were also conducted in the dark in order to distinguish between photochemical and chemical reactions.

| Compound | Sandy Soil (SS) | Bentonitic Soil (BS) | Kaolinitic Soil (KS) |
|---|---|---|---|
| $SiO_2$ | 78 | 33,5 | 33,5 |
| Kaolin [$Al_2Si_2O_5(OH)_4$] | - | - | 60 |
| Bentonite [$Al_2O_34SiO_2H_2O$] | 20 | 60 | - |
| $CaCO_3$ | 0,5 | 5 | 5 |
| $Fe_2O_3$ | 0,25 | 0,25 | 0,25 |
| $MnO_2$ | 0,25 | 0,25 | 0,25 |
| Humic Acid | 1 | 1 | 1 |

**Table 13**. Composition of model synthetic soils (wt%).

## 4.2 RESULTS AND DISCUSSION

Soil experiments with rivastigmine (**1c**) were unsuccessful. Indeed, in all experimental conditions (dark/light and wet/dry soils), despite the use of very polar solvents for extraction, the recovery of the organic material was <10%. It is likely that the drug is strongly retained mainly for dipole-dipole and ionic interactions between the polar groups of the basic rivastigmine and acidic sites of the soil.

Starting from loratidine (**1d**) NMR analysis of the mixtures after 1 h showed that in sandy soil the drug was converted, in a small amount, to isomer **4d**. This product was also observed under irradiation in solution (see chapter 2, section *2.4.2*), and its formation does not depend on the water amount in the medium. From the other soils the drug was recovered unchanged even after 10 h of irradiation. Evidently, the higher $SiO_2$ content in sandy soil plays a role in favouring the isomerization reaction (Scheme 25).
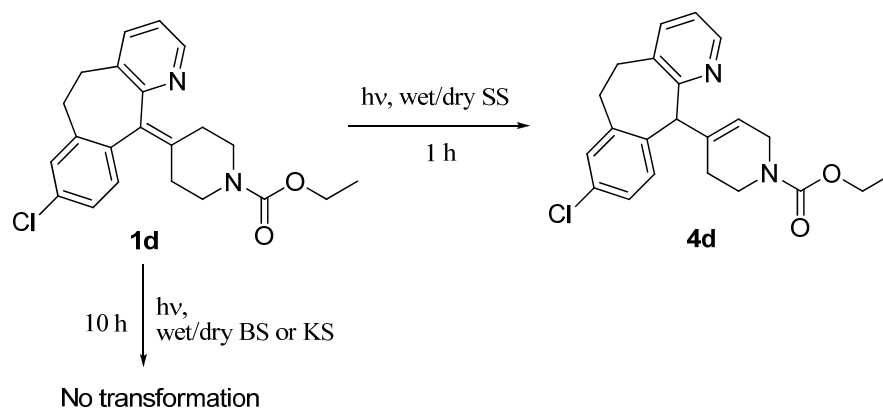


**Scheme 25**. Phototransformation of loratidine in model soils.

17-α-ethinylestradiol (**1o**) was recovered unchanged after 10 hours of UVB irradiation in all three soils. The same result was obtained either by using high-pressure mercury lamp with pyrex filter or by using wet soils and irradiating with both lamps. The photostability of the drug, already observed in solution, is enhanced in soil. This could be due to an inefficient photosensitization of these soils on ethinylestradiol or, more likely, to a filter action of the soils. These results give a further evidence of the environmental issue of this compound that is widely used, recalcitrant and with endocrine disrupting potency (Shved et al. 2008).

Photodegradation of carboxin (**1p**) was observed only in sandy soil (Scheme 26). After 2 h of irradiation the proton spectrum showed that carboxin was converted for ca. 25%. Chromatography of the irradiation mixture led to the isolation of products **2p-4p** that were identified by comparison of their NMR spectra with those reported (Cermola and Iesce 2002).
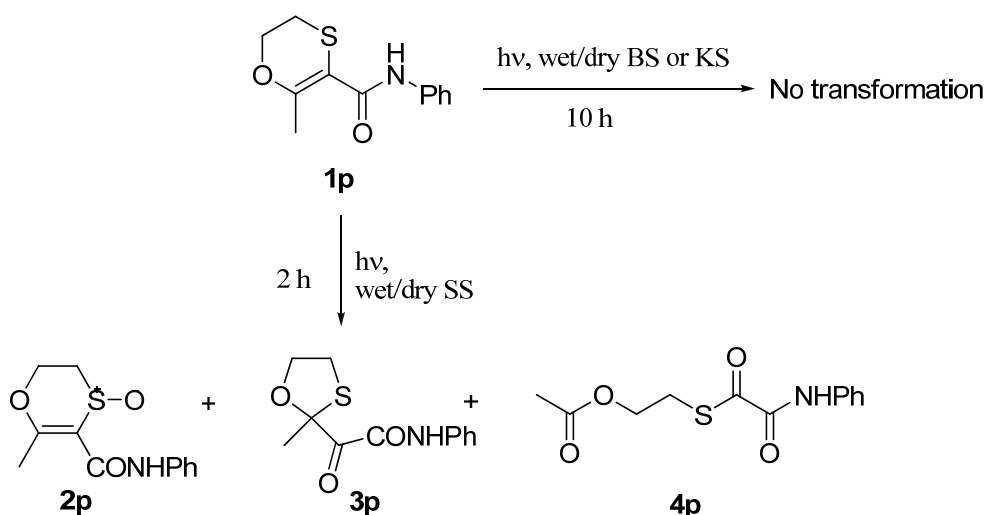


**Scheme 26**. Phototransformation of carboxin in model soils.

As demonstrated previously (DellaGreca et al. 2004b), products **2p-4p** should be formed by photooxidative pathways. The excited pesticide undergoes oxygen addition to sulphur giving sulfoxide **2p** or to the double bond giving the diradicals ***a*** or ***b***. The latter through intra- o intermolecular reactions afford amide **4p** or oxathiolane **3p** (Scheme 27).
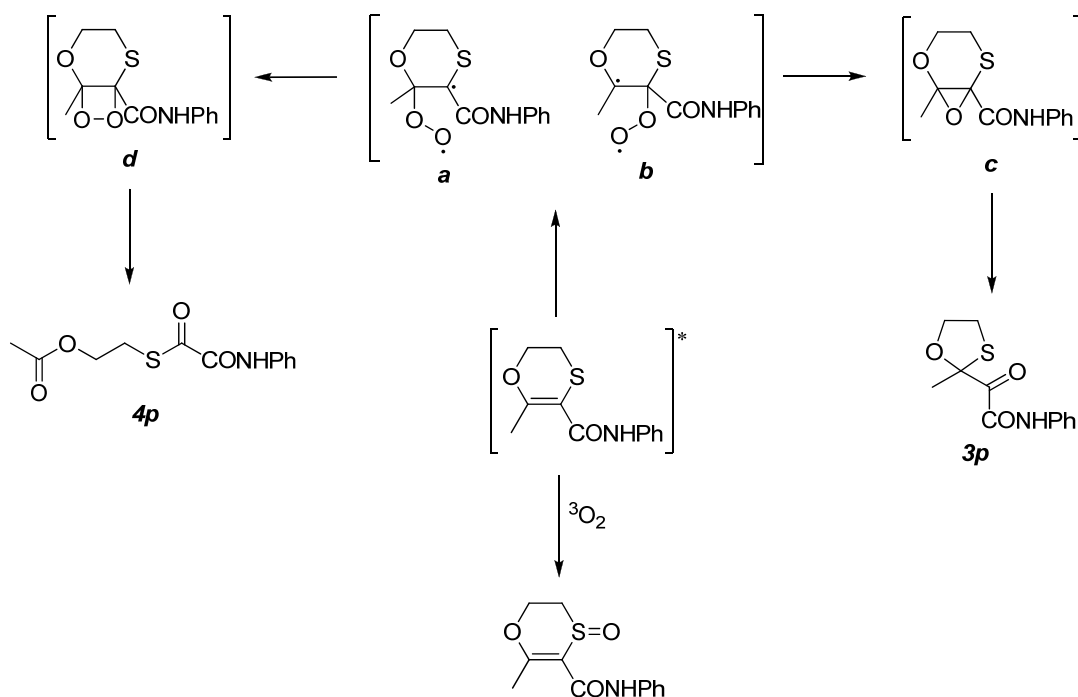
**Scheme 27**. Phototransformation mechanisms of carboxin.

Irradiation on wet SS led to the same products in different ratio. Table 14 reports the percentages deduced from the irradiation mixture after 2h by integration of isolated signals for each compound. As shown in Table 14 the degradation of the pesticide is slower in dry soil than in wet soil.

| Irradiation medium | 1p | 2p | 3p | 4p |
|---|---|---|---|---|
| Dry SS | 75 | 10 | 5 | 10 |
| Wet SS | 65 | 20 | 7 | 8 |
| Water | - | 52 | 28 | 20 |

**Table 14**. Percentage product distribution after 2 h of UV-B irradiation of carboxin in different media.

Noteworthy is the presence of amide **4p** that confirms the tendency of carboxin to undergo oxygen addition to the double bond. This compound was not detected by carboxin exposure to sunlight in water; under these conditions only hydrolysis products were observed (DellaGreca et al. 2004b). Evidently, long exposition times and the presence of water induce hydrolysis of amide **4p**.

## 4.3 CONCLUSION

The phototransformation of xenobiotics has been observed only in sandy soil, probably due to the different amount of silica and/or $CaCO_3$ respect to the other model soils. The greater amount of silica may promote acid-catalyzed processes while the greater amount of carbonate may have a filter action, inhibiting the photolysis of xenobiotics. In some cases, the phototransformation has been faster in wet soils than in dry soils, showing the important role of water in pollutant degradation.

Although simple synthetic soils have been used, the results evidence some of the factors that can have an influence on the photochemical behavior of a xenobiotic:

1) the presence of acidic or basic reactive sites that may cause ionic bonds of saline type and hence the non-recovery of the organic material as observed for rivastigmine

2) the depth of the layer and the filter action that reduce significantly the light absorption as observed for loratidine and ethinylestradiol

3) the presence of moisture that can favor phototransformation as oserved for carboxin.

# 5.0 CONCLUSIONS

In this PhD thesis the photochemical behavior of some xenobiotics under environmental-like conditions has been investigated. These compounds are characterized by the presence in the molecular structure of an indole moiety or a carbamate function. In particular, direct photolysis studies have been carried out on drugs indomethacin, etodolac, loratidine and rivastigmine, on pesticides chlorpropham and phenisopham and on carbamic model compounds. Indirect photolysis of rivastigmine and nicotine have also been examined. Finally, for some xenobiotics photochemical experiments in soil have been carried out. In all the cases photoproducts have been isolated and/or spectroscopically characterized.

Acute and chronic tests of some xenobiotics and their photoproducts on non-target organisms are in progress in collaboration with Second University of Naples.

From a chemical point of view, interesting photochemical data have been obtained.

Investigation on indomethacin, a non-steroidal anti-inflammatory drug (NSAID), has evidenced the role of the aryl portion in the formation of ionic species prior to the decarboxylation, and the results give a further support to the general photodecarboxylation mechanism of arylalkanoic acids. The results are in agreement with the classification of NSAID arylalkanoic acids into two different groups depending on the ability of the aryl ring to act as an electron-acceptor (ketoprofen, suprofen, tolmetin) or an electron-donor (naproxen, carprofen, indomethacin) (De Guidi et al. 2005; Pitchumani and Madhavan 2004). During the last decade the photochemistry of NSAIDS has received considerable attention mainly to establish the molecular bases of their phototoxic properties (Bosca et al. 2004; De Guidi et al. 2005; Musa and Eriksson 2010; Nayak 2010). The involvement of radical and electrophilic species could account for the phototoxic effects, sometime observed, in therapeutic uses of indomethacin (Stern and Bigby 1984). These effects could be also associated with its ability to generate reactive oxygenated species (ROS) (Onoue and Tsuda 2006). Indeed, as observed in other 2-, 3-, 2,3- alkylsubstituted indoles (Iesce et al. 2005; Mudry and Frasca 1973) self-sensitized photooxygenation of the heterocyclic ring occurs, and this type of reaction has also been observed for the other indolic drug examined, etodolac.

Investigation on rivastigmine and its main human metabolite has evidenced a peculiar photochemical behavior. Both compounds undergo a β-cleavage of the benzylamine moiety resulting in photosolvolysis reaction, previously observed for

benzyl ethers or esters (Fleming and Pincock 1999; Turro et al. 2010). In particular, the photodegradation involves the tertiary amino site and leads mainly to ion-derived products characterized by departure of $Me_2N$-group. It is reported that amines bearing *N*-substituents that are capable of stabilizing the formed aminium radicals have lower oxidation potentials as compared to those with *N*-electron withdrawing substituents as amides and carbamates (Yoon et al. 2004). This could account for the unreactivity of the carbamic-N function of rivastigmine as compared with the reactivity of the benzylaminic function (Yoon et al. 2004). It is noteworthy that the conversion of rivastigmine is slow by direct irradiation with UV-B light or sunlight, but it is promoted by ketones or photoelectron-transfer sensitizers such as anthraquinone. The main photoproduct, a ketone, influences the photodegradation rate of the drug acting as photosensitizer. This poses a problem in a possible indirect photosensitive effect of rivastigmine.

Pesticides chlorpropham and phenisopham contain a carbamate and a bis-carbamate function, respectively; in phenisopham one of the functions is similarly substituted as in chlorpropham. Neverthless, the two pesticides behave differently: the first one undergoes a nucleophilic photosubstitution of chlorine with water on the aromatic ring, while in phenisopham photo-Fries rearrangements occur involving the cleavage of the *N*-aryl *O*-aryl carbamate moiety. However investigation on model compounds evidences that *N*-aryl *O*-aryl substitution is not a sufficient condition to have a photo-induced breaking of the carbamate bond. This breaking is completely overcome in the presence of a chlorine on the aromatic ring. Moreover, substitution on the carbamic nitrogen as well as the presence of a *N*-substituent in the *O*-aryl moiety appears determinant to accelerate the photo-Fries reaction. In the future it would be important to investigate on the substituent effects on the *O*-aryl ring.

All the photochemical experiments evidence the determinant role of water as solvent. This is probably due to the fact that water can favor photoionization reactions, stabilize ionic intermediates and trap electrophilic species.

Some experiments using rivastigmine and nicotine have been carried out under indirect photolysis conditions in Clermont-Ferrand (France) in collaboration with *Laboratoire de Photochimie Moléculaire et Macromoléculaire*-University Blaise Pascal. The results show that the degradation rate of both compounds depends on the $HO^{\bullet}$ source ($H_2O_2$, nitrates, nitrites). Faster degradation has been observed in the presence of nitrates and nitrites and is probably due to collateral reactions between xenobiotics and

photogenerated reactive nitrogen species. For rivastigmine the formation of nitro derivatives has been confirmed by LC-MS. Nitro compounds are often more toxic than the parent compounds (Suzuki et al. 1982), and hence for a complete environmental risk assessment the reactivity toward hydroxyl radical and also toward nitro reactive species that are naturally present in surface waters should be considered.

Investigation on the photochemistry in soils of some bioactive compounds has led to less satisfying results. Despite the simple synthetic model soils used each compound examined behaves differently depending on the light absorption property, the formation of saline bonds due to the presence of acidic or basic reactive sites, filter effects. In addition to these factors in real soils other factors have to be considered as the presence of microorganisms or xenobiotics, the type of texture, the pH, etc. Hence, attempts to foresee the photochemical behavior of an organic molecule in soil from that observed in water are inadequate.

In conclusion, the whole of the results during the three years' work has furnished information on the photochemical behavior of bioactive compounds under environmental-like conditions. Moreover, it gives deeper insight into the substituent and solvent effects in the photochemistry of some important compound classes as indoles, benzyl derivatives and carbamates.

# 6.0 EXPERIMENTAL SECTION

## 6.1 MATERIALS AND METHODS

### 6.1.1 Materials

Indomethacin (**1a**) (99%), hydrogen peroxide (30 %), sodium carbonate (99.5 %) and sodium nitrate (99 %) were purchased from Fluka.

Etodolac (**1b**) (>98%), rivastigmine (**1c**) tartrate, loratidine (**1d**), phenisopham (**1f**) were supplied by Kemprotec.

3-(1-dimethylaminoethyl) phenol (**1c'**) (99%) was purchased by Carlo Erba.

(*S*)-(-)-Nicotine (**1n**) (99 %), aniline, 3-chloroaniline, 4-chloroaniline and *N*-ethylaniline were purchased by Alfa Aesar.

Chlorpropham (**1e**), carboxin (**1p**), ethinylestradiol (**1o**), 4-chlorobenzoic acid (**7a**), 1-(carboethoxy)-4-piperidinone (**2d**), 3-chloro-*N*-ethylaniline, 4-chloro-*N*-ethylaniline, phenyl chloroformate, 3-hydroxyacetanilide (**7m**), phenyl isocyanate, triethylamine, p-nitroanisole (PNA), pyridine (py), 9,10-anthraquinone, phosphoric acid (85% in water), sodium chloride (98 %), terephthalic acid (98 %), 4-hydroxybenzoic acid (**9**), manganese (IV) oxide (99.99%), calcium carbonate, humic acid sodium salt, iron (III) oxide (>99%), kaolin, bentonite and Silica gel (0.063-0.2) were purchase by Sigma-Aldrich.

Compounds **2i**, **3i**, **4l**, **6l**, and were supplied by Aurora Building Blocks.

Sodium sulphate anhydrous (99.5 %), formic acid (98% in water) and sodium nitrite (98%) were purchased from Prolabo; 2-hydroxyterephthalic acid (97 %) was purchased from Atlantic research chemical.

All chemicals were used without further purification unless otherwise indicated.

Aqueous solutions were prepared using Milli-Q water obtained from a Milli-Q gradient system (Millipore). Solvents were of HPLC grade and they were supplied by Sigma-Aldrich.

### 6.1.2 Apparatus

NMR spectra were recorded on a Varian Inova-500 instrument operating at 499.6 and 125.6 MHz for $^1$H and $^{13}$C, respectively, and referenced with deuterated solvents (CDCl$_3$ or CD$_3$OD). The carbon multiplicity was evidenced by DEPT experiments. The proton couplings were evidenced by $^1$H-$^1$H COSY experiments. The heteronuclear chemical shift correlations were determined by HMQC and HMBC pulse sequences.

IR spectra were recorded on a Jasco FT/IR-430 instrument equipped with single reflection ATR using $CHCl_3$ as solvent.

UV–Vis spectra were recorded with a Varian Cary 300 UV–Vis spectrophotometer or on a PerkinElmer Lambda 7 spectrophotometer.

A Varian Cary Eclipse fluorescence spectrofluorimeter was used, adopting a 5 nm bandpass on both excitation and emission.

Electronic impact mass spectra (EI-MS) were obtained with a GC–MS QP5050A (Shimadzu) equipped with a 70 eV EI detector.

Ion chromatography analyses are performed using a a DIONEX DX-320 equipped with an IonPac AG11 (guard-column 4μ 50 mm) and an IonPac AS11 (analytical column 5 x 250 mm) for anions and a DIONEX ICS-1500 equipped with an IonPac CG16 (guard-column 4 x 50 mm) and an IonPac CS16 (analytical column 5 x 250 mm) for cations. The elution step was performed using a KOH concentration gradient as follow: at initial time [KOH] = 0.2 mM increasing up to 0.43 mM at 4.5 min, followed by a linear gradient to 11.7 mM up to 18 min. the [KOH] was then linearly increased up to 33.5 mM within 3 min. The flow rate was 1 ml $min^{-1}$.

pH was measured with a Metrohm combined glass electrode, connected to a Metrohm 713 pH-meter.

Total organic carbon (TOC) and $HCO_3^-/CO_3^{2-}$ in natural water were quantified by TOC-5050A Analyser (Shimadzu) using calibration curves previously performed by using standard solutions.


*Chromatographic separation*

Analytical and preparative TLCs were made on Kieselgel 60 $F_{254}$ plates with 0.2 mm, 0.5 or 1 mm layer thickness, respectively (Merck).

Column chromatography was performed using Silica gel (0.063-0.2) (Aldrich) or using Lichroprep C-18 resin (40-63 μm) (Merck).


*Chromatographic analysis*

HPLC experiments were carried out on four HPLC systems.

A Waters 1525 binary pump HPLC equipped with UV diode-array detector with a Sinergy Hydro RP18 (4 μm, 250 mm x 4.6 mm) column was used.

An Agilent 1100 Series binary pump HPLC equipped with a UV detector with a Gemini C18 (5 μm, 250 mm x 4.6 mm) column was used.

An HPLC system (Waters Alliance) equipped with a diode array detector was used for rivastigmine analysis. An Eclipse XDB-C18 column (Agilent, 4.6 x 150 mm, 5 μm).

An HPLC system (Waters Em-Power) equipped with a diode array detector was used for nicotine analysis. An Eclipse XDB-C18 column (Agilent, 4.6 x 150 mm, 5 μm).

LC-MS analyses were run on an Agilent1100 MSD instrument using a Sphere Clone C18 (Phenomenex, 4.6 x 250 mm, 5 μm) column. The gradient elution was: at initial time 30 % acetonitrile and 70 % water acidified with 1% formic acid, followed by a linear gradient to 75 % acetonitrile within 55 min. Then, the same ratio was maintained constant for 20 min. The flow rate was 0.4 ml min$^{-1}$ and the UV detector was set at 254 nm.

GC-MS analyses were run on a GC–MS QP5050A (Shimadzu) using a capillary Zebron ZB-5MS column (Phenomenex, 30 m x 0.25 mm i.d. x 0.25 μm), the flow rate was 1.0 ml min$^{-1}$, He as carrier gas, with a temperature gradient: 60°C for 3 min, up to 150°C at 12°C/min, from 150°C up to 230°C at 18°C/min, from 230°C up to 280°C at 19°C/min, 280°C for 5 min.


*Irradiation set-up*

System I: photoreactor (Multirays, Helios Italquartz) equipped with four lamps with a maximum at 254 nm (UV-C).

System II: photoreactor (Multirays, Helios Italquartz) equipped with six 15W lamps with a maximum at 310 nm (UV-B). The incident photon flux (4.98 x 10$^{21}$ photons m$^{-2}$ s$^{-1}$) in solution was calculated using PNA/pyridine actinometer (Dulin and Mill 1982).

System III: photoreactor (Multirays, Helios Italquartz) equipped with four lamps with a maximum at 366 nm (UV-A).

System IV: thermostated pyrex cylindrical reactor (total volume 100 ml) surrounded by six Duke GL20E 20 W lamps. The temperature was held at 293 ± 2 K. Emission spectrum reaching solution was measured with an Ocean Optics SD 2000 CCD spectrophotometer (calibrated using a DH-2000-CAL Deuterium Tungsten Halogen reference lamp) and normalized to the actinometry results using PNA/pyridine actinometer (Dulin and Mill 1982). The incident photon flux in solution was 6.10 x 10$^{19}$ photons m$^{-2}$ s$^{-1}$.

System V: a thermostated cylindrical reactor of 40 ml, cooled by water circulation at a temperature of 15 ± 2°C in order to limit thermal reactions, was located at one focal point of the lamp in order to maintain a constant irradiation of the whole sample and

was equipped on the top with a pyrex filter removing the wavelengths lower than ~285 nm. Samples were continuously stirred with a magnetic stirrer to ensure homogeneity. The emission spectrum of the Xenon lamp (see Fig. 54, chapter 3) was recorded using an optical fiber coupled with a CCD spectrophotometer (Ocean Optics SD 2000). A reference lamp (DH-2000-CAL, Ocean Optics) was used for calibration. The emission spectrum reaching the reactor surface was calculated to be 4.31 x $10^{19}$ photons cm$^{-2}$ s$^{-1}$ over the wavelength range 290-400 nm.

System VI: a high-pressure Hg-lamp GR.E. 500W (Helios Italquartz) horizontally placed at a distance of 15 cm from sample.

All irradiation experiments were performed in triplicate.

### 6.1.3 Calibration curves

For each xenobiotic the calibration curve was obtained by analyzing stock solutions by HPLC and plotting the peak areas versus the theoretical concentrations. The data were subjected to the least squares regression analysis.

### 6.1.4 Kinetic constants and quantum yields determination

Xenobiotic solution was irradiated and at fixed time intervals an aliquot (500 µL) was withdrawn and analysed by HPLC. The time evolution of xenobiotic could be fitted with a pseudo-first order equation $C_0 = C_t e^{-kt}$ where $C_0$ was the initial xenobiotic concentration, $C_t$ the concentration at time t and k the pseudo-first order degradation rate constant.

Assuming xenobiotic as the only absorbing species present in water, the polychromatic quantum yield degradation ($\Phi$) was calculated in the overlap range of xenobiotics absorption spectrum with lamp emission spectrum, as follows:

$$\Phi = \frac{R_X^d}{I_a} \qquad\qquad \text{(Eq.5)}$$

where $R_X^d$ is the xenobiotic degradation rate (M s$^{-1}$) and $I_a$ is the absorbed photon flux *per* unit of surface and unit of time. The latter was calculated from:

$$I_a = \int_{\lambda_1}^{\lambda_2} I_0(\lambda)\left(1 - 10^{-\varepsilon(\lambda)d[X]}\right) d\lambda \qquad\qquad (Eq.6)$$

where $I_0$ is the incident photon flux, $\varepsilon$ is the molar absorption coefficient of xenobiotic, $d$ the optical path length inside the cells and $[X]$ the initial xenobiotic concentration.

## 6.2 DIRECT PHOTOLYSIS

### 6.2.1 Indomethacin

_HPLC systems_

HPLC system A: Agilent Waters 1525 binary pump HPLC equipped with UV diode-array detector was used for kinetics using a Sinergy Hydro RP18 (4 μm, 250 mm x 4.6 mm) column. Injection 100 μl. The mobile phase was made of eluent A (Milli-Q water) and B (methanol-acetonitrile (1:1, v/v) (A-B, 1:1 v/v). The flow rate was 0.4 ml min⁻¹.

HPLC system B: Agilent 1100 Series binary pump HPLC equipped with a UV detector set at 254 nm was used for qualitative analysis using a Gemini C18 (5 μm, 250 mm x 4.6 mm) column. Injection 250 μl. The mobile phase was made of eluent A (water with 1% formic acid) and B (acetonitrile) (A-B, 1:1 v/v). The flow rate was 0.8 ml min⁻¹.

_Stability in aqueous solution in the dark_

Indomethacin solutions ($1 \times 10^{-5}$ M) in water:acetonitrile (95:5, v/v) at pH 4, 7 and 9 were prepared. The acid and alkaline solutions were made using NaOH and HCl to adjust pH level. All solutions were kept in the dark and analysed by HPLC showing no degradation of drug after 48 h.

_Phototransformation kinetics and quantum yield_

Indomethacin solutions ($1 \times 10^{-5}$ M) were prepared in water/acetonitrile (95:5, v/v). Stock solutions, in quartz tubes (25 ml) were irradiated by System I, System II and by sunlight. The concentration change with time was monitored by HPLC (system A). The kinetic constants and the quantum yield were determined as reported in section _6.1.4_.

Three samples of drug solution (1 x $10^{-5}$ M, 20 ml) in open quartz tubes were irradiated by System I, System II and sunlight, respectively, and analysed time by time by HPLC (system B). The photoproducts were identified by HPLC comparing their $R_f$s with those of standard compounds which were isolated and characterized by performing preparative photochemical experiments (see below).

A drug solution (1 x $10^{-5}$ M, 20 ml) in a closed tube saturated with argon was irradiated by System I and analysed time by time by HPLC (system B).

A further sample (1 x $10^{-5}$ M, 20 ml) was kept in the dark and analysed by HPLC (system B) at 10, 20 and 30 days.

*Preparative experiments for photoproducts isolation*

Indomethacin (50 mg) was dissolved in 140 ml of water-acetonitrile (1:1, v/v, 1 x $10^{-3}$ M) and irradiated by System I for 4 h. After evaporation of the solvents, the mixture was chromatographed on a RP-18 open column by eluting with (water-1% formic acid)-acetonitrile (3:7, v/v) and gave compounds **8a** (5.7 mg), **9a** (1.1 mg), **7a** (5.8 mg), **6a** (3.6 mg), **1a** (14.8 mg), **2a** (4.3 mg), **3a** (10.4 mg), **5a** (1.0 mg).

In another experiment the drug (36 mg) was dissolved in 20 ml of water-acetonitrile (1:1, v/v, 5 x $10^{-3}$ M) and exposed to sunlight (October-November 2010, Naples). After 45 d, evaporation of the solvents gave a residue which was chromatographed as above leading to compounds **8a** (3.2 mg), **9a** (3.1 mg), **7a** (4.8 mg), **6a** (1.2 mg), **4a** (3.9 mg), **3a** (11.3 mg), **5a** (1.8 mg).

Compounds **3a** (Weedon and Wong 1991), **5a** (Weedon and Wong 1991) and **8a** (Torisu et al. 2005) were identified by comparison of NMR data with those reported. Acid **7a** was identified by comparison of NMR with those of an authentic sample. Unknown compounds **2a**, **4a**, **6a** and **9a** were characterized by MS, IR and NMR data.

*1-(4-Chlorobenzoyl)-3-hydroxymethyl-5-methoxy-2-methyl-1H-indole* (**2a**): ESI-MS: *m/z* 352 [M+Na]$^+$; IR $\nu_{max}$ (CHCl$_3$) 3453, 1683, 1478 cm$^{-1}$; $^1$H-NMR (CD$_3$OD) $\delta$ 7.66 (d, 2H, *J*=8.7 Hz), 7.47 (d, 2H, *J*=8.7 Hz), 7.10 (d, 1H, *J*=2.7 Hz), 6.83 (d, 1H, *J*=9.0 Hz), 6.67 (dd, 1H, *J*=2.7 Hz and *J*=9.0 Hz), 4.82 (s, 2H), 3.84 (s, 3H), 2.43 (s, 3H); $^{13}$C-NMR (CD$_3$OD) $\delta$ 168.5, 156.3, 139.7, 129.7, 136.5, 131.4, 131.1, 130.3, 129.4, 118.7, 115.2, 112.2, 101.4, 56.0, 55.8, 13.3.

*1-(4-Chlorobenzoyl)-5-methoxy-2-methyl-1H-indole-3-carboxylic acid* (**4a**): ESI-MS *m/z* 344 [M+H]$^+$; IR $\nu_{max}$ (CHCl$_3$) 3019, 1707, 1672, 1476 cm$^{-1}$; $^1$H-NMR (CD$_3$OD) $\delta$

7.71 (s, 1H), 7.70 (d, 2H, $J$=8.4 Hz), 7.50 (d, 2H, $J$=8.4 Hz), 6.88 (d, 1H, $J$=9.0 Hz), 6.75 (dd, 1H, $J$=9.0 Hz and $J$=2.7 Hz), 3.89 (s, 3H), 2.77 (s, 3H); $^{13}$C-NMR (CD$_3$OD) $\delta$ 170.3, 168.6, 156.9, 147.4, 141.1, 132.6, 132.0, 130.8, 129.7, 129.2, 128.4, 114.3, 113.4, 104.2, 56.0, 15.0.

*2-Acetamido-4-(4-chlorobenzoyl)-5-methoxybenzoic acid* (**6a**): ESI-MS: *m/z* 348 [M+H]$^+$; IR $\nu_{max}$ (CHCl$_3$) 3419, 3002, 1673, 1588, 1461 cm$^{-1}$; $^1$H-NMR (CD$_3$OD) $\delta$ 8.51 (s, 1H), 7.81 (s, 1H), 7.75 (d, 2H, $J$=9.0 Hz), 7.48 (d, 1H, $J$=9.0 Hz), 3.72 (s, 3H), 2.15 (s, 3H); $^{13}$C-NMR (CD$_3$OD) $\delta$ 199.0, 175.1, 175.0, 156.2, 141.2, 138.3, 134.0, 132.8, 131.1, 130.9, 130.3, 120.2, 114.2, 56.3, 12.6.

*2-Acetamido-5-methoxybenzoic acid* (**9a**): ESI-MS: *m/z* 232 [M+Na]$^+$; IR $\nu_{max}$ (CHCl$_3$) 3423, 2995, 1670, 1611, 1466 cm$^{-1}$; $^1$H-NMR (CD$_3$OD) $\delta$ 8.37 (d, 1H, $J$= 9.2 Hz), 7.62 (d, 1H, $J$=2.8 Hz), 6.96 (dd, 1H, $J$=9.2 Hz and $J$=2.8 Hz), 3.79 (s, 3H), 2.15 (s, 3H); $^{13}$C-NMR (CD$_3$OD) $\delta$ 174.0, 170.1, 155.2, 134.2, 125.0, 122.5, 118.8, 117.1, 56.4, 25.4.

*Photodegradation of photoproducts **2a, 3a, 5a, 8a***

1 x 10$^{-4}$ M solutions of products **2a**, **3a**, **5a** and **8a** in water/acetonitrile (95:5, v/v, 20 mL) were prepared by 1:10 dilution with water of each 1 x 10$^{-3}$ M solution.

Each solution in open quartz tube was irradiated by System I and analysed time by time by HPLC (system B). The photoproducts were identified by HPLC as above.

A further solution of each sample was kept in darkness and analysed by HPLC (system B) at 1, 5 and 10 days.

### 6.2.2  Etodolac

*HPLC systems*

HPLC system C: Agilent 1100 Series binary pump HPLC equipped with a UV detector set at 230 nm, using a Gemini C18 (5 $\mu$m, 250 mm x 4.6 mm) column with an isocratic elution at a flow rate of 0.8 mL min$^{-1}$ (formic acid 1.0% (A)/CH$_3$CN (B) 1:1, v/v) was used for kinetic analysis. Injection 250 $\mu$l.

HPLC system D: Agilent 1100 Series binary pump HPLC equipped with a UV detector set at 254 nm using a Gemini C18 (5 $\mu$m, 250 mm x 4.6 mm) column was used for qualitative analysis. The column was equilibrated with a mixture of A (H$_2$O containing 1% formic acid)–B (acetonitrile) 9:1 (v/v) at a flow rate of 0.8 mL min$^{-1}$. The run

followed this programme: isocratic B 10% from the start to 6 min, an increase of B up to 50% from 6 to 7 min, isocratic B 50% for 8 min, an increase of B up to 90% from 15 to 20 min and isocratic B 90% for 10 min. Injection 250 μl.

LC-MS analyses were run on an Agilent1100 MSD instrument using a Gemini C18 (5 μm, 250 mm x 4.6 mm) column. Injection 100 μl. Mobile phase: water with 1% formic acid (A) and acetonitrile (B). The gradient elution was: at initial time B 30 % and A 70 %, followed by a linear gradient to A 75 % within 55 min, the ratio was maintained constant for 5 min, than the ratio return to B 30% in 3 min.

## Stability in aqueous solution in the dark

Etodolac solutions ($5 \times 10^{-5}$ M) in water:acetonitrile (9:1, v/v) at pH 4, 7 and 9 were prepared. The acid and alkaline solutions were made using NaOH and HCl to adjust pH level. All solutions were kept in the dark and analysed by HPLC showing no degradation of drug after 48 h.

## Phototransformation kinetics and quantum yield

Etodolac solution ($1 \times 10^{-4}$ M) in water/acetonitrile (9:1, v/v) was irradiated by System II, in quartz tubes (25 mL). The concentration change with time was monitored by HPLC (system C). The kinetic constant and the quantum yield were determined as reported in section *6.1.4*.

## Sunlight irradiation of etodolac

Two solutions of etodolac in water/acetonitrile (9:1, v/v) at different concentration ($5 \times 10^{-5}$ M and $1 \times 10^{-3}$ M) were exposed to sunlight in a closed quartz tube in December-January 2012-2013 in Naples and analysed by HPLC (system D) and LC-MS after 1, 2 and 3 days.

## Preparative experiments for photoproducts isolation

Etodolac (50 mg) was dissolved in 174 mL of water-acetonitrile (9:1, v/v, $1 \times 10^{-3}$ M) and irradiated by System II for 1 h. After evaporation of the solvents, the mixture was separated by preparative TLC. Elution with $Et_2O$ gave compound **2b** (30 mg), etodolac (8 mg) and an intractable material (8 mg).

*2-(2,7'-diethyl-3'-oxo-4,5-dihydro-2H-spiro[furan-3,2'-indoline]-2-yl)acetic acid* (**2b**): ESI-MS: *m/z* 304 [M+H]$^+$, *m/z* 326[M+Na]$^+$; UV λ$_{max}$ (H$_2$O/CH$_3$CN 9:1) nm 214 (log ε

4.2), nm 255 (log ε 3.6), nm 225 (log ε 3.4); IR $\nu_{max}$ (CHCl$_3$) 3443, 3193, 2978, 1710, 1421 cm$^{-1}$; $^1$H-NMR (500 MHz, CD$_3$OD): δ 7.12-7.08(m, 2H), 6.98 (t, 1H, $J$=7.5 Hz), 4.34-4.30 (m, 1H), 4.18 (q, 1H, $J$=8.5 Hz), 2.79 (d, 1H, $J$=14.0 Hz), 2.75-2.72 (m, 1H), 2.64-2.59 (m, 2H), 2.16-2.11 (m, 1H), 1.93 (dd, 1H, $J$= 14.0 and $J$=6.5Hz), 1.50 (dd, 1H, $J$= 14.0 and $J$=6.5Hz), 1.19 (t, 3H, $J$=7.5 Hz ),0.57 (t, 3H, $J$=7.5 Hz).$^{13}$C NMR (126 MHz, CD$_3$OD) δ 181.3, 175.0, 140.3, 133.7, 129.4, 127.7, 124.1, 124.0, 89.9, 65.9, 60.8, 39.7, 38.0, 28.7, 25.4, 15.4, 9.0.

*Irradiation experiments for mechanistic purposes*

Two 1 x 10$^{-3}$ M solutions of etodolac in H$_2$O/CH$_3$CN (9:1, v/v) and CH$_3$CN were prepared by dissolving 5 mg in 17.4 mL. Each solution was irradiated in open quartz tubes with UV-B lamps and analysed by HPLC (system D), LC-MS and $^1$H-NMR at selected times. A 1 x 10$^{-3}$ M solutions in H$_2$O/CH$_3$CN (9:1, v/v) was irradiated in closed quartz tubes after saturating with argon. The solution was analysed by HPLC (system D), LC-MS and $^1$H-NMR at selected times.

## 6.2.3  Rivastigmine

*Chemicals*

Rivastigmine (**1c**) was obtained by dissolving the salt (rivastigmine tartrate) in NaHCO$_3$ (sat.) and extracting with ethyl acetate.

*HPLC system*

HPLC experiments were carried out on an Agilent 1100 HPLC system, equipped with an UV detector, using a RP-18 column (Gemini, 5 μm, 110 A, 250 mm × 4.6 mm). The flow was set to 0.8 mL/min. The detector lamp was set at 254 nm. The column was equilibrated with a mixture of A (H$_2$O containing 1% formic acid)–B (acetonitrile) 9:1 (v/v). The run followed this programme: isocratic B 10% from the start to 7 min, an increase of B up to 90% from 7 to 12 min, isocratic B 90% for 11 min, return to B 10% in 2 min.

*Stability in aqueous solution in the dark*

Rivastigmine solutions (5 x $10^{-5}$ M) in water at pH 4, 7 and 9 were prepared. The acid and alkaline solutions were made using NaOH and HCl to adjust pH level. All solutions were kept in the dark and analysed by HPLC showing no degradation of drug after 48 h.

*Phototransformation kinetics and quantum yield*

Rivastigmine water solution (5 x $10^{-5}$ M) was irradiated in a photochemical setup (system IV). The concentration change with time was monitored by HPLC. The kinetic constant and the quantum yield were determined as reported in section *6.1.4*.

*Sunlight irradiation of rivastigmine*

A solution of rivastigmine in water (1 x $10^{-5}$ M) was exposed to sunlight in closed pyrex tubes in September–October 2010 in Naples and analysed by HPLC after 6, 12 and 20 days.

*Preparative experiments for photoproducts isolation*

A solution of rivastigmine (32 mg) was dissolved in 128 mL of Milli-Q $H_2O/CH_3CN$ (9:1, v/v, 1 x $10^{-3}$ M) and irradiated in open tubes with UV-B lamps for 5 h. Then, the solvents were evaporated under vacuum and the residue (20 mg) was separated by preparative TLC. Elution with $CH_2Cl_2$/AcOEt (8:2, v/v) gave a mixture of **4c** and **5c** (<1 mg), ketone **2c** (4 mg), alcohol **3c** (7 mg), an intractable material (5 mg) and rivastigmine (2 mg) at decreasing Rfs.

Rivastigmine (15 mg) dissolved in 60 mL of acetonitrile (1 x $10^{-3}$ M) was exposed in open tubes to UV-B lamps (System II) for 1 h. After evaporation of the solvent, preparative TLC of the residue as above gave ketone **2c** (10 mg) and the drug (1 mg). A solution of rivastigmine (15 mg) in methanol (60 mL, 1 x $10^{-3}$ M) was saturated with argon and irradiated in closed tubes to UV-B lamps for 5 h. After evaporation of the solvent, preparative TLC of the residue as above gave a fraction (1 mg) composed of **4c** and **5c** (in ca. 1:1 molar ratio), ether **6c** (3 mg) and rivastigmine (9 mg) (Fig. 2). Products **2c**, **3c** and **6** were fully characterized. Alkene **4c** and alkane **5c** were recovered as a 1:1 mixture in small amounts, therefore only $^1$H NMR data could be obtained and refer to this mixture.

*3-Acetylphenyl N-ethyl-N-methyl carbamate* (**2c**): EI-MS *m/z* 221 [M]$^{+\bullet}$, 177, 86, 58; UV $\lambda_{max}$ ($CH_3OH$) nm: 282 (log $\varepsilon$ 3.2); IR $\nu_{max}$ ($CHCl_3$) 1717, 1693, 1607, 1406 and

1168 cm$^{-1}$; $^1$H-NMR (500 MHz, CDCl$_3$) δ 7.70 (br s, 1H), 7.79 (d, 1H, *J*=8.0 Hz), 7.47 (t, 1H, *J*=8.0 Hz), 7.34 (br d, 1H, *J*=7.0 Hz), 3.49 and 3.41(q, 2H, *J*=7.0 Hz), 3.09 and 3.00 (s, 3H), 1.27 and 1.20 (t, 3H, *J*=7.0 Hz), 2.60 (s, 3H); $^{13}$C-NMR (126 MHz, CDCl$_3$) δ 197.2, 154.5, 154.3, 151.8, 138.4, 129.4, 126.7, 125.0, 121.6, 44.1, 19.9, 13.2, 12 .4.

*3-(1-Hydroxyethyl)phenyl N-ethyl-N-methyl carbamate* (**3c**): EI-MS *m/z* 223 [M]$^{+•}$, 86, 77, 58; UV λ$_{max}$ (CH$_3$OH) nm 252 (log ε 2.9); IR ν$_{max}$ (CHCl$_3$) 3626, 3501, 1716, 1600, 1172, 1014 cm$^{-1}$; $^1$H-NMR (500 MHz, CDCl$_3$) δ 7.32 (t, 1H, *J*=8.5 Hz), 7.18 (d, 1H, *J*=8.5 Hz), 7.14 (br s, 1H), 7.01 (br d, 1H, *J*=8.0 Hz), 4.88 (q, 1H, *J*=6.4 Hz), 3.48 and 3.41 (q, 2H, *J*=6.9 Hz), 3.07 and 2.99 (s, 3H), 1.48 (d, 3H, *J*=6.4 Hz), 1.24 and 1.19 (t, 3H, *J*=6.9 Hz); $^{13}$C-NMR (126 MHz, CDCl$_3$) δ 154.6, 154.4, 151.6, 147.4, 129.2, 122.1, 120.7, 118.8, 70.0, 44.1, 34.2, 33.8, 25.0, 13.2, 12.5.

*3-Vinylphenyl N-ethyl-N-methyl carbamate* (**4c**) and *3-ethylphenyl N-ethyl-N-methyl carbamate* (**5c**): (1:1 mixture); selected $^1$H-NMR signals for alkene **4c**: (500 MHz, CDCl$_3$) δ 7.30 (t, 1H, *J*=7.8 Hz), 7.22 (d, 1H, *J*=7.8 Hz), 7.16 (br s, 1H), 6.68 (dd, 1H, *J*=17.6 Hz and *J*=11.0 Hz), 5.74 and 5.26 (d, 2H, *J*=17.6 Hz and *J*=11.0 Hz); selected $^1$H-NMR signals for alkane **5c**: (500 MHz, CDCl$_3$) δ 7.25 (t, 1H, *J*=8.0 Hz), 7.02 (d, 1H, *J*=8.0 Hz), 6.95 (br s,1H), 2.65 (q, 2H, *J*=7.0 Hz), 1.23 (t, 3H, *J*=8.0 Hz); overlapping $^1$H-NMR signals: δ 6.92 (br s, 2H), 3.47 and 3.40 (2q, 4H, *J*=6.0 Hz), 3.06 and 2.99 (2s, 6H), 1.22 and 1.17 (2t, 6H, *J*=6.0 Hz).

*3-(1-methoxyethyl)phenyl N-ethyl-N-methyl carbamate* (**6c**): EI-MS *m/z* 237 [M]$^{+•}$, 236, 206, 86, 58; UV λ$_{max}$ (CH$_3$OH) nm: 261 (log ε 2.7); IR ν$_{max}$ (CHCl$_3$) 1715, 1608, 1236, 1168 cm$^{-1}$; $^1$H-NMR (500 MHz, CDCl$_3$) δ 7.06 (br s, 1H), 7.04 (br d, 1H, *J*=7.8 Hz), 7.33 (t, 1H, *J*=7.8 Hz), 7.13 (d, 1H, *J*=8.5 Hz), 4.29 (q, 1H, *J*=6.5 Hz), 1.42 (d, 3H, *J*=6.5 Hz), 3.48 and 3.41 (q, 2H, *J*=6.9 Hz), 1.25 and 1.19 (t, 3H, *J*=6.9 Hz), 3.07 and 2.99 (s, 3H), 3.23 (s, 3H); $^{13}$C-NMR (126 MHz, CDCl$_3$) δ 145.1, 119.5, 151.7, 120.8, 129.2, 122.8, 79.3, 23.8, 154.6, 154.3, 44.1, 13.2, 12.5, 34.2, 33.8, 56.6.


*Irradiation experiments for mechanistic purposes*

Four 1 x 10$^{-3}$ M solutions of rivastigmine in H$_2$O/CH$_3$CN (9:1, v/v), CH$_3$CN, CH$_3$OH, CH$_3$OH/CH$_3$CN (9:1, v/v) were prepared by dissolving 5 mg in 20 mL. Each solution was irradiated in open quartz tubes with UV-B lamps (System II) and analysed by HPLC and $^1$H-NMR at selected times. Similar irradiation experiments were performed as above in closed quartz tubes after saturating with argon. A further series of solutions

treated as above were irradiated for 1 h. Then, the solvents were evaporated and each residue was carefully analysed by $^1$H-NMR. The photoproducts in each mixture were identified by comparing the NMR signals with those of compounds, which were isolated and characterized by performing preparative photochemical experiments (see above). All the experiments were performed in triplicate. Samples of all solutions were kept in the dark and analysed as above showing no degradation after 48 h.

*Irradiation experiments with sensitizers.*

Three solutions of rivastigmine (5 mg) in 100 mL of H2O/CH3CN (9:1, v/v, 5 x 10$^{-4}$ M) in the presence of 0.3, 0.5, 0.7 equiv. of ketone **2c** were irradiated in closed quartz tubes with UV-B lamps (System II) and analysed by HPLC. Two solutions of rivastigmine (5 mg) in 100 mL of H2O/CH3CN (1:1, v/v, 5 x 10$^{-4}$ M) with and without 0.5 equiv. of 9,10-anthraquinone were irradiated in closed quartz tubes with UV-A lamps (centred at λ=360 nm) and analysed by HPLC.

*Laser flash photolysis studies*

For 266/355 nm excitation, experiments were carried out using the fourth/third harmonic of a Quanta Ray GCR 130-01 Nd:YAG laser system instrument, used in a right-angle geometry with respect to the monitoring light beam. The single pulses were ca. 9 ns in duration, with energy of ~60 mJ/pulse. Individual cuvette samples (V = 3 mL) were used for a maximum of four consecutive laser shots. The transient absorbance at the pre-selected wavelength was monitored by a detection system consisting of a pulsed xenon lamp (150 W), monochromator and a photomultiplier (1P28). A spectrometer control unit was used for synchronising the pulsed light source and programmable shutters with the laser output. The signal from the photomultiplier was digitised by a programmable digital oscilloscope (HP54522A). A 32 bits RISC-processor kinetic spectrometer workstation was used to analyse the digitised signal. The pseudo-first order decay constants of transient species were obtained by fitting the absorbance *vs* time data with single or double exponential equations. The error was calculated as 3σ from the fit of the experimental data. All experiments were performed at ambient temperature (295 ± 2 K) in aerated and argon-saturated solutions.

### 6.2.4 3-(1-Dimethylaminoethyl) phenol (1c')

*HPLC system*

HPLC experiments were carried out on an Agilent 1100 HPLC system, equipped with an UV detector, using a RP-18 column (Gemini, 5 μm, 110 A, 250 mm × 4.6 mm). The flow was set to 0.8 mL/min. The detector lamp was set at 254 nm. The column was equilibrated with a mixture of A ($H_2O$ containing 0.1% formic acid)–B (acetonitrile). The run followed this programme: isocratic B 10% from the start to 18 min, an increase of B up to 90% from 18 to 20 min, isocratic B 90% for 5 min, return to B 10% in 2 min.

*Stability in aqueous solution in the dark*

Solutions of compound **1c'** ($1 \times 10^{-3}$ M) in water:acetonitrile (9:1, v/v) at pH 4, 7 and 9 were prepared. The acid and alkaline solutions were made using NaOH and HCl to adjust pH level. All solutions were kept in the dark and analysed by HPLC showing no degradation of drug after 24 h.

*Phototransformation kinetics and quantum yield calculation*

Solutions of compound **1c'** in $H_2O/CH_3CN$ (9:1 v/v) at different concentrations ($5 \times 10^{-5}$ M and $1 \times 10^{-3}$ M) were irradiated in open quartz tubes (20 x 1 cm, 25 mL) by System II. The concentration change with time was monitored by HPLC. The kinetic constant and the quantum yield were determined as reported in section *6.1.4*.

*Preparative experiments for photoproducts isolation*

A solution of compound **1c'** (60 mg) was dissolved in 400 mL of Milli-Q $H_2O/CH_3CN$ (9:1, v/v, $1 \times 10^{-3}$ M) and irradiated in open tubes with UV-B lamps (System II) for 1 h. Then, the solvents was evaporated under vacuum and the residue was separated by preparative TLC. Elution with hexane/AcOEt (6:4, v/v) gave photoproduct **2c'** (44 mg). Compound **2c'** was identified by comparing its spectroscopic data [$^1$H-NMR (500 MHz, CD$_3$OD): δ 7.12 (t, 1H, *J*=8.0 Hz), 6.83-6.80 (m, 2H), 6.67-6.64(m, 1H), 4.74 (q, 1H, *J*=6.5 Hz),1.40(d, 3H, *J*=6.5 Hz); $^{13}$C-NMR (126 MHz, CD$_3$OD) δ 158.4, 149.2, 130.3, 117.7, 114.9, 113.3, 70.8, 25.5] with those reported (Sharma and Moses 2010).

*Irradiation experiments for mechanistic purposes*

Two $1 \times 10^{-3}$ M solutions of compound **1c'** in $H_2O/CH_3CN$ (9:1, v/v) were prepared by dissolving 5 mg in 30 mL. The first solution was irradiated (System II) in open quartz

tubes, the second solution was irradiated (System II) in closed quartz tubes after saturating with argon. Irradiations were analysed by HPLC and $^1$H-NMR. The photoproduct in each mixture was identified by comparing the NMR signals with those of standard compounds, which was isolated and characterized by performing preparative photochemical experiments (see above).

## *6.2.5  Loratidine*

### *HPLC system*

HPLC experiments were carried out on an Agilent 1100 HPLC system, equipped with an UV detector set at 254 nm, using a RP-18 column (Gemini, 5 μm, 110 A, 250 mm x 4.6 mm) with an isocratic elution at a flow rate of 0.8 mL min$^{-1}$ (formic acid 1.0% (A)/CH$_3$CN (B) 4:6, v/v).

### *Stability in aqueous solution in the dark*

Loratidine (**1d**) solutions (1 x 10$^{-4}$ M) in H$_2$O/CH$_3$CN (9:1, v/v) at pH 4, 7 and 9 were prepared. The acid and alkaline solutions were made using NaOH and HCl to adjust pH level. All solutions were kept in the dark and analysed by HPLC showing no degradation of drug after 48 h.

### *Phototransformation kinetics and quantum yield*

Loratidine solution (1 x 10$^{-4}$ M) in H$_2$O/CH$_3$CN (9:1, v/v) was irradiated by System II, in quartz tubes (25 mL). The concentration change with time was monitored by HPLC. The kinetic constant and the quantum yield were determined as reported in section *6.1.4*.

### *Sunlight irradiation of loratidine*

A solution of loratidine 1 x 10$^{-4}$ M in H$_2$O/CH$_3$CN (9:1, v/v) was exposed to sunlight in a closed quartz tube in February 2013 in Naples and analysed by HPLC after 1, 2 and 4 days.

### *Preparative experiments for photoproducts isolation*

Loratidine (50 mg) was dissolved in 130 mL of H$_2$O/CH$_3$CN (75:25, v/v, 1 x 10$^{-3}$ M) and irradiated by UV-B lamps (System II). The irradiation mixture was analysed at

different time by HPLC and GC-MS. After 1 h of irradiation the solvents were evaporation under vacuum, and the mixture was separated by preparative TLC. Elution with $Et_2O$ gave compounds **2d** (15 mg), **3d** (8 mg), **4d** (13 mg) and loratidine (5 mg).

*8-Chloro-6,11-dihydro-5H-benzo[5,6]cyclohepta[1,2-b]pyridine* (**3d**): EI-MS: *m/z* 229 $[M]^{+\bullet}$; UV $\lambda_{max}$ ($CH_3OH$) nm 279 (log $\varepsilon$ 3.1); IR $\nu_{max}$ ($CHCl_3$) 1650, 1070 $cm^{-1}$; ^{1}H-NMR (500 MHz, $CDCl_3$): $\delta$ 8.38 (s, 1H), 7.66 (d, 1H, *J*=7.3 Hz), 7.30 (d, 1H, *J*=8.0 Hz), 7.18-7.13 (m, 2H), 4.56 (s, 2H), 3.20 (br s, 4H); ^{13}C-NMR (126 MHz, $CDCl_3$) $\delta$ 156.9, 146.5, 140.8, 137.7, 136.0, 133.8, 132.3, 130.7, 128.9, 126.3, 120.2, 35.7, 31.3.

*1(2H)-Pyridinecarboxylic acid, 4-(8-chloro-6,11-dihydro-5H-benzo[5,6]cyclohepta [1,2-b]pyridin-11-yl)-3,6-dihydro-, ethyl ester* (**4d**): EI-MS: *m/z* 382 $[M]^{+\bullet}$; UV $\lambda_{max}$ ($CH_3OH$) nm 266 (log $\varepsilon$ 3.8); IR $\nu_{max}$ ($CHCl_3$) 3684, 1690, 1371 $cm^{-1}$; ^{1}H-NMR (500 MHz, $CDCl_3$): $\delta$ 8.39 (d, 1H, *J*=4.0 Hz), 7.42 (d, 1H, *J*=7.3 Hz), 7.20-7.12 (m, 4H), 4.86 (br s, 1H), 4.80 (br s, 1H), 4.10 (q, 2H, *J*=7.1 Hz), 3.88 (m, 2H), 3.53-3.30 (m, 4H), 2.81 (m, 1H), 2.71 (m, 1H), 1.87 (m, 1H), 1.79 (m, 1H); ^{13}C-NMR (126 MHz, $CDCl_3$) $\delta$ 157.0, 155.5, 146.8, 141.8, 138.5, 135.9, 135.9, 135.0, 133.1, 133.0, 131.1, 129.8, 126.3, 122.4, 121.1, 62.3, 61.2, 43.4, 40.5, 31.3, 29.9, 28.0, 14.9.

<u>*Irradiation experiments for mechanistic purposes*</u>

A 1 x $10^{-3}$M solution of loratidine in $H_2O/CH_3CN$ (75:25, v/v) was irradiated (System II) in closed quartz tubes after saturating with argon. The solution was analysed by HPLC and ^{1}H-NMR at selected times.

A 1 x $10^{-3}$M solution of loratidine in $CH_3CN$ was irradiated (System II) in open quartz tubes. The solution was analysed by HPLC and ^{1}H NMR at selected times.

## 6.2.6  Chlorpropham

<u>HPLC system</u>

HPLC experiments were carried out on an Agilent 1100 HPLC system, equipped with an UV detector (set at 230 nm), using a RP-18 column (Gemini, 5 μm, 110 A, 250 x 4.6 mm). A mixture of A ($H_2O$ containing 1% formic acid) – B (acetonitrile) 1:1 v/v was used as mobile phase at a constant flow rate of 1.2 mL/min.

*Stability in aqueous solution in the dark*

Chlorpropham solutions ($5 \times 10^{-5}$ M) in water:acetonitrile (9:1, v/v) at pH 4, 7 and 9 were prepared. The acid and alkaline solutions were made using NaOH and HCl to adjust pH level. All solutions were kept in the dark and analysed by HPLC showing no degradation of drug after 48 h.

*Phototransformation kinetics and quantum yield*

Chlorpropham (**1e**) solution ($5 \times 10^{-5}$ M) in water/acetonitrile (9:1, v/v) was irradiated by System II, in quartz tubes (25 mL). The concentration change with time was monitored by HPLC. The kinetic constant and the quantum yield were determined as reported in section *6.1.4*.

*Sunlight irradiation of chlorpropham*

Chlorpropham solutions ($5 \times 10^{-5}$ M) in $H_2O/CH_3CN$ (9:1 v/v) were exposed to sunlight in five closed quartz tubes in July-August 2012 in Naples and analysed by HPLC after 10, 30 and 60 days. After 60 days the five solutions were unified and concentrated. The resulting mixture has analysed carefully by HPLC and $^1$H-NMR using authentic phenol **2e** as standard.

*Preparative experiments for photoproducts isolation*

A $1 \times 10^{-3}$ M solution of chlorpropham (40 mg) in 188 mL of $H_2O/CH_3CN$ (9:1 v/v) was irradiated in open quartz tubes with UV-B lamps for 1 h. Then, the solvents were evaporated under vacuum and the residue was analysed by NMR and then was separated by preparative TLC. Elution with $CH_2Cl_2$/AcOEt (9:1 v/v) gave chlorpropham **1e** (24 mg), photoproduct **2e** (10 mg) and **3e** (4 mg). Compound **2e** was identified by comparing its spectroscopic data ($^1$H-NMR) with those reported (Guzik 1978), compound and **3e** was fully characterized.

*Isopropyl 3-hydroxyphenylcarbamate* (**2e**): EI-MS *m/z* 195 [M]$^{+\bullet}$, 153, 136, 109; UV $\lambda_{max}$ ($H_2O/CH_3CN$ 9:1 v/v) nm 235 (log $\varepsilon$ 3.7), 280 nm (log $\varepsilon$ 3.1); IR $\nu_{max}$ (CHCl$_3$) 3576, 3425, 1729, 1604, 1525 cm$^{-1}$; $^1$H-NMR (500 MHz, CDCl$_3$) δ 7.33 (br s, 1H), 7.13, (t, 1H, *J*=8.1 Hz), 6.65 (d, 1H, *J*=8.0 Hz), 6.63 (s, 1H), 6.56 (d, 1H, *J*=8.0 Hz), 6.38 (br s, 1H), 5.01 (sept, 1H, *J*=6.5 Hz), 1.30 (d, 6H, *J*=6.5 Hz); $^{13}$C-NMR (126 MHz, CDCl$_3$) δ 157.1, 153.7, 139.2, 130.2, 110.8, 110.6, 106.0, 69.4, 22.3.

*Isopropyl 3-acetamidophenylcarbamate* (**3e**): oil; EI-MS *m/z* 236 $[M]^{+\bullet}$, 194, 177, 152, 108; UV $\lambda_{max}$ ($H_2O/CH_3CN$ 1:1 v/v) 225 nm (log 3.7), 280 nm (log 2.7); IR $\nu_{max}$ ($CHCl_3$) 3417, 1724, 1683, 1606, 1515, 1219, 1110 $cm^{-1}$; $^1$H-NMR (500 MHz, $CDCl_3$) δ 7.65 (s, 1H), 7.23 (d, 2H, *J*=7.1 Hz), 7.15 (br s, 1H), 7.11 (m, 1H), 6.56 (br s, 1H), 5.00 (sept, 1H, *J*=6.3 Hz), 2.16 (s, 3H), 1.30 (d, 6H, *J*=6.2 Hz); $^{13}$C-NMR (126 MHz, $CDCl_3$) δ 163.6, 153.4, 138.7, 138.6, 129.6, 114.3, 109.7, 68.9, 24.6, 22.0.

*Photoproduct **2e** irradiation*

A solution of **2e** (4 mg) in 20 mL of $H_2O/CH_3CN$ (9:1 v/v, 1 x $10^{-3}$ M) was irradiated in open quartz tubes with UV-B lamps (System II) and analysed by HPLC and $^1$H-NMR at selected times. After 10h analyses have showed no degradation.

*Irradiation in different solvents*

Four 1 x $10^{-3}$ M solutions of chlorpropham in $H_2O/CH_3CN$ (99:1, v/v), $H_2O/CH_3CN$ (9:1, v/v), $H_2O/CH_3CN$ (1:1, v/v), $CH_3CN$ were prepared by dissolving 5 mg in 23 mL. Each solution was irradiated for 1 h in open quartz tubes with UV-B lamps (System II) and analysed by HPLC and $^1$H-NMR. The photoproducts in each mixture were identified by comparing the NMR signals with those of standard compounds, which were isolated and characterized by performing preparative photochemical experiments (see above).

## 6.2.7 Phenisopham

### HPLC system

HPLC experiments were carried out on an Agilent 1100 HPLC system, equipped with an UV detector (set at 230 nm), using a RP-18 column (Gemini, 5 μm, 110 A, 250 x 4.6 mm). A mixture of A ($H_2O$ containing 1% formic acid) – B (acetonitrile) 1:1 v/v was used as mobile phase at a constant flow rate of 1.2 mL/min.

### Stability in aqueous solution in the dark

Phenisopham solutions (5 x $10^{-5}$ M) in water:acetonitrile (9:1, v/v) at pH 4, 7 and 9 were prepared. The acid and alkaline solutions were made using NaOH and HCl to adjust pH level. All solutions were kept in the dark and analysed by HPLC showing no degradation of drug after 48 h.

*Phototransformation kinetics and quantum yield*

Phenisopham (**1f**) solution (5 x $10^{-5}$ M) in water/acetonitrile (9:1, v/v) was irradiated by System II, in quartz tubes (25 mL). The concentration change with time was monitored by HPLC. The kinetic constant and the quantum yield were determined as reported in section *6.1.4*.

*Sunlight irradiation of phenisopham*

Phenisopham solutions (5 x $10^{-5}$ M) in $H_2O/CH_3CN$ (9:1 v/v) were exposed to sunlight in five closed quartz tubes in July-August 2012 in Naples and analysed by HPLC after 10, 30 and 60 days. After 60 days the five solutions were unified and concentrated. The resulting mixture has analysed carefully by HPLC and $^1$H-NMR using compounds **2f-6f** as standard.

*Preparative experiments for photoproducts isolation*

A 1 x $10^{-3}$ M solution of phenisopham (50 mg) in 146 mL of $H_2O/CH_3CN$ (7:3 v/v) was irradiated in open quartz tubes with UV-B lamps (System II) for 2 h. Then, the solvents were evaporated under vacuum and the residue was separated by preparative TLC. Elution with $CH_2Cl_2/AcOEt$ (9:1 v/v) gave phenisopham **1f** (15 mg), photoproducts **5f** (2 mg), **2f** (<1 mg), **6f** (4 mg) and **4f** (25 mg) at decreasing Rfs. Product **2f** was identified by comparison of its proton spectrum with that reported (Guzik 1978). Products **4f**, **5f** and **6f** were fully characterized.

*Isopropyl 2-(ethyl(phenyl)carbamoyl)-3-hydroxyphenylcarbamate* (**4f**): oil; EI-MS *m/z* 342 $[M]^{+\bullet}$, 180, 162, 121, 106; UV $\lambda_{max}$ ($H_2O/CH_3CN$ 1:1 v/v) nm 230 (log ε 3.0), 270 nm (log ε 2.4); IR $\nu_{max}$ ($CHCl_3$) 3561, 3411, 1731, 1685, 1635, 1627, 1210 cm$^{-1}$; $^1$H-NMR (500 MHz, $CDCl_3$) δ 7.19-7.17 (m, 2H), 7.07 (t, 2H, *J*=8.0 Hz), 7.01 (d, 2H, *J*=9.0 Hz), 6.90 (br s, 1H), 6.81 (d, 1H, *J*=8.1 Hz), 6.50 (d, 1H, *J*=8.0 Hz), 4.96 (sept, 1H, *J*=6.5 Hz), 4.10 (m, 1H), 3.86 (m, 1H), 1.33-1.20 (m, 9H). $^{13}$C-NMR (126 MHz, $CDCl_3$) δ 171.0, 168.0, 154.6, 152.7, 141.1, 135.5, 131.5, 128.6, 127.3, 126.6, 112.3, 111.4, 68.9, 45.2, 22.1, 14.2.

*Isopropyl 4-(ethyl(phenyl)carbamoyl)-3-hydroxyphenylcarbamate* (**5f**): oil; EI-MS *m/z* 342 $[M]^{+\bullet}$, 222, 180, 148, 121; UV $\lambda_{max}$ ($H_2O/CH_3CN$ 1:1 v/v) nm 232 (log ε 1.9), 273 nm (log ε 2.4); IR $\nu_{max}$ ($CHCl_3$) 3628, 3424, 1730, 1630, 1626, 1209 cm$^{-1}$; $^1$H-NMR (500 MHz, $CDCl_3$) δ 11.57 (s, 1H), 7.33 (t, 2H, *J*=9.0 Hz), 7.27 (m, 1H), 7.10 (d, 2H, *J*=9.0 Hz), 6.86 (d, 1H, *J*=2.0 Hz), 6.54 (d, 1H, *J*=9.0 Hz), 6.43-6.35 (br m, 2H), 4.96

(sept, 1H, *J*=6.5 Hz), 3.93 (q, 2H, *J*=7.0 Hz), 1.25 (d, 6H, *J*=6.5 Hz), 1.21 (t, 3H, *J*=7.0 Hz); $^{13}$C-NMR (126 MHz, CDCl$_3$) δ 170.7, 162.5, 152.9, 152.7, 152.4, 141.9, 131.5, 129.6, 127.5, 127.2, 107.5, 106.1, 69.0, 46.5, 21.9, 12.5.

*Isopropyl 4-(ethyl(phenyl)carbamoyl)-5-hydroxyphenylcarbamate* (**6f**): oil; EI-MS *m/z* 342 [M]$^{+\bullet}$, 180, 162, 121, 106; UV λ$_{max}$ (H$_2$O/CH$_3$CN 1:1 v/v) nm 233 (log ε 3.3), 278 nm (log ε 2.7); IR ν$_{max}$ (CHCl$_3$) 3583, 3300, 1722, 1648, 1627, 1214 cm$^{-1}$; $^1$H-NMR (500 MHz, CDCl$_3$) δ 9.29 (s, 1H), 7.78 (d, 1H, *J*=1.5 Hz), 7.26-7.23 (m, 2H), 7.16 (t, 1H, *J*=8.0 Hz), 6.99 (d, 2H, *J*=8.0 Hz), 6.74 (d, 1H, *J*=8.0 Hz), 6.60 (br s, 1H), 6.09 (dd, 1H, *J*=8.0 Hz and *J*=1.5 Hz), 4.99 (sept, 1H, *J*=6.5 Hz), 3.98 (q, 2H, *J*=7.0 Hz), 1.31 (d, 6H, *J*=6.5 Hz), 1.24 (t, 3H, *J*=7.0 Hz); $^{13}$C-NMR (126 MHz, CDCl$_3$) δ 170.4, 158.4, 156.9, 153.7, 143.9, 140.9, 132.4, 129.7, 127.6, 126.9, 108.9, 106.4, 69.4, 46.0, 22.5, 13.4.

## *Photoproducts irradiation*

Solutions of amides **4f** (1.5 mg), **5f** (1.5 mg) and **6f** (1.5 mg) in 22 mL of H$_2$O/CH$_3$CN (8:2 v/v, 2 x 10$^{-4}$ M) were irradiated in open quartz tubes with UV-B lamps (System II) and analysed by $^1$H-NMR. After 4h analyses showed no degradation.

Solution of aniline **3f** (1.2 mg) in 20 mL of H$_2$O/CH$_3$CN (9:1 v/v, 5 x 10$^{-4}$ M) was irradiated in open quartz tubes with UV-B lamps (System II) and analysed by $^1$H-NMR. After 4 h analyses showed complete degradation in a not identified products mixture.

## 6.2.8 Model carbamic compounds

### *HPLC system*

HPLC system used was HPLC system D, see section 6.2.2.

### *Synthesis of model carbamic compounds 1g-l*

In a typical experimental procedure, to a solution of each aniline (15 mmol) in dichloromethane dry (26 mL), 1.6 mL of phenyl chloroformate (13 mmol) was added dropwise. The mixture was stirred at 0°C for 1 h and then it was kept at room temperature for 30 min. The reaction mixture was neutralized with a saturated solution of sodium hydrogen carbonate and extracted with CH$_2$Cl$_2$ (3 x 50 mL). The combined organic layers were washed with brine, dried with anhydrous sodium sulfate, filtered and evaporated under reduced pressure. The residue was purified by silica column

chromatography using light petroleum/diethyl ether 7:3 v/v (light petroleum/EtOAc 7:3 and 9:1 v/v for compounds **1i** and **1k**, respectively) to give carbamic compounds **1g-l** with yields generally > 95%.

Products **1g** (Shivarkar et al. 2004), **1i** (Shivarkar et al. 2004), **1k** (Shivarkar et al. 2004), and **1l** (Imori and Togo 2006) were identified by comparison of their NMR spectra with those reported in literature. New products **1h** and **1j** were fully characterized.

*Phenyl 3-chlorophenyl(ethyl)carbamate* (**1h**): oil; EI-MS *m/z* 275 [M]$^{+\bullet}$, 182, 153; UV $\lambda_{max}$ (H$_2$O/CH$_3$CN 1:1) nm 236 (log ε 3.7); IR $\nu_{max}$ (CHCl$_3$) 1731, 1401 cm$^{-1}$; $^1$H-NMR (500 MHz, CDCl$_3$) δ 7.36-7.17 (m, overlapped signals, 9H), 3.83 (br q, 2H), 1.25 (br t, 3H); $^{13}$C NMR (126 MHz, CDCl$_3$) δ 153.3, 151.2, 142.6, 134.5, 130.0, 129.2, 127.5, 127.1, 125.4, 121.5, 45.8, 13.6.

*Phenyl 4-chlorophenyl(ethyl)carbamate* (**1j**): mp 75.9-76.7 °C; EI-MS *m/z* 275 [M]$^{+\bullet}$, 182, 153; UV $\lambda_{max}$ (H$_2$O/CH$_3$CN 1:1) nm 238 (log ε 4.1); IR $\nu_{max}$ (CHCl$_3$) 1722, 1394 cm$^{-1}$; $^1$H-NMR (500 MHz, CDCl$_3$): δ 7.38-7.25 (m, overlapped signals, 6H), 7.18 (t, 1H, *J*=7.3 Hz), 7.10 (br s, 2H), 3.81 (br q, 2H), 1.23 (br t, 3H); $^{13}$C-NMR (126 MHz, CDCl$_3$) δ 153.3, 151.1, 139.8, 132.4, 129.1, 128.5, 125.2, 121.4, 45.6, 13.4.

## *Synthesis of model carbamic compounds 1m*

To a solution of 3-hydroxyacetanilide (**7m**) (6.6 mmol) in dichloromethane dry (6.3 mL) and triethylamine in catalytic amount (one drop) 0.7 mL of phenyl isocyanate (6.3 mmol) was added dropwise. The mixture was stirred at room temperature for 1 h. To the reaction mixture 6 mL of water was added and the mixture was extracted with CH$_2$Cl$_2$ (3 x 6 mL). The combined organic layers were washed with brine, dried with anhydrous sodium sulfate, filtered and evaporated under reduced pressure. The product **1m** was purified by crystallization with chloroform-methanol-petroleum ether and fully characterized.

*3-acetamidophenyl phenylcarbamate* (**1m**): mp 171.3-174.8 °C; EI-MS *m/z* 270 [M]$^{+\bullet}$, 150, 120; UV $\lambda_{max}$ (H$_2$O/CH$_3$CN 1:1) nm 238 (log ε 5.2); IR $\nu_{max}$ (CHCl$_3$) 3428, 1758 (C=O), 1692, 1515, 1079, 1009 cm$^{-1}$; $^1$H-NMR (500 MHz, CDCl$_3$) δ 7.55 (t, 1H, *J*=1.8 Hz), 7.48 (d, 2H, *J*=7.9 Hz), 7.37-7.29 (m, 4H), 7.06 (t, 1H, *J*=7.4 Hz), 6.93 (dd, 1H, *J*=7.9 Hz and *J*=1.8 Hz), 2.12 (s, 3H); $^{13}$C-NMR (126 MHz, CDCl$_3$) δ 171.7, 154.0, 152.5, 141.0, 139.7, 130.4, 129.9, 124.5, 120.1, 118.3, 117.8, 114.6, 23.8.

1 x 10$^{-3}$ M solutions of each model carbamate (**1g-m**) in H$_2$O/CH$_3$CN 1:1 (v/v) were irradiated in open quartz tubes by System II. The solutions were analysed by HPLC and $^1$H-NMR at different times. The irradiation experiments were not stopped until starting compound was degraded at least for 20-30%. The content of all tubes was collected and evaporated. The residue was analysed by $^1$H-NMR and then chromatographed.

Samples of all solutions were kept in the dark and analysed as above showing no degradation after 48 h.

Irradiation of compound **1g** (50 mg, 202 mL of solvents) was run for 4 h. The residue was analysed by NMR and then separated by TLC, eluting with light petroleum/EtOAc 7:3 (v/v), to give unreacted **1g** (28 mg) and photoproducts **2g** (9 mg) and **3g** (10 mg). Compound **2g** was identified by comparison of their proton NMR spectra with those reported in literature (Akita et al. 2005). Compound **3g** was fully characterized.

*Phenyl (3-acetamidophenyl)carbamate* (**3g**): oil; EI-MS *m/z* 270 [M]$^{+\bullet}$, 176, 134, 94; UV λ$_{max}$ (H$_2$O/CH$_3$CN 1:1) nm 228 (log ε 3.8); IR ν$_{max}$ (CHCl$_3$) 3436, 1754, 1695, 1532, 1099, 1015 cm$^{-1}$; $^1$H-NMR (500 MHz, CDCl$_3$) δ 7.75 (br s, 1H), 7.39 (t, 2H, *J*=7.9 Hz), 7.29-7.22 (m, 4H), 7.18 (d, 3H, *J*=7.5 Hz), 7.04 (br s, 1H), 2.16 (s, 3H); $^{13}$C-NMR (126 MHz, CDCl$_3$) δ 168.4, 151.6, 150.5, 138.6, 138.1, 129.7, 129.4, 125.7, 121.6, 115.0, 114.5, 110.1, 24.6.

Irradiation of compound **1h** (50 mg, 182 mL of solvents) was carried out for 14 h. The residue was analysed by NMR and then separated by TLC, eluting with light petroleum/Et$_2$O 6:4 (v/v), to give unreacted **1h** (38 mg) and photoproducts **2h** (4 mg) and **3h** (6 mg). Photoproducts were fully characterized.

*Phenyl ethyl(3-hydroxyphenyl)carbamate* (**2h**): oil; EI-MS *m/z* 257 [M]$^{+\bullet}$, 164, 136; UV λ$_{max}$ (H$_2$O/CH$_3$CN 1:1) nm 275 (log ε 3.4); IR ν$_{max}$ (CHCl$_3$) 3597, 3349, 2293, 2256, 1716 (C=O), 1594, 1401 cm$^{-1}$; $^1$H-NMR (500 MHz, CDCl$_3$): δ 7.38 (t, 2H, *J*=7.6 Hz), 7.23 (t, 1H, *J*=8.0 Hz), 7.30 (t, 1H, *J*=7.3 Hz), 7.10 (d, 2H, *J*=4.5 Hz), 6.87 (d, 1H, *J*=7.9 Hz), 6.78 (s, 1H), 6.72 (d, 1H, *J*=7.8 Hz), 3.80 (br q, 2H), 1.24 (br t, 3H); $^{13}$C-NMR (126 MHz, CDCl$_3$) δ 156.2, 153.7, 151.3, 142.5, 129.9, 129.2, 125.3, 121.6, 119.4, 114.6, 114.2, 45.8, 13.5.

*Phenyl 3-acetamidophenyl(ethyl)carbamate* (**3h**): oil; EI-MS *m/z* 298 [M]$^{+\bullet}$, 205, 177, 135; UV λ$_{max}$ (H$_2$O/CH$_3$CN 1:1) nm 275 (log ε 3.2), 244 (log ε 4.0); IR ν$_{max}$ (CHCl$_3$)

3438 (N-H), 3342 , 1716, 1607, 1397 cm$^{-1}$; $^1$H-NMR (500 MHz, CDCl$_3$): δ 7.61 (s, 1H), 7.52 (s, 1H), 7.33-7.29 (m, overlapped signals, 4H), 7.16 (t, 1H, $J$=7.1 Hz), 7.10 (br s, 2H), 7.04 (d, 1H, $J$=7.2 Hz), 3.81 (br q, 2H), 2.12 (s, 3H), 1.24 (br t, 3H). $^{13}$C-NMR (126 MHz, CDCl$_3$) δ 168.3, 153.6, 151.2, 141.8, 138.7, 129.3, 129.1, 125.2, 122.8, 121.6, 118.7, 118.1, 45.8, 24.4, 13.5.

Irradiation of compound **1i** (70 mg, 255 mL of solvents) was carried out for 2 h. The residue was analysed by NMR and then separated by TLC, eluting with light petroleum/Et$_2$O 6:4 (v/v), to give unreacted **1i** (6 mg) and photoproducts **2i** (5 mg), **3i** (11 mg) and **8i** (=**1k**) (20 mg) and polymeric material (24 mg). Compound **8i** (=**1k**) was identified by comparison of their proton NMR spectra with those reported in literature (Shivarkar et al. 2004). Compounds **2i** and **3i**, were identified by comparison of their proton NMR spectra with those of authentic samples.

Irradiation of compound **1j** (90 mg, 327 mL of solvents) was carried out for 10 h. The residue was analysed by NMR and then separated by TLC, eluting with light petroleum/Et$_2$O 3:7 (v/v), to give unreacted **1j** (64 mg), photoproduct **3j** (10 mg), and polymeric material (8 mg).

*Phenyl 4-acetamidophenyl(ethyl)carbamate* (**3j**): mp 156.6-159.0 °C; EI-MS *m/z* 298 [M]$^{+\bullet}$, 205, 177, 135; UV λ$_{max}$ (H$_2$O/CH$_3$CN 1:1) nm 250 (log ε 10.2); IR ν$_{max}$ (CHCl$_3$) 3441, 1717, 1602, 1517, 1389 cm$^{-1}$; $^1$H-NMR (500 MHz, CD$_3$OD): δ 7.63 (d, 4H, $J$=9.0 Hz), 7.34 (br m, 2H), 7.31 (d, 2H, $J$=9.3 Hz), 7.20 (br m, 1H), 7.05 (br s, 1H), 4.10 (q, 2H, $J$=7.1 Hz), 2.16 (s, 3H), 1.24 (t, 3H, $J$=7.1 Hz). $^{13}$C-NMR (126 MHz, CD$_3$OD) δ 172.2, 154.3, 153.2, 130.9, 129.6, 127.0, 123.2, 122.2, 47.5, 24.3, 14.0.

Irradiation of compound **1k** (80 mg, 375 mL of solvents) was carried out for 42 h. The residue was analysed by NMR and then separated by TLC, eluting with light petroleum/Et$_2$O 1:1 (v/v), to give unreacted **1k** (74 mg), a mixture of **1k** and **4k** (3 mg, ca. 7:3 molar ratio), a mixture of **6k** and **9** (2 mg, ca 2:3 molar ratio). **4k** and **6k** were identified by comparing the NMR signals with those reported after rejecting the signals of **1k** and **9**, respectively.

Compounds **4k** (Ma et al. 2012) and **6k** (Ma et al. 2012) were identified by comparison of their proton NMR spectra with those reported in literature. Compound **9** was identified by comparison of their proton NMR spectra with those of authentic samples.

Irradiation of compound **1l** (45 mg, 187 mL of solvents) was carried out for 42 h. The residue was analysed by NMR and then separated by TLC, eluting with light petroleum/Et$_2$O 1:1 (v/v), to give unreacted **1l** (32 mg) and photoproducts **6l** (3 mg), **9** (5 mg), a mixture of products among which **4l** was identified (20%). All photoproducts were identified by comparison of their proton NMR spectra with those of authentic samples.

Irradiation of compound **1m** (70 mg, 260 mL of solvents) was carried out for 42 h. The residue was analysed by NMR and then separated by TLC, eluting with CH$_2$Cl$_2$/EtOAc 9:1 (v/v), to give unreacted **1m** (55 mg), **6m** (3 mg), **7m** (2 mg) and a fraction (5 mg) composed of **4m** and **5m** (in ca. 1:1.2 molar ratio).

*2-Acetamido-6-hydroxy-N-phenylbenzamide* (**4m**) and *4-acetamido-2-hydroxy-N-phenyl benzamide* (**5m**): (1:1.2 mixture); selected ^{1}H-NMR signals for **4m**: (500 MHz, CD$_3$OD) δ 7.20 (t, 1H, $J$=8.0 Hz), 6.66 (d, 1H, $J$=8.3 Hz), 6.40 (d, 1H, $J$=7.8 Hz); selected ^{1}H-NMR signals for **5m**: (500 MHz, CD$_3$OD) δ 7.82 (d, 1H, $J$=8.8 Hz), 6.58 (d, 1H, $J$=2.3 Hz), 6.44 (d, 1H, $J$=8.8 Hz).

*2-Acetamido-4-hydroxy-N-phenylbenzamide* (**6m**): selected ^{1}H-NMR signals (500 MHz, CD$_3$OD) δ 7.69 (t, 1H, $J$=8.2 Hz), 7.63-7.55 (m, 3H), 7.41 (m, 2H), 7.13 (d, 1H, $J$=8.1 Hz), 6.88 (d, 1H, $J$=8.2 Hz), 2.21 (s, 3H).

*Irradiation in different solvents*

A 1 x 10$^{-3}$ M solution of **1g** in H$_2$O/CH$_3$CN (7:3, v/v) was prepared by dissolving 5 mg in 20 mL and was irradiated for 1 h in open quartz tubes with UV-B lamps (System II) and analysed by HPLC and ^{1}H-NMR. The analysis showed the presence of **1g**, **2g** and **3g** in 70, 25 and 5 %, respectively. The photoproducts in each mixture were identified by comparing the NMR signals with those of standard compounds, which were isolated and characterized by performing preparative photochemical experiments (see above).

## 6.3   INDIRECT PHOTOLYSIS

### 6.3.1 Detection of hydroxyl radicals

The hydroxyl radical formation rate ($R^f_{\bullet OH}$) was determined by using Terephthalic acid (TA) as trapping molecule. TA reacts with hydroxyl radical leading to the formation of

2-hydroxyterephthalic acid (TAOH) with a yield ($Y_{TAOH}$) determined as the ratio between the initial formation rate of TAOH ($R_{TAOH}^{f}$) and the initial degradation rate of TA ($R_{TA}^{d}$) ranged between 12 and 30 % which depends on the pH and temperature of aqueous media (Charbouillot et al. 2011). This method represents a simple and fast detection of photogenerated $^{\bullet}$OH with a high sensitivity that allows us to detect up to 10 nM of $^{\bullet}$OH.

In order to calculate the formation rate of $^{\bullet}$OH as a function of different aqueous media composition, different solutions were irradiated (System V) in the same media used for xenobiotics photochemical experiments. An aliquot of solution (3 mL) was withdrawn and putted in a fluorescence cuvette at fixed intervals times. The cuvette was transferred into a spectrofluorimeter and TAOH was quantified by using a calibration curve previously performed by using standard solution of TAOH. The concentration of TA used during all experiments was comprised between 500 µM and 1 mM in order to trap all photogenerated $^{\bullet}$OH.


## 6.3.2 Rivastigmine

### HPLC system

HPLC system (Waters Alliance) equipped with a diode array detector was used for rivastigmine analysis. An Eclipse XDB-C18 column (Agilent, 4.6 x 150 mm, 5 µm) and a gradient elution at a flow rate of 1.0 mL min$^{-1}$ were used. The gradient was: at initial time 10 % acetonitrile and 90 % water acidified with 3‰ phosphoric acid for 7 min, followed by a linear gradient to 90 % acetonitrile within 8 min. Then, the same ratio was maintained constant for 8 min followed by a linear gradient to 10 % acetonitrile within 2 min. This ratio was maintained constant for 5 min. UV detector was settled at 210 nm.

An LC-MS system (Agilent 1100 Series, binary pump) equipped with an ESI ion source (MSD VL) and an UV detector was used for rivastigmine degradation products identification. The adopted column was a Sphere Clone C18 column (Phenomenex, 4.6 x 250 mm, 5 µm) and the gradient elution was: at initial time 30 % acetonitrile and 70 % water acidified with 1% formic acid, followed by a linear gradient to 75 % acetonitrile within 55 min. Then, the same ratio was maintained constant for 20 min. The flow rate was 0.4 mL min$^{-1}$ and the UV detector was settled at 254 nm.

*Photoinduced degradation and data analysis.*

The experiments were performed either in milli-q water or in natural water. The solutions in milli-q water were prepared by mixing different concentrations of hydrogen peroxide (188μM, 376μM, 550μM 752μM), or nitrates (200μM, 400μM, 5mM) or nitrites (5.4μM, 10μM, 50μM, 100μM) to a constant concentration of rivastigmine (45μM). The irradiations were carried out with irradiation System V. In order to follow the irradiation experiments the solutions were analysed by HPLC injecting an aliquot (200μL) taken at different times.

The time evolution of rivastigmine in the presence of photochemical sources of $^{\bullet}OH$ could be fitted with a pseudo-first order equation $C_0 = C_t e^{-kt}$ where $C_0$ was the initial rivastigmine concentration, $C_t$ the concentration at time $t$ and k the pseudo-first order degradation rate constant. The error bounds associated to the rate data represent $3\sigma$, derived from the scattering of the experimental data around the fitting curves (intra-series variability).

*Phototransformation products identification*

Three experiment were conducted using a rivastigmine concentration of ($4 \times 10^{-3}$ M) in the presence of hydrogen peroxide 3.5mM (experiment A), nitrates 15mM (experiment B) and nitrite 50 μM (experiment C). After 48 hours of irradiation the solution were analysed using an LC- MS.

*Irradiations in natural waters*

Lake, river and rain waters, sampled on July 2011, were collected in order to perform hydroxyl radical measurement and rivastigmine degradation studies. River water and lake water come from Artiere river and Chambon lake respectively, both located in the Puy de Dôme region, France. Artiere river passes through Clermont-Ferrand agglomeration, Chambon lake is in the massif of Dore mountains at 877 m above sea level. Rain water was collected on the 1st November 2011 at the "Cézeaux" (south of Clermont-Ferrand) located at 394 m of altitude on the south of Clermont-Ferrand city.

Natural water samples, collected using a glass bottle, were filtered on 0.20 μm membranes (Minisart®, Sartorium Stedim) and stored under refrigeration. Irradiation experiments were performed the day after, while, for analysis by ion chromatography (IC) inorganic and organic concentrations were determined no more than 24 hours after

sampling. An suitable amount of rivastigmine was added to natural waters in order to obtain a 45μM concentration of drug. The solutions were irradiated by System V.


## 6.3.3 Nicotine

### HPLC system

An HPLC system (Waters Em-Power) equipped with a diode array detector was used for nicotine analysis. An Eclipse XDB-C18 column (Agilent, 4.6 x 150 mm, 5 μm) and an isocratic elution at a flow rate of 0.6 mL min$^{-1}$ were used (formic acid 0.5%(A)/MeOH(B) 98:2, v/v). UV detector was settled at 259 nm.


### Stability in aqueous solution in the dark

A nicotine solution (25 x 10$^{-6}$ M) in water was kept in the dark and analysed by UV-visible spectrum and HPLC showing no degradation of drug after 48 h.


### Photoinduced degradation and data analysis

The experiments were performed either in milli-q water. The solutions in milli-q water were prepared by mixing different concentrations of hydrogen peroxide (200μM, 250μM, 350μM, 700μM), or nitrates (500μM, 1mM, 2.5mM, 5mM) or nitrites (10μM, 25μM, 50μM) to a constant concentration of nicotine (25μM). The irradiations were carried out with irradiation System V. In order to follow the irradiation experiments the solutions were analysed by UV-visible spectra and by HPLC injecting an aliquot (200μL) taken at different times.

The time evolution of nicotine in the presence of photochemical sources of $^{\bullet}$OH could be fitted with a pseudo-first order equation $C_0 = C_t e^{-kt}$ where $C_0$ was the initial rivastigmine concentration, $C_t$ the concentration at time $t$ and k the pseudo-first order degradation rate constant. The error bounds associated to the rate data represent $3\sigma$, derived from the scattering of the experimental data around the fitting curves (intra-series variability).

## 6.4 PHOTOTRANSFORMATION IN SOIL

### 6.4.1 Model soils preparation

Three type of model soils were used during phototransformation experiments. The three model soils prepared are: sandy soil (SS), bentonitic soil (BS) and kaleonitic soil (KS). Each soil was prepared mixing the components according to the procedure reported in literature (Lo and Yang 1999):

| Compound | Sandy Soil (SS) | Bentonitic Soil (BS) | Kaolinitic Soil (KS) |
|---|---|---|---|
| $SiO_2$ | 78 | 33,5 | 33,5 |
| Kaolin [$Al_2Si_2O_5(OH)_4$] | - | - | 60 |
| Bentonite [$Al_2O_3 4SiO_2 H_2O$] | 20 | 60 | - |
| $CaCO_3$ | 0,5 | 5 | 5 |
| $Fe_2O_3$ | 0,25 | 0,25 | 0,25 |
| $MnO_2$ | 0,25 | 0,25 | 0,25 |
| Humic Acid | 1 | 1 | 1 |

**Table 13**. Composition of synthetic soils (wt%).

### 6.4.2 Phototransformation in dry soils

Xenobiotic-soil dispersions were prepared by adding a xenobiotic solution (10 mg in 20 mL of $CH_3OH$) to 5 g of model soil to obtain a concentration xenobiotic/soil of 2 mg (xenobiotic)/ 1g (soil). The mixture was stirred at room temperature for 5 h to allow evaporation of the solvent and the homogeneous distribution of xenobiotic in the soil. The xenobiotic-soil samples were distributed uniformly on the surface of a plate (diameter 18.5 cm) to give an average soil thickness of about 0.5-1.5 mm. The samples of soil were speared in two samples, the first was irradiate by System VI and the second one was kept in the dark.

After irradiation the xenobiotic was extracted with organic solvents from soil layer by vacuum filtration on büchner funnel with filter paper. In particular, the soil was washed with organic solvents (20 mL of $CH_2Cl_2$, 20 mL of $CH_3OH$). All the solvents were evaporated under reduced pressure and the residue was analysed by NMR. Analogues procedure was applied to extract xenobiotics from soils kept in the dark.

### 6.4.3 Phototransformation in wet soils

Xenobiotic-soil dispersions were prepared by adding a xenobiotic solution (10 mg in 20 mL of $CH_3OH$) to 5 g of model soil to obtain a concentration xenobiotic/soil of 2 mg (xenobiotic)/ 1g (soil). The mixture was stirred at room temperature for 5 h to allow evaporation of the solvent and the homogeneous distribution of xenobiotic in the soil. The samples of soil were speared in two samples and in both 10 mL of water was added. One soil sample was irradiated by System VI and the second one was kept in the dark. The xenobiotic-soil samples were distributed uniformly on the surface of a plate (diameter 18.5 cm) to give an average soil thickness of about 0.5-1.5 mm.

After irradiation the xenobiotics were extracted from soil by vacuum filtration on büchner funnel with filter paper, the soil was washed with organic solvents (50 mL of $CH_2Cl_2$ and 2x50 mL of AcOEt/$CH_3OH$ (7:3 v/v). The solvents were evaporated under reduced pressure and the residue was analysed by NMR. Analogues procedure was applied to extract the material from soils kept in the dark.

### 6.4.4 Rivastigmine

*Phototransformation in dry soils*

Samples rivastigmine-soil were prepared as reported in section 6.4.2 and were irradiated by System II and System VI for 30 minute, 1 and 2 hours.

*Phototransformation in wet soils*

Samples rivastigmine-soil were prepared as reported in section 6.4.3 and were irradiated by System II and System VI for 30 minute, 1 and 2 hours.

### 6.4.5 Loratidine

*Phototransformation in dry soils*

Samples loratidine-soil were prepared as reported in section 6.4.2  and were irradiated by System II and System VI for 30 minute, 1, 2, 3, 4 and 5 hours.

*Phototransformation in wet soils*

Samples loratidine-soil were prepared as reported in section 6.4.3 and were irradiated by System II and System VI for 30 minute, 1, 2, 3, 4 and 5 hours.

*Procedures for isolation and characterization of phototransformation products*

From irradiation (5h) of loratidine in sandy soil, both dry and wet, the photoproduct **4d** was isolated by preparative TLC (elution with Et$_2$O/Petroleum ether (9:1 v/v)). Photoproduct **4d** was identified by comparing the NMR signals with those of standard compound, which was isolated and characterized by performing preparative aqueous photochemical experiments (section 6.2.5).

## 6.4.6 17-α-Ethinylestradiol

*Phototransformation in dry soils*

Samples 17-α-ethinylestradiol-soil were prepared as reported in section 6.4.2 and were irradiated by System II and System VI for 3, 5, 10, 15, and 20 hours.

*Phototransformation in wet soils*

Samples 17-α-ethinylestradiol-soil were prepared as reported in section 6.4.3 and were irradiated by System II and System VI for 3, 5, 10, 15, and 20 hours.

## 6.4.7 Carboxin

*Phototransformation in dry soils*

Samples of carboxin in sandy soil were prepared as reported in section 6.4.2 and were irradiated by System II for 2 hours.

*Phototransformation in wet soils*

Samples of carboxin in sandy soil were prepared as reported in section 6.4.3 and were irradiated by System II for 2 hours.

*Procedures for isolation and characterization of phototransformation products*

From irradiation (2h) of carboxin in sandy soil, both dry and wet, the photoproducts **2p**, **3p** and **4p** were isolated by preparative TLC and were identified by comparing their spectroscopic data with those reported in literature (Cermola and Iesce 2002; DellaGreca et al. 2004b).

# 6.0 BIBLIOGRAPHY

Abounassif MA, El-Obeid HA, Gadkariem EA. 2005. Stability studies on some benzocycloheptane antihistaminic agents. J. Pharm. Biomed. Anal. 36(5):1011-1018.

Agnihotri VP. 1986. Degradation of carboxin by mycoflora isolated from sugarcane rhizosphere. Indian Phytopathol. 39(3):418-22.

Akita S, Umezawa N, Higuchi T. 2005. On-bead fluorescence assay for serine/threonine kinases. Org. Lett. 7(25):5565-5568.

Albinet A, Minero C, Vione D. 2010. Photochemical generation of reactive species upon irradiation of rainwater: negligible photoactivity of dissolved organic matter. Sci. Total Environ. 408(16):3367-3373.

Andreozzi R, Raffaele M, Nicklas P. 2003. Pharmaceuticals in STP effluents and their solar photodegradation in aquatic environment. Chemosphere 50(10):1319-1330.

Armbrust KL, Crosby DG. 1991. Fate of carbaryl, 1-naphthol, and atrazine in seawater. Pac. Sci. 45(3):314-20.

Balasubramanya RH, Patil RB. 1980. Degradation of carboxin and oxycarboxin by microorganisms. Plant Soil 57(2-3):457-61.

Bar-On P, Millard CB, Harel M, Dvir H, Enz A, Sussman JL, Silman I. 2002. Kinetic and structural studies on the interaction of cholinesterases with the anti-alzheimer drug rivastigmine. Biochemistry 41(11):3555-3564.

Benowitz NL. 1998. Nicotine safety and toxicity. Benowitz NL, editor. New York: Oxford University Press 203 p.

Berendes U, Blaschke G. 1996. Simultaneous determination of the phase II metabolites of the non steroidal anti-inflammatory drug etodolac in human urine. Enantiomer 1(4-6):415-422.

Bezares-Cruz JC, Poyer IC, Nienow A, Hua I, Jafvert CT. 2007. Direct and indirect (via $H_2O_2$) UV photodegradation of nicotine in water. Abstracts of Papers, 233rd ACS National Meeting, Chicago (IL), United States, March 25-29, 2007:SUST-149.

Bhadouria BS, Mathur VB, Kaul R. 2012. Monitoring of organochlorine pesticides in and around Keoladeo National Park, Bharatpur, Rajasthan, India. Environ. Monit. Assess. 184(9):5295-5300.

Bi N-M, Ren M-G, Song Q-H. 2010. Photo-Ritter reaction of arylmethyl bromides in acetonitrile. Synth. Commun. 40(17):2617-2623.

Bosca F, Marin ML, Miranda MA. 2004. Photodecarboxylation of acids and lactones: antiinflammatory drugs. In: Lenci F, Horspool W, editors. CRC Handbook of Organic Photochemistry and Photobiology. 2nd ed. Boca Raton (Fl): CRC Press. p 64/1-64/10.

Bosca F, Miranda MA, Vano L, Vargas F. 1990. New photodegradation pathways of Naproxen, a phototoxic non-steroidal anti-inflammatory drug. J. Photochem. Photobiol. A, 54(1):131-4.

Boule P. 1999. Part L: Reactions and processes: environmental photochemistry. In: Boule P, editor. The Handbook of Environmental Chemistry. New York: Springer-Verlag. p 359.

Boule P, Meunier L, Bonnemoy F, Boulkamh A, Zertal A, Lavedrine B. 2002. Direct phototransformation of aromatic pesticides in aqueous solution. Int. J. Photoenergy 4(2):69-78.

Boxall ABA, Sinclair CJ, Fenner K, Kolpin D, Maund SJ. 2004. When synthetic chemicals degrade in the environment. Environ. Sci. Technol. 38(19):368A-375A.

Brown LR, Flavin C, Kane H. 1996. Contains important information on key agricultural and environmental trends. In: Institute W, editor. Vital signs: the trends that are shaping our future. New York: Island Press. p 169.

Buerge IJ, Kahle M, Buser H-R, Mueller MD, Poiger T. 2008. Nicotine derivatives in wastewater and surface waters: application as chemical markers for domestic wastewater. Environ. Sci. Technol. 42(17):6354-6360.

Burrows HD, Canle L M, Santaballa JA, Steenken S. 2002. Reaction pathways and mechanisms of photodegradation of pesticides. J. Photochem. Photobiol. B, 67(2):71-108.

Buxton GV, Greenstock CL, Helman WP, Ross AB. 1988. Critical review of rate constants for reactions of hydrated electrons, hydrogen atoms and hydroxyl radicals ($^\bullet$OH/$^\bullet$O$^-$) in aqueous solution. J. Phys. Chem. Ref. Data 17(2):513-886.

Calamari D, Zuccato E, Castiglioni S, Bagnati R, Fanelli R. 2003. Strategic survey of therapeutic drugs in the rivers Po and Lambro in northern Italy. Environ. Sci. Technol. 37(7):1241-1248.

Cermola F, DellaGreca M, Iesce MR, Montanaro S, Previtera L, Temussi F, Brigante M. 2007. Irradiation of fluvastatin in water. J. Photochem. Photobiol. A, 189(2-3):264-271.

Cermola F, Iesce MR. 2002. Substituent and solvent effects on the photosensitized oxygenation of 5,6-dihydro-1,4-oxathiins. Intramolecular oxygen transfer *vs* normal cleavage of the dioxetane intermediates. J. Org. Chem. 67(14):4937-4944.

Cerniglia CE. 1992. Biodegradation of polycyclic aromatic hydrocarbons. Biodegradation 3(2-3):351-68.

Charbouillot T, Brigante M, Mailhot G, Maddigapu PR, Minero C, Vione D. 2011. Performance and selectivity of the terephthalic acid probe for $^\bullet$OH as a function of temperature, pH and composition of atmospherically relevant aqueous media. J. Photochem. Photobiol. A, 222(1):70-76.

Chiron S, Comoretto L, Rinaldi E, Maurino V, Minero C, Vione D. 2009. Pesticide by-products in the Rhone delta (Southern France). The case of 4-chloro-2-methylphenol and of its nitroderivative. Chemosphere 74(4):599-604.

Chiron S, Minero C, Vione D. 2007. Occurrence of 2,4-dichlorophenol and of 2,4-dichloro-6-nitrophenol in the Rhone river delta (Southern France). Environ. Sci. Technol. 41(9):3127-3133.

Chowdhury MAZ, Banik S, Uddin B, Moniruzzaman M, Karim N, Gan SH. 2012. Organophosphorus and carbamate pesticide residues detected in water samples collected from paddy and vegetable fields of the Savar and Dhamrai Upazilas in Bangladesh. Int. J. Environ. Res. Public Health 9:3318-3329.

Claridge RFC, Fischer H. 1983. Self-termination and electronic spectra of substituted benzyl radicals in solution. J. Phys. Chem. 87(11):1960-7.

Clonfero E. 1997. Genetic toxicity of urban air particulate matter. Med. Lav. 88(1):13-23.

Cohen SG, Stein NM. 1971. Kinetics of photoreduction of benzophenones by amines. Deamination and dealkylation of amines. J. Amer. Chem. Soc. 93(24):6542-51.

Cosa G, Scaiano JC. 2004. Laser techniques in the study of drug photochemistry. Photochem. Photobiol. 80(2):159-174.

Dabestani R, Sik RH, Davis DG, Dubay G, Chignell CF. 1993. Spectroscopic studies of cutaneous photosensitizing agents. XVIII. Indomethacin. Photochem. Photobiol. 58(3):367-73.

Daughton CG, Ternes TA. 1999. Pharmaceuticals and personal care products in the environment: agents of subtle change? Environ. Health Perspect. Suppl. 107(6):907-938.

David B, Lhote M, Faure V, Boule P. 1998. Ultrasonic and photochemical degradation of chlorpropham and 3-chloroaniline in aqueous solution. Water Res. 32(8):2451-2461.

De Bertrand N, Barcelo D. 1991. Photodegradation of the carbamate pesticides aldicarb, carbaryl and carbofuran in water. Anal. Chim. Acta 254(1-2):235-44.

De Guidi G, Ragusa S, Cambria MT, Belvedere A, Catalfo A, Cambria A. 2005. Photosensitizing effect of some nonsteroidal antiinflammatory drugs on natural and artificial membranes: dependence on phospholipid composition. Chem. Res. Toxicol. 18(2):204-212.

DellaGreca M, Brigante M, Isidori M, Nardelli A, Previtera L, Rubino M, Temussi F. 2004a. Phototransformation and ecotoxicity of the drug Naproxen-Na. Environ. Chem. Lett. 1(4):237-241.

DellaGreca M, Iesce MR, Cermola F, Rubino M, Isidori M. 2004b. Phototransformation of carboxin in water. Toxicity of the pesticide and its sulfoxide to aquatic organisms. J. Agric. Food Chem. 52(20):6228-6232.

Demtroeder W. 2008. Laser spectroscopy. Demtroeder W, editor. Berlin: Springer-Verlag.

Disanayaka BW, Weedon AC. 1987. Charge transfer fluorescence of some *N*-benzoylindoles. Can. J. Chem. 65(2):245-50.

Duggan DE, Hogans AF, Kwan KC, McMahon FG. 1972. Metabolism of indomethacin in man. J. Pharmacol. Exp. Ther. 181(3):563-75.

Dulin D, Mill T. 1982. Development and evaluation of sunlight actinometers. Environ. Sci. Technol. 16(11):815-20.

EEA. 2011. European Environmental Agency. Environmental Risk Assessment: approaches, experiences and information sources. http://www.eea.europa.eu/publications/GH-07-97-595-EN-C2/riskindex.html.

Eke KR. 1996. Pesticides in the aquatic environment in England and Wales. Pestic. Outlook 7(2):15-20.

Ekiz-Guecer N, Reisch J. 1991. Photochemical studies, 58. Photostability of indomethacin in the crystalline state. Pharm. Acta Helv. 66(3):66-7.

Ellis JB. 2006. Pharmaceutical and personal care products (PPCPs) in urban receiving waters. Environ. Pollut. 144(1):184-189.

Escher BI, Fenner K. 2011. Recent advances in environmental risk assessment of transformation products. Environ. Sci. Technol. 45(9):3835-3847.

ExToxNet. 1996. Extension Toxixology Network. Pesticide information profiles (PIPs): Carboxin. http://extoxnet.orst.edu/pips/carboxin.htm. Oregon State University.

Farre M, Perez S, Kantiani L, Barcelo D. 2008. Fate and toxicity of emerging pollutants, their metabolites and transformation products in the aquatic environment. TrAC, Trends Anal. Chem. 27(11):991-1007.

Fava L, Orru MA, Scardala S, Alonzo E, Fardella M, Strumia C, Martinelli A, Finocchiaro S, Previtera M, Franchi A and others. 2010. Pesticides and their metabolites in selected Italian groundwater and surface water used for drinking. Ann. Ist. Super. Sanita 46(3):309-316.

Fischer M, Warneck P. 1996. Photodecomposition of nitrite and undissociated nitrous acid in aqueous solution. J. Phys. Chem. 100(48):18749-18756.

Fleming SA, Pincock JA. 1999. Photochemical cleavage reactions of benzyl-heteroatom sigma bonds. In: Ramamurthy V, Schanze KS, editors. Organic Molecular Photochemistry: Marcel Dekker. p 211-281.

Galadi A, Julliard M. 1996. Photosensitized oxidative degradation of pesticides. Chemosphere 33(1):1-15.

González MC, San Román E. 2005. Environmental photochemistry in heterogeneous media. In: Boule P, Bahnemann D, Robertson P, editors. Handbook of Environmental Chemistry. Berlin: Springer. p 49–75.

Griveau Y, Bremer H, Pfenning M; 20090616, assignee. 2009. Ternary herbicidal compositions comprising aminopyralid and imazamox and at least one other herbicide. Germany patent 2009-EP57408-2009153246.

Guzik FF. 1978. Photolysis of isopropyl 3-chlorocarbanilate in water. J. Agric. Food Chem. 26(1):53-5.

Halling-Sorensen B, Nors Nielsen S, Lanzky PF, Ingerslev F, Holten Lutzhoft HC, Jorgensen SE. 1998. Occurrence, fate and effects of pharmaceutical substances in the environment - A review. Chemosphere 36(2):357-93.

Harris J. 1982. Rates of direct aqueous photolysis. In: McGraw-Hill, editor. Handbook of Chemical Property Estimation Methods: Environmental Behavior of Organic Compounds. New York: American Chemical Society

Hebert VR, Miller GC. 1990. Depth dependence of direct and indirect photolysis on soil surfaces. J. Agric. Food Chem. 38(3):913-18.

Hoshina K, Horiyama S, Matsunaga H, Haginaka J. 2011. Simultaneous determination of non-steroidal anti-inflammatory drugs in river water samples by liquid chromatography-tandem mass spectrometry using molecularly imprinted polymers as a pretreatment column. J. Pharm. Biomed. Anal. 55(5):916-922.

Huang J, Mabury SA. 2000. The role of carbonate radical in limiting the persistence of sulfur-containing chemicals in sunlit natural waters. Chemosphere 41(11):1775-1782.

Huerta-Fontela M, Galceran MT, Martin-Alonso J, Ventura F. 2008. Occurrence of psychoactive stimulatory drugs in wastewaters in north-eastern Spain. Sci. Total Environ. 397(1-3):31-40.

Iesce MR, Cermola F, De Lorenzo F, Graziano ML, Caliendo B. 2002. Photochemical behavior of the systemic fungicide carboxin. Environ. Sci. Pollut. Res. Int. 9(2):107-109.

Iesce MR, Cermola F, Temussi F. 2005. Photooxygenation of heterocycles. Curr. Org. Chem. 9(2):109-139.

Iesce MR, della Greca M, Cermola F, Rubino M, Isidori M, Pascarella L. 2006. Transformation and ecotoxicity in carbamic pesticides in water. Environ. Sci. Pollut. Res. Int. 13(2):105-109.

Imori S, Togo H. 2006. Efficient demethylation of *N,N*-dimethylanilines with phenyl chloroformate in ionic liquids. Synlett(16):2629-2632.

Isidori M, Coppola E, Iesce MR, Cermola F, Papa G, Parrella A. 2012. Comparative abiotic or biotic degradation of carboxin by two Entisols with different surface properties or Pseudomonas aeruginosa strain: A toxicity study using the crustacean Thamnocephalus platyurus. J. Environ. Sci. Health, Part B 47(9):891-900.

Iwafune T, Inao K, Horio T, Iwasaki N, Yokoyama A, Nagai T. 2010. Behavior of paddy pesticides and major metabolites in the Sakura River, Ibaraki Japan. J. Pestic. Sci. 35(2):114-123.

Jahan K, Ordonez R, Ramachandran R, Balzer S, Stern M. 2008. Modeling biodegradation of nonylphenol. Water, Air, Soil Pollut.: Focus 8(3-4):395-404.

Janex-Habibi M-L, Huyard A, Esperanza M, Bruchet A. 2009. Reduction of endocrine disruptor emissions in the environment: The benefit of wastewater treatment. Water Res. 43(6):1565-1576.

Jjemba PK. 2006. Excretion and ecotoxicity of pharmaceutical and personal care products in the environment. Ecotoxicol. Environ. Saf. 63(1):113-130.

Johnston LJ, Schepp NP. 1993. Reactivities of radical cations: characterization of styrene radical cations and measurements of their reactivity toward nucleophiles. J. Am. Chem. Soc. 115(15):6564-71.

Jorgensen SE, Halling-Sorensen B. 2000. Drugs in the environment. Chemosphere 40(7):691-699.

Jou F-Y, Freeman GR. 1977. Shapes of optical spectra of solvated electrons. Effect of pressure. J. Phys. Chem. 81(9):909-15.

Jurgens MD, Holthaus KIE, Johnson AC, Smith JJL, Hetheridge M, Williams RJ. 2002. The potential for estradiol and ethinylestradiol degradation in English rivers. Environ. Toxicol. Chem. 21(3):480-488.

Kalshetty BM, Gani RS, Chandrasekhar VM, Kalashetti MB. 2012. Synthesis and evaluation of some new ethoxy-indole derivatives as potential antimicrobial agents. J. Chem., Biol. Phys. Sci. 2(4):1759-1772.

Kaneko S, Okumura K, Numaguchi Y, Matsui H, Murase K, Mokuno S, Morishima I, Hira K, Toki Y, Ito T and others. 2000. Melatonin scavenges hydroxyl radical and protects isolated rat hearts from ischemic reperfusion injury. Life Sci. 67(2):101-112.

Kim I, Yamashita N, Tanaka H. 2009. Photodegradation of pharmaceuticals and personal care products during UV and UV/$H_2O_2$ treatments. Chemosphere 77(4):518-525.

Kopf G, Schwack W. 1995. Photodegradation of the carbamate insecticide ethiofencarb. Pestic. Sci. 43(4):303-9.

Kress N, Herut B, Galil BS. 2004. Sewage sludge impact on sediment quality and benthic assemblages off the Mediterranean coast of Israel - A long-term study. Marine Environmental Research 57(3):213-233.

Lam MW, Tantuco K, Mabury SA. 2003. PhotoFate: a new approach in accounting for the contribution of indirect photolysis of pesticides and pharmaceuticals in surface waters. Environ. Sci. Technol. 37(5):899-907.

Larson RA, Zepp RG. 1988. Reactivity of the carbonate radical with aniline derivatives. Environ. Toxicol. Chem. 7(4):265-74.

Lee YJ, Padula J, Lee HK. 1988. Kinetics and mechanisms of etodolac degradation in aqueous solutions. J. Pharm. Sci. 77(1):81-6.

Leifer A. 1988. The kinetics of environmental aquatic photochemistry: theory and practice. Leifer A, editor. Washington: American Chemical Society 304 p.

Lentza-Rizos C, Balokas A. 2001. Residue levels of chlorpropham in individual tubers and composite samples of postharvest-treated potatoes. J. Agric. Food Chem. 49(2):710-714.

Leonard BE. 1995. Mechanisms of action of antidepressants. CNS Drugs 4(1):1-12.

Liu B, Wu F, Deng N-S. 2003. UV-light induced photodegradation of 17α-ethynylestradiol in aqueous solutions. J. Hazard. Mater. 98(1-3):311-316.

Lo IMC, Yang XY. 1999. EDTA extraction of heavy metals from different soil fractions and synthetic soils. Water, Air, Soil Pollut. 109(1-4):219-236.

Lopez-Serna R, Petrovic M, Barcelo D. 2012. Direct analysis of pharmaceuticals, their metabolites and transformation products in environmental waters using on-line TurboFlow[TM] chromatography-liquid chromatography-tandem mass spectrometry. J. Chromatogr. A, 1252:115-129.

Ma F, Xie X, Zhang L, Peng Z, Ding L, Fu L, Zhang Z. 2012. Palladium-catalyzed amidation of aryl halides using 2-dialkylphosphino-2'-alkoxyl-1,1'-binaphthyl as ligands. J. Org. Chem. 77(12):5279-5285.

Mack J, Bolton JR. 1999. Photochemistry of nitrite and nitrate in aqueous solution: a review. J. Photochem. Photobiol. A, 128(1-3):1-13.

Mallory FB, Mallory CW. 1988. Organic reactions. In: Dauben WG, editor. Organic Reactions. Malabar: Krieger Publishing Company.

Matamoros V, Duhec A, Albaiges J, Bayona JM. 2009. Photodegradation of carbamazepine, ibuprofen, ketoprofen and 17α-ethinylestradiol in fresh and seawater. Water, Air, Soil Pollut. 196(1-4):161-168.

Mateen A, Chapalamadugu S, Kaskar B, Bhatti AR, Chaudhry GR. 1994. Microbial metabolism of carbamate and organophosphate pesticides. Biol. Degrad. Biorem. Toxic Chem.:198-233.

Mateo CA, Urrutia A, Rodriguez JG, Fonseca I, Cano FH. 1996. Photooxygenation of 1,2,3,4-tetrahydrocarbazole: synthesis of spiro[cyclopentane-1,2'-indolin-3'-one]. J. Org. Chem. 61(2):810-12.

McGimpsey WG, Goerner H. 1996. Photoionization of indole, *N*-methylindole and tryptophan in aqueous solution upon excitation at 193 nm. Photochem. Photobiol. 64(3):501-509.

Mehnert E, Schock SC, Barnhardt ML, Caughey ME, Chou SFJ, Dey WS, Dreher GB, Ray C. 1995. The occurrence of agricultural chemicals in Illinois' rural private wells: results from the pilot study. Ground Water Monit. Rem. 15(1):142-9.

Metcalf RL. 1971. Pesticides in the environment. In: White-Stevens R, editor. Chemistry and Biology of Pesticides. New York: Marcel Dekker.

Meyer I, Oertling H, Hillebrand N, Goemann C, Brodhage R; 20100525, assignee. 2010. Menthyl carbamate compounds as active anti-cellulite ingredients. Germany patent 2010-EP57117-2010089421.

Mill T. 1999. Predicting photoreaction rates in surface waters. Chemosphere 38(6):1379-1390.

Miranda MA, Galindo F. 2004. Photo-Fries reaction and related processes. In: Lenci F, Horspool W, editors. CRC Handbook of Organic Photochemistry and Photobiology. Boca Raton (Fl): CRC Press. p 42-1-11.

Moore DE, Chappuis PP. 1988. A comparative study of the photochemistry of the non-steroidal anti-inflammatory drugs, naproxen, benoxaprofen and indomethacin. Photochem. Photobiol. 47(2):173-80.

Morais S, Dias E, de Lourdes Pereira M. 2012. Human exposure to pesticides. In: Jokanović M, editor. The Impact of Pesticides. First Edition ed. Cheyenne (WY): AcademyPublish.org.

Mudry CA, Frasca AR. 1973. Photooxidation of indole derivatives. Tetrahedron 29(4):603-13.

Murray KE, Thomas SM, Bodour AA. 2010. Prioritizing research for trace pollutants and emerging contaminants in the freshwater environment. Environ. Pollut. 158(12):3462-3471.

Musa KAK, Eriksson LA. 2010. Theoretical investigation of NSAID photodegradation mechanisms. Quantum Biochem. 2:805-834.

Mustazza C, Borioni A, Del Giudice MR, Gatta F, Ferretti R, Meneguz A, Volpe MT, Lorenzini P. 2002. Synthesis and cholinesterase activity of phenylcarbamates related to rivastigmine, a therapeutic agent for Alzheimer's disease. Eur. J. Med. Chem. 37(2):91-109.

Nakagawa M, Matsuki K, Hasegawa K, Hino T. 1982. Isolation and reactions of 7a-hydroperoxy-1,2,3,4,6,7,7a,12b-octahydroindolo[2,3-a]quinolizine. J. Chem. Soc., Chem. Commun.(13):742-3.

Nayak P. 2010. Commonly used photosensitizing medications: their adverse effects and precautions to be considered. Int. J. Pharm. Sci. Rev. Res. 4(2):135-140.

Nelieu S, Kerhoas L, Sarakha M, Einhorn J. 2004. Nitrite and nitrate induced photodegradation of monolinuron in aqueous solution. Environ. Chem. Lett. 2(2):83-87.

Nienow AM, Hua I, Poyer IC, Bezares-Cruz JC, Jafvert CT. 2009. Multifactor statistical analysis of $H_2O_2$-enhanced photodegradation of nicotine and phosphamidon. Ind. Eng. Chem. Res. 48(8):3955–3963.

OECD. 2000. Draft document: Phototransformation of chemicals in water - Direct and indirect photolysis: OECD Publishing.

OECD. 2008. Test No. 316: Phototransformation of chemicals in water - Direct photolysis: OECD Publishing.

Oldroyd DL, Weedon AC. 1991. Solvent- and wavelength-dependent photochemistry of N-benzoylindole and N-ethoxycarbonylindole. J. Photochem. Photobiol. A, 57(1-3):207-16.

Oldroyd DL, Weedon AC. 1994. Intramolecular photochemical cycloaddition reactions of N-[(ω-alkenyloxy)carbonyl]indoles and N-(ω-alkenoyl)indoles. J. Org. Chem. 59(6):1333-43.

Onoue S, Tsuda Y. 2006. Analytical studies on the prediction of photosensitive/phototoxic potential of pharmaceutical substances. Pharm. Res. 23(1):156-164.

Paiga P, Morais S, Correia M, Alves A, Delerue-Matos C. 2009. Screening of carbamates and ureas in fresh and processed tomato samples using microwave-assisted extraction and liquid chromatography. Anal. Lett. 42(2):265-283.

Pari K, Sundari CS, Chandani S, Balasubramanian D. 2000. β-Carbolines that accumulate in human tissues may serve a protective role against oxidative stress. J. Biol. Chem. 275(4):2455-2462.

Pawelczyk E, Knitter B, Knitter K. 1977. Kinetics of drug decomposition. Part 50: Graphic method for calculation of zero-order rate constants of sequential reaction of indomethacin photodegradation. Pharmazie 32(8-9):483-5.

Petrick LM, Svidovsky A, Dubowski Y. 2011. Thirdhand smoke: heterogeneous oxidation of nicotine and secondary aerosol formation in the indoor environment. Environ. Sci. Technol. 45(1):328-333.

Pincock JA, Wedge PJ. 1994. The photochemistry of methoxy-substituted benzyl acetates and benzyl pivalates: homolytic vs heterolytic cleavage. J. Org. Chem. 59(19):5587-95.

Pitchumani K, Madhavan D. 2004. Induced diastereoselectivity in photodecarboxylation reactions. In: Lenci F, Horspool W, editors. CRC Handbook of Organic Photochemistry and Photobiology 2nd ed. Boca Raton (Fl): CRC Press. p 65/1-65/14.

Pommier F, Frigola R. 2003. Quantitative determination of rivastigmine and its major metabolite in human plasma by liquid chromatography with atmospheric-pressure chemical-ionization tandem mass spectrometry. J. Chromatogr., B: Anal. Technol. Biomed. Life Sci. 784(2):301-313.

Ramanathan R, Reyderman L, Kulmatycki K, Su AD, Alvarez N, Chowdhury SK, Alton KB, Wirth MA, Clement RP, Statkevich P and others. 2007. Disposition of loratadine in healthy volunteers. Xenobiotica 37(7):753-769.

Rao BM, Srinivasu MK, Kumar KP, Bhradwaj N, Ravi R, Mohakhud PK, Reddy GO, Kumar PR. 2005. A stability indicating LC method for rivastigmine hydrogen tartrate. J. Pharm. Biomed. Anal. 37(1):57-63.

Rodriguez S, Santos A, Romero A. 2011. Effectiveness of AOP's on abatement of emerging pollutants and their oxidation intermediates: Nicotine removal with Fenton's Reagent. Desalination In Press, Corrected Proof.

RxList. The Internet Drug Index; http://www.rxlist.com/indocin-drug.htm.

Salem MY, El-Kosasy AM, El-Bardicy MG, Abd El-Rahman MK. 2010. Spectrophotometric and spectrodensitometric methods for the determination of rivastigmine hydrogen tartrate in presence of its degradation product. Drug Test. Anal. 2(5):225-233.

Samanidou V, Fytianos K, Pfister G, Bahadir M. 1988. Photochemical decomposition of carbamate pesticides in natural waters of northern Greece. Sci. Total Environ. 76(1):85-92.

Sanz-Asensio J, Plaza-Medina M, Martinez-Soria MT, Perez-Clavijo M. 1999. Study of photodegradation of the pesticide ethiofencarb in aqueous and non-aqueous media, by gas chromatography-mass spectrometry. J. Chromatogr. A, 840(2):235-247.

Schutt L, Bunce NJ. 2004. Photodehalogenation of aryl halides. In: Horspool W, Lenci, F. , editor. CRC Handbook of Organic Photochemistry and Photobiology. 2nd ed. Boca Raton (Fl): CRC Press. p 38-1-18.

Schwarzenbach RP, Gschwend PM, Imboden DM. 2003. Environmental organic chemistry. Hoboken: John Wiley & Sons.

Semple KT, Reid BJ, Fermor TR. 2001. Impact of composting strategies on the treatment of soils contaminated with organic pollutants. Environ. Pollut. 112(2):269-283.

Shankar MV, Nelieu S, Kerhoas L, Einhorn J. 2007. Photo-induced degradation of diuron in aqueous solution by nitrites and nitrates: kinetics and pathways. Chemosphere 66(4):767-74.

Sharma P, Moses JE. 2010. Ethynyldiisopropylsilyl: a new alkynylsilane protecting group and "Click" linker. Org. Lett. 12(12):2860-2863.

Shivarkar AB, Gupte SP, Chaudhari RV. 2004. Carbamate synthesis via transfunctionalization of substituted ureas and carbonates. J. Mol. Catal. A: Chem. 223(1-2):85-92.

Shved N, Berishvili G, Baroiller J-F, Segner H, Reinecke M. 2008. Environmentally relevant concentrations of $17\alpha$-ethinylestradiol (EE2) interfere with the growth hormone (GH)/insulin-like growth factor (IGF)-I system in developing bony fish. Toxicol. Sci. 106(1):93-102.

Sinclair CJ, Boxall ABA. 2003. Assessing the ecotoxicity of pesticide transformation products. Environ. Sci. Technol. 37(20):4617-4625.

Sinkkonen S, Paasivirta J. 2000. Degradation half-life times of PCDDs, PCDFs and PCBs for environmental fate modeling. Chemosphere 40(9-11):943-949.

Sleiman M, Destaillats H, Smith JD, Liu C-L, Ahmed M, Wilson KR, Gundel LA. 2010. Secondary organic aerosol formation from ozone-initiated reactions with nicotine and secondhand tobacco smoke. Atmos. Environ. 44(34):4191-4198.

Sobolewski AL, Domcke W. 2000. Photoinduced charge separation in indole-water clusters. Chem. Phys. Lett. 329(1-2):130-137.

Soumillion JP, De Wolf B. 1981. A link between photoreduction and photosubstitution of chloroaromatic compounds. J. Chem. Soc., Chem. Commun.(9):436-7.

Steger-Hartmann T, Kuemmerer K, Hartmann A. 1997. Biological degradation of cyclophosphamide and its occurrence in sewage water. Ecotoxicol. Environ. Saf. 36(2):174-179.

Stern RS, Bigby M. 1984. An expanded profile of cutaneous reactions to nonsteroidal anti-inflammatory drugs. Reports to a specialty-based system for spontaneous reporting of adverse reactions to drugs. JAMA-J. Am. Med. Assoc. 252(11):1433-7.

Strickmann DB, Blaschke G. 2001. Isolation of an unknown metabolite of the nonsteroidal anti-inflammatory drug etodolac and its identification as 5-hydroxyetodolac. J. Pharm. Biomed. Anal. 25(5-6):977-984.

Suzuki J, Okazaki H, Nishi Y, Suzuki S. 1982. Formation of mutagens by photolysis of aromatic compounds in aqueous nitrate solution. Bull. Environ. Contam. Toxicol. 29(5):511-16.

Suzumura K, Yasuhara M, Narita H. 1999. Superoxide anion scavenging properties of fluvastatin and its metabolites. Chem. Pharm. Bull. 47(10):1477-1480.

Temussi F, Bassolino G, Cermola F, DellaGreca M, Iesce MR, Montanaro S, Previtera L, Rubino M. 2010. Investigation on the phototransformation of tadalafil in aqueous media. 6-Epimerization *vs* solvent trapping reaction. Photochem. Photobiol. Sci. 9(8):1139-1144.

Temussi F, Passananti M, Previtera L, Iesce MR, Brigante M, Mailhot G, DellaGreca M. 2012. Phototransformation of the drug rivastigmine: photoinduced cleavage of benzyl-nitrogen sigma bond. J. Photochem. Photobiol. A, 239:1-6.

The European Parliament and of the Council. 2006. Registration, Evaluation, Authorisation and Restriction of Chemicals (REACH). Official Journal of the European Union. p 1-516.

Tomlin CDS. 1997. The pesticide manual. Tomlin CDS, editor. Surrey (UK): British Crop Protection Council. 1606 p.

Tomlin CDS. 2001. Pesticides and agricultural chemicals. GWA Milne, editor. Aldershot (UK): Gower Publishing Ltd.

Torisu K, Kobayashi K, Iwahashi M, Egashira H, Nakai Y, Okada Y, Nanbu F, Ohuchida S, Nakai H, Toda M. 2005. Development of a prostaglandin D2 receptor antagonist: discovery of a new chemical lead. Eur. J. Med. Chem. 40(5):505-519.

Turro NJ, Ramamurthy V, Scaiano JC. 2010. Modern molecular photochemistry of organic molecules. Sausalito: University Science Books.

US EPA. 1992. Environmental Protection Agency. National survey of pesticides in drinking water wells: phase II report. EPA 570/8-91-020.

US EPA. 1996. Environmental Protection Agency. Prevention, pesticides and toxic substances. R.E.D. FACTS: Chlorpropham. U.S. Environmental Protection Agency.

US EPA. 2008. Illinois Environmental Protection Agency. Report on pharmaceuticals and personal care products in Illinois drinking water. http://www.epa.state.il.us/water/pharmaceuticals-in-drinking-water.pdf.

US EPA. 2009. Environmental Protection Agency. Nicotine; Product cancellation order. Vol. 74(No. 105):26695.

US EPA. 2012. Environmental Protection Agency. Pesticides: health and safety. http://www.epa.gov/pesticides/health/human.htm

Vaal M, van der Wal JT, Hoekstra J, Hermens J. 1997. Variation in the sensitivity of aquatic species in relation to the classification of environmental pollutants. Chemosphere 35(6):1311-1327.

Valcárcel Y, González Alonso S, Rodríguez-Gil JL, Gil A, Catalá M. 2011. Detection of pharmaceutically active compounds in the rivers and tap water of the Madrid Region (Spain) and potential ecotoxicological risk. Chemosphere 84(10):1336-1348.

Valenti TW, Jr., Perez-Hurtado P, Chambliss CK, Brooks BW. 2009. Aquatic toxicity of Sertraline to Pimephales promelas at environmentally relevant surface water pH. Environ. Toxicol. Chem. 28(12):2685-2694.

Vaughan PP, Blough NV. 1998. Photochemical formation of hydroxyl radical by constituents of natural waters. Environ. Sci. Technol. 32(19):2947-2953.

Vialaton D, Richard C. 2000. Direct photolyses of thiobencarb and ethiofencarb in aqueous phase. J. Photochem. Photobiol. A, 136(3):169-174.

Vielhaber G, Oertling H, Titze N, Goemann C, Brodhage R; 20100525, assignee. 2010. Cyclohexyl carbamate compounds as skin and/or hair lightening actives. Germany patent 2010-EP57115-2010122178.

Vione D, Bagnus D, Maurino V, Minero C. 2010. Quantification of singlet oxygen and hydroxyl radicals upon UV irradiation of surface water. Environmental Chemistry Letters 8(2):193-198.

Vione D, Maurino V, Minero C, Pelizzetti E. 2005. Reactions induced in natural waters by irradiation of nitrate and nitrite ions. In: Boule P, Bahnemann D, Robertson P, editors. Handbook of Environmental Chemistry. Berlin: Springer. p 221-253.

Wang Z-Y, Xu X-X, Hu Z-D, Kang J-W. 2006. Sensitive method for enantioseparation of rivastigmine with highly sulfated cyclodextrin as chiral selector by capillary electrophoresis. Chin. J. Chem. 24(10):1384-1387.

Wayne RP. 2005. Basic Concepts of Photochemical Transformations. In: Boule PB, Detlef; Robertson, Peter;, editor. Handbook of Environmental Chemistry. Berlin: Springer. p 1-47.

Weedon AC, Wong DF. 1991. The photochemistry of Indomethacin. J. Photochem. Photobiol. A, 61(1):27-33.

Weyman GS, Rufli H, Weltje L, Salinas ER, Hamitou M. 2012. Aquatic toxicity tests with substances that are poorly soluble in water and consequences for environmental risk assessment. Environ. Toxicol. Chem. 31(7):1662-1669.

Wright J. 2003. Environmental chemistry. Wright J, editor. London Routledge.

Wu A-B, Cheng H-W, Hu C-M, Chen F-A, Chou T-C, Chen C-Y. 1997. Photolysis of indomethacin in methanol. Tetrahedron Lett. 38(4):621-622.

Yao Y, Li Z-s. 2008. Inhibition mechanism of cholinesterases by carbamate: a theoretical study. Chem. Res. Chin. Univ. 24(6):778-781.

Yoon UC, Su Z, Mariano PS. 2004. The dinamics and photochemicalm consequences of aminium radical reactions. In: Horspool W, Lenci F, editors. CRC Handbook of Photochemistry and Photobiology. 2nd ed. Boca Raton: CRC Press. p 101-120.

Zarrelli A, Della Greca M, Parolisi A, Iesce MR, Cermola F, Temussi F, Isidori M, Lavorgna M, Passananti M, Previtera L. 2012. Chemical fate and genotoxic risk associated with hypochlorite treatment of nicotine. Sci. Total Environ. 426:132-138.

Zhao Y. 2010. Auxin biosynthesis and its role in plant development. Annu. Rev. Plant Biol. 61:49-64.

Zuo Y, Zhang K, Deng Y. 2006. Occurrence and photochemical degradation of $17\alpha$-ethinylestradiol in Acushnet River Estuary. Chemosphere 63(9):1583-1590.

# SCIENTIFIC PRODUCTION LIST

PUBLICATIONS:

*PhD Thesis Publications*

Temussi F., Cermola F., DellaGreca M., Iesce M.R., Passananti M., Previtera L., Zarrelli A., "Determination of photostability and photodegradation products of indomethacin in aqueous media" Journal of pharmaceutical and biomedical analysis (2011), 56(4), 678-683.

Temussi F., Passananti M., Previtera L., Iesce M.R., Brigante M., Mailhot G., DellaGreca M., "Phototransformation of drug rivastigmine: photoinduced cleavage of benzyl-nitrogen sigma bond" Journal of photochemistry and photobiology A: chemistry (2012), 239, 1-6.

Passananti M., Temussi F., Iesce M.R., Mailhot G., Brigante M., "The impact of the hydroxyl radical photochemical sources on the rivastigmine drug transformation in mimic and natural waters" Water Research. Submitted.

Passananti M., Temussi F., Isidori M, Iesce M.R., DellaGreca M., Lavorgna M., "Chlorpropham and Phenisopham: phototransformation and ecotoxicity of carbamates in the aquatic environment" Environmental Science and Pollution Research. Submitted.

*Other Publications*

Cermola F., Iesce M.R., Astarita A., Passananti M., "Dye-sensitized photooxygenation of 2,5-bis(glycosyl)furans" Letters in Organic Chemistry (2011), 8(5), 309-314.

Zarrelli A., DellaGreca M., Parolisi A., Iesce M.R., Cermola F., Temussi F., Isidori M., Lavorgna M., Passananti M., Previtera L., "Chemical fate and genotoxic risk associated with hypochlorite treatment of nicotine" Science of the total environment (2012), 426, 132-138.

COMMUNICATIONS:

Temussi F., Bassolino G., DellaGreca M., Iesce M.R., Passananti M., Previtera L., Rega N., Savarese M., "Photochemical reactivity of *N*-benzylamides"; oral communication, XXV International Conference on Photochemistry (ICP 2011), Beijing, Cina, 7-12 August 2011.

Passananti M., Brigante M., Mailhot G., Previtera L., Temussi F., Iesce M.R., "Indirect photolysis and degradation of xenobiotics in aqueous media. Role and impact of the hydroxyl radical"; poster communication, 12th European Meeting on Environmental Chemistry (EMEC12), Clermont-Ferrand, France, 7-10 December 2011.

Passananti M., Cermola F., DellaGreca M., Iesce M.R., Previtera L., Temussi F., "The photochemical behavior of carbamate herbicides and structurally related compounds"; oral communication, Italian Photochemistry Meeting 2012 (IPM 2012), Bologna, Italy, 11-12 October 2012.